MIMO RADIO-OVER-FIBRE DISTRIBUTED ANTENNA SYSTEM FOR NEXT GENERATION WIRELESS COMMUNICATION

Yumeng Yang

Department of Engineering

University of Cambridge

This dissertation is submitted for the degree of

Doctor of Philosophy

Sidney Sussex College

September 20th, 2017

I would like to dedicate this thesis to my parents …

Declaration

I hereby declare that except where specific reference is made to the work of others, the contents of this dissertation are original and have not been submitted in whole or in part for consideration for any other degree or qualification in this, or any other University. This dissertation is the result of my own work and includes nothing which is the outcome of work done in collaboration, except where specifically indicated in the text. This dissertation contains less than 65,000 words including appendices, bibliography, footnotes, tables and equations and has less than 150 figures.

Yumeng Yang

September 20th, 2017

Acknowledgements

First of all, I would like to acknowledge my supervisor, Prof. Richard Penty, for his guidance during my PhD study. I am grateful for his inspiration and continuous support in the past four years. I would also like to thank my advisor, Prof. Ian White, whose comments and suggestions contribute to the complement of this thesis. Their help and supports benefit me a lot, not only in the field of radio over fibre technology but also on the way to become an independent researcher.

I want to thank Dr Michael Crisp and Dr Tongyun Li especially, who provided me with infinite helps to the first steps in my PhD study. They spent their valuable time to discuss academic problems with me. Also thanks for Adrian Wonfer and George Gordon for their constant help in my research.

Other group members also gave me valuable support, including Peter Vasilyev, Nikos Bamiedakis, Jinlong Wei, Sithamparanathan Sabesan, Qixiang Cheng, Xuhan Guo, Jiannan Zhu, Jian Chen, Sicheng Zou, Xin Li, Minsheng Ding, Shuai Yang, Priyanka De Souza, Eric Lowe. Thank them all for their help. I would like to give my special thanks to Minsheng Ding and Shuai Yang, who have been my best friends and companions during my PhD and ordered delivery food with me in the very late nights.

Most importantly, I would like to express my gratitude to my parents (Hefa Yang and Danwen Shen), who gave me the strongest supports all the time. Without their spiritual encouragement and meticulous supports, it is impossible for me to finish this work. I am particularly grateful to my wife – Wen Sun. She gave me unconditional companionship and understanding at my most difficult time.

In the end, when I am writing this thesis, my grandfather is suffering from cancer. I hope he can get well. Best wishes to him.

Abstract

This thesis introduces low-cost implementations for the next generation distributed antenna system (DAS) using analogue radio over fibre. A multiple-input-multiple-output (MIMO) enabled radio over fibre (RoF) system using double sideband (DSB) frequency translation system is proposed. In such a system, the 2x2 MIMO signals can be transmitted to the remote antenna units (RAUs) from the base station via a single optical link. By using the DSB frequency translation, the original single-input-single-output (SISO) DAS can be upgraded into the MIMO DAS without implementing parallel optical links. Experimentally, the DSB frequency translation 2x2 MIMO RoF system transmits 2x2 LTE MIMO signals with 20MHz bandwidth in each channel via a 300m MMF link. The condition number of the system is <10dB within the power equaliser bandwidth which means the MIMO system is well-conditioned and the crosstalk between the channels can be compensated by the MIMO signal processing.

To install the DSB frequency translation system in a wideband service-agnostic DAS, the original MIMO signals need to be translated into unoccupied frequency bands over the DAS, which are usually occupied by specific applications that are not to be transmitted over the DAS. The frequency spectrum allocation of the wireless services is analysed showing that by choosing a particular LO frequency (2.2GHz in the UK), in the DSB frequency translation system, the original MIMO signals can always be translated into unoccupied frequency bands so that the same infrastructure can support multiple services.

The idea of DSB frequency translation system can not only support MIMO radio over fibre but can also improve the SFDR of a general radio over fibre system. Because when the upper sideband and the lower sideband of the signal after translation are converted back to the original frequency band, the noise adds incoherently but the signals add-up coherently, this gives the system theoretically 2dB 3rd order SFDR improvement. If the idea of the DSB frequency translation is extended into a higher number of sidebands, the system SFDR can be further improved. Experimentally, the system 3rd order SFDR can be improved beyond the intrinsic

optical link by 2.7dB by using quadruple sideband (QSB) frequency translation. It means the optical bandwidth in a general RoF system can be traded for the electrical SFDR.

By integrating the analogue and the digital RoF systems, a hybrid DAS has been demonstrated, showing that the EVM dynamic range for the 4G LTE service (using digital RoF link) can be improved to be similar to the 3G UMTS service (using analogue RoF link), so that fewer number of RAUs for the LTE services are needed.

List of Publications

[1] Y. Yang, M. J. Crisp, R. V. Penty and I. H. White, "Low-Cost MIMO Radio Over Fiber System for Multiservice DAS Using Double Sideband Frequency Translation," in *Journal of Lightwave Technology*, vol. 34, no. 16, pp. 3818-3824, Aug.15, 15 2016.

[2] Y. Yang, M. J. Crisp, T. Li, R. V. Penty, I. H. White, "MIMO Capable RoF System with Improved SFDR using Quadruple Sidebands, " *2017 IEEE International Topical Meeting on Microwave Photonics (MWP)*, Beijing, China, 2017.

[3] R. V. Penty, G. Gordon, Y Yang, M. J. Crisp, T. Wilkinson, I. White, "Methods for Transmitting MIMO Radio Signals Over Fibre," *2017 IEEE International Topical Meeting on Microwave Photonics (MWP)*, Beijing, China, 2017. (Invited)

Contents

List of Figures

List of Tables

Nomenclature

2G	Second-generation wireless telephone technology
3G	Third-generation wireless telephone technology
3GPP	The 3rd Generation Partnership Project
4G	Fourth-generation wireless telephone technology
64QAM	64 quadrature amplitude modulation
ADC	Analogue to Digital Converter
AP	Access point
APD	Avalanche Photodiode
CW	Continuous Wave
DAC	Digital to Analogue Converter
DAS	Distributed antenna system

DDAS	Digitized Distributed Antenna System
DSB	Double Sideband
DSP	Digital Signal Processing
EDFA	Erbium-doped fibre amplifier
EVM	Error Vector Magnitude
FDD	Frequency-division duplexing
FPGA	Field Programmable Gate Array
GSM	Global system for mobile
IF	Intermediate Frequency
LO	Local Oscillator
LoS	Line-of-Sight
LTE	Long-term evolution
MIMO	Multiple-Input Multiple-Output
PoE	Power over Ethernet
POI	Point of Interface
QoS	Quality of Service
RAU	Remote Antenna Unit

RF	Radio Frequency
RoF	Radio over fibre
RRU	Remote Radio Unit
SFDR	Spurious-free Dynamic Range
SSB	Single Sideband
TDD	Time-division duplexing
UMTS	Universal mobile telecommunication service
VNA	Vector Network Analyser
VSG	Vector Signal Generator

Chapter 1 Introduction

1.1 MIMO-enabled RoF for Indoor Wireless Coverage

1.1.1 A brief historical background of modern wireless communication

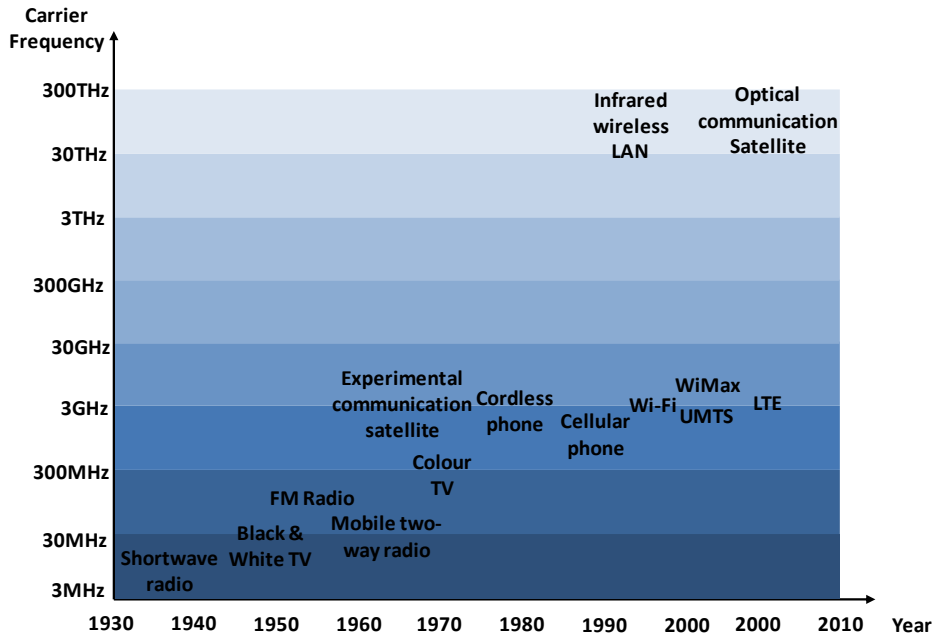

Figure 1.1 Milestones of wireless communication [1]

In several years following 1894, the commercial wireless telegraphy system was invented by Guglielmo Marconi, and human voice was first transmitted wirelessly in 1900 [1]. In the past century, wireless communication grew rapidly. Particularly in recent decades, the development

of cellular networks has revolutionised many lives and is still experiencing fast growth. Figure 1.1 shows some of the milestones of the wireless communication.

In fact, the revolutionary change in wireless communication is happening in every decade, and the overall trend of the development is to a higher frequency and higher data rate. Nowadays, the wireless communication has been a critical part of people's daily lives. Currently, there are 6.9 billion mobile cellular subscriptions worldwide [2].

Various of wireless standards have been defined and deployed rapidly to satisfy the demand on the wireless capacity, including the 1st generation (1G) to the 4th generation (4G) cellular networks and other wireless services, such as IEEE 802.11 series (Wi-Fi) and IEEE 802.16 series (WiMAX). After the cellular concept was raised by researchers in the Bell Laboratories in the 1970s [1], the booming of cellular networks became one of the most revolutionary events in human's communication history.

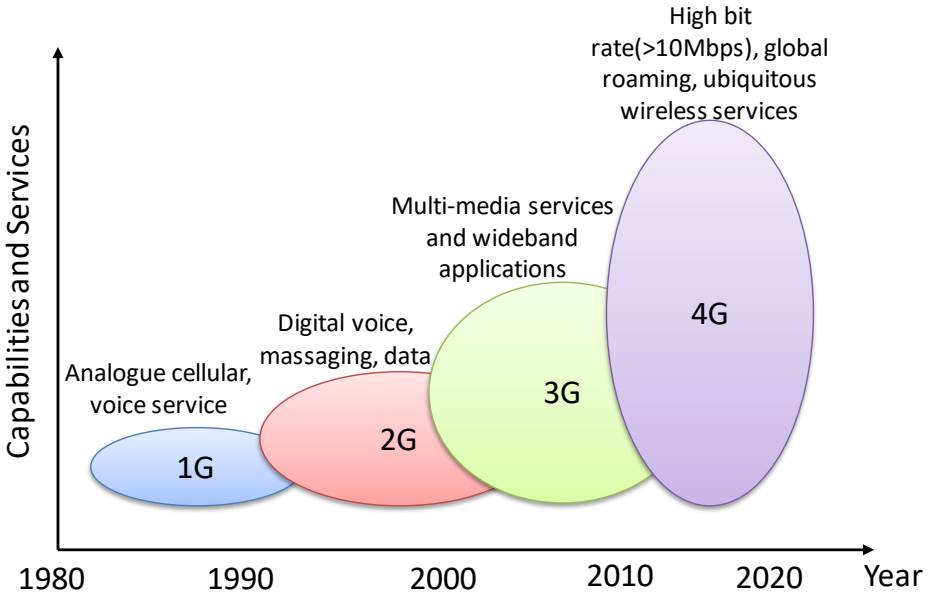

Figure 1.2 Evolution of cellular networks from the 1980s [4]

The 1G standards were introduced in the 1980s but limited by the high cost, low capability and few users, it is only deployed in some restricted regions. However, the 2G global system for mobile communications (GSM) lowered the price to a level that major public consumers can

accept. Since then, the 2G networks have been spreading into all over the world [3]. Compared with the analogue 1G services, the digital 2G services can support not only the voice communication but also messaging and low-speed data services, as shown in Figure 1.2. At the same period with the 2G network, the code-division multiple access (CDMA) has been specified in Qualcomm® IS-95 and IS-2000 standards. These two standards have enhanced the commercialisation of the 2G system [4].

To cope with the wideband multi-media data communication, a higher speed network was developed. The wideband code division multiple access (WCDMA) became one of the key technologies in the 3rd generation cellular network [4]. The first release of the 3GPP long-term evolution (LTE) technology has been deployed as one of the key 4G candidate systems in 2009. The 4G network can provide much higher data rate (>10Mbps) than previous generations of cellular networks.

1.1.2 Need and challenges for indoor wireless coverage of MIMO signals

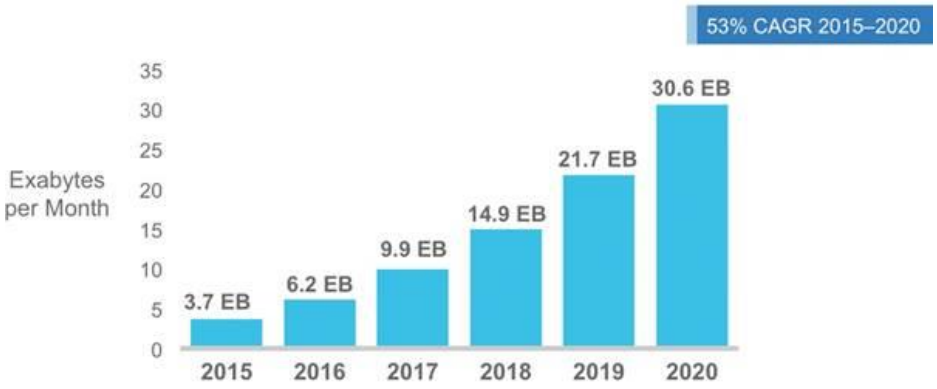

Figure 1.3: Cisco's forecast on mobile data generated per month globally [5]

Following the 4G mobile deployment, an enormous amount of mobile data is now being made. Cisco® predicts that by 2020, 30.6 Exabytes wireless data will be produced per month [5], as

shown in Figure 1.3. And by 2020, the number of portable devices will be beyond 10 billion and 40% of them will be smartphones (Figure 1.4). By 2018, 4G will make up 15% of connections and 51% of total traffic [5]. In the 4G standards, such as long-term evolution (LTE) and LTE-advanced, the use of MIMO techniques can increase data throughput and improve transmission reliability without increasing the occupied spectrum.

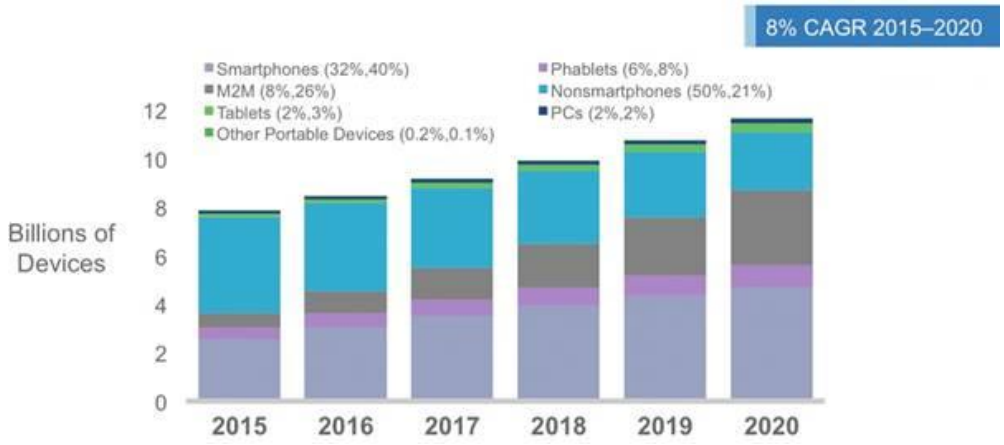

Figure 1.4: Cisco's forecast on global mobile device growth [5]

However, 80-90% of wireless data traffic originates in the indoor environments [6], where propagation conditions are usually poor with a high degree of multipath. The users suffer from a bad data connection or the drop of call in the inbuilding area. Non Line-of-sight (LoS) propagation and high attenuation through the building structure seriously lower the quality of service (QoS) for wireless services users inside buildings.

Therefore, it is necessary to find a cost-effective way to cover the indoor area by LTE and MIMO services.

1.1.3 Solutions for indoor wireless coverage

Various solutions have been developed to improve indoor wireless coverage, such as signal repeaters, femtocells (or small cells), and distributed antenna systems (DAS).

The signal repeater is a straightforward and the lowest cost solution. It is a bi-directional amplifier, which picks up and amplifies off-air downlink signals as signal sources, and also delivers users' uplink signal back to free space. However, the signal repeater can only provide service via a line-of-sight radio link to a neighbouring macro base station, as shown in Figure 1.5. The signal quality of the repeater is poorer than the small cells and distributed antenna systems. All these factors make the signal repeater unsuitable for most indoor environments, for example, buildings with complicated structures and large stadiums/shopping malls with high user density.

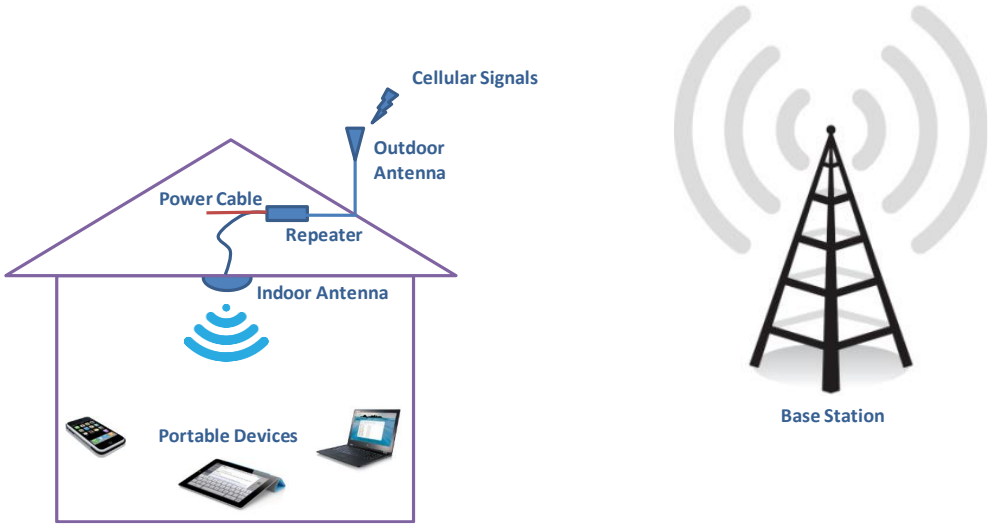

Figure 1.5: Architecture of a signal repeater [7]

The small cell delivers baseband signals from the operator core network to remote access points (APs). Typically, there are two types of small cell structures.

As in Figure 1.6, the traditional **stand-alone small cell system** is a smaller version of macro basestation. It connects the access point to the internet, then to the operator's core network. Although it has a direct connection with the existing internet protocol (IP) network, this kind of system requires high-cost small cell APs and is usually designed for a single operator and a limited number of users. Because the stand-alone small cells are not related to each other, inter-cell interference occurs at the cell borders. Usually, this small cell system is provided by mobile operators for homes without mobile signal coverage, such as the Home Signal Box from Three UK® and the Sure Signal from Vodafone® [8] [9].

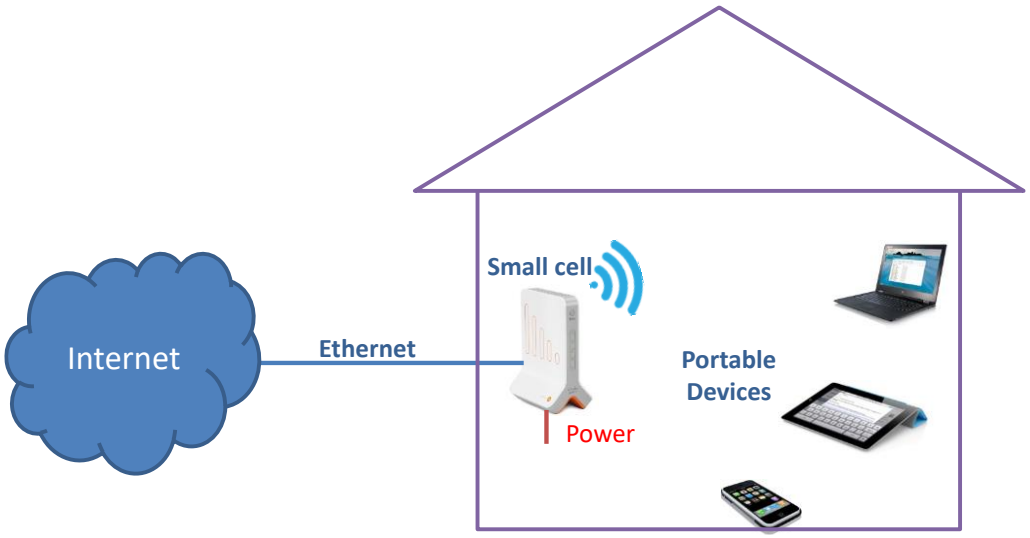

Figure 1.6 Architecture of a stand-alone small cell [9]

Figure 1.7 shows the layout of the **small cell system using a remote radio head (RRU)**. Compared with the stand-alone small cell product, the RRU small cell system centralises some of the signal processing from remote ends to the baseband controller. Because the centralised controller controls all the RRUs, there is no inter-cell interference. Thus it can provide wider signal coverage area to end users than the stand-alone small cell product. However, because of the complex digital data processing at both baseband controllers and RRUs, the RRU small cell system is a relatively high-cost solution.

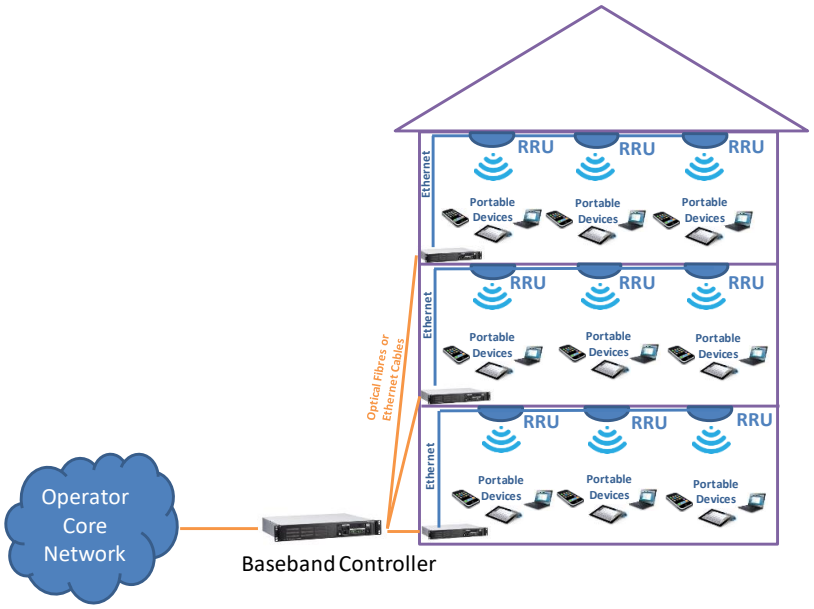

Figure 1.7 Architecture of a small cell system using RRUs [10]

In modern small cell systems, there are many attempts to lower the cost, such as using power over Ethernet (PoE) which makes the RRUs very easy to install, for example, Ericsson® RadioDot™ [10], Huawei® LampSite™ [11] and ZTE® QCell™ [12]. The small cell is now considered as a competitive solution for indoor wireless coverage, especially for office use. However, limited by the complexity of the signal processing and the requirement for the opening of the baseband ports from the mobile operator, the small cell system usually supports only a single operator. Thus it is not suitable for high user density areas where multiple operators and multiple services are required, such as sports stadiums, airports and shopping malls.

The DAS delivers base station signals, either in digital or in analogue forms, to remote antenna units (RAUs), as shown in Figure 1.8. Many indoor DASs use radio-over-fibre (RoF) technology to transmit signals between a base station and remote antenna units because of its versatility, flexibility, scalability and low cost [13]. It is predicted that by 2022, the DAS market will worth 10.78 billion US dollars [14].

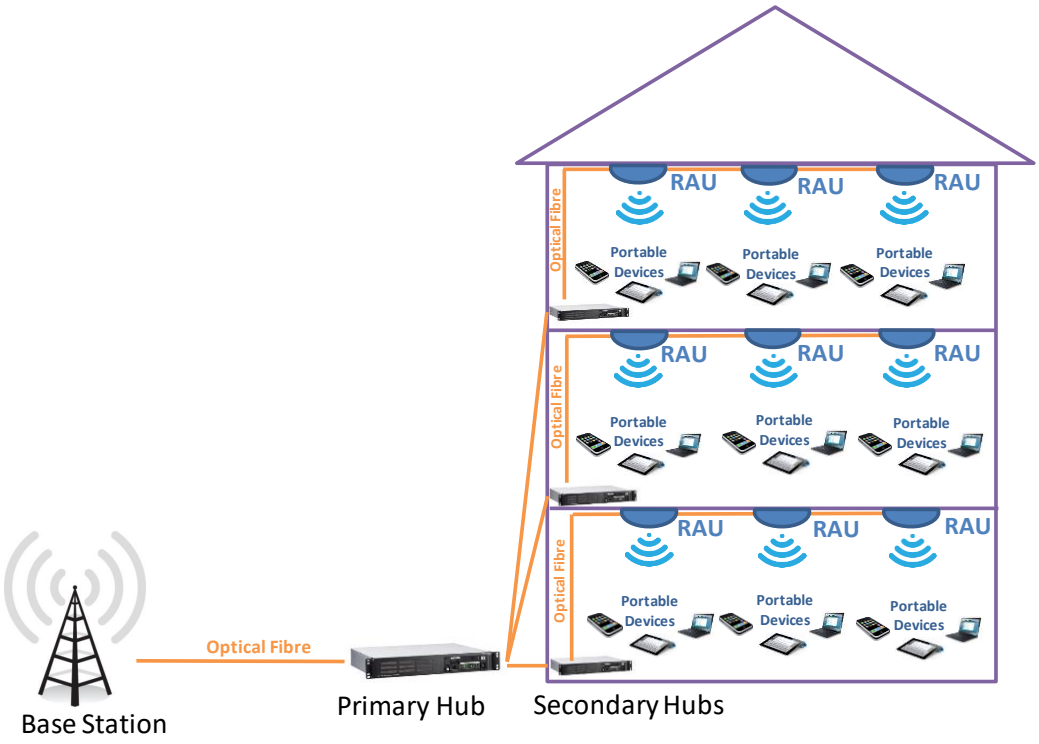

Figure 1.8 Typical architecture of a DAS [15]

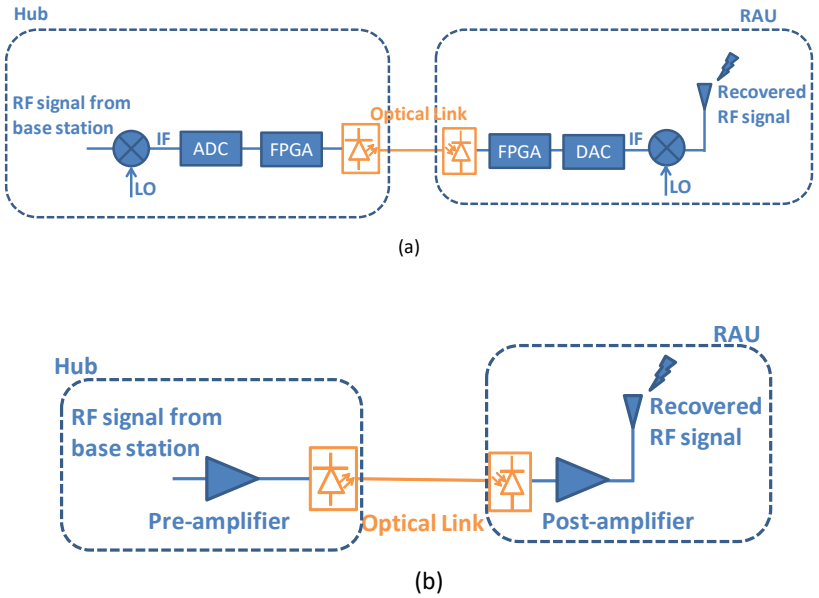

Figure 1.9 Typical Layout of a single link DAS: (a) Digital DAS; (b) Analogue DAS [16] [17]

Digital DAS (DDAS), as shown in Figure 1.9 (a), converts original base station RF signals into a lower intermediate frequency (IF), and then digitises IF signals using an ADC. In some DDASs, an FPGA follows the ADC to do digital data processing, such as data rate compression [17] [18]. The digital data after the FPGA is then transmitted via optical links to the RAUs where it is reconverted to the original basestation RF signal. Compared with analogue DASs, the DDAS has larger tolerance to long distance RF performance degradation and is easy to be controlled by system administrators, but the massive amount of data generated by sampling base station signals make the DDAS approach hard to cope with very high capacity applications, such as MIMO and future 5G network.

Analogue DASs, as shown in Figure 1.9 (b), transmit RF signals from base stations to RAUs via a directly modulated optical link without any digitisation [19]. The simplicity makes the analogue DAS low-cost and capable of handling large bandwidth signals. However, because the signal quality can be degraded by the nonlinearity and noise of active devices in the analogue DAS, such as such as power amplifiers and optical components in the link, the system needs to be very carefully designed to make sure it has satisfactory RF performance.

Table 1.1 Comparison among different indoor signal coverage solutions

	Repeater	Stand-alone Small Cell	RRU Small Cell	Digital DAS	Analogue DAS
Coverage area	Small	Small	Medium	Large	Large
Multi-operator	No	No	No	Yes	Yes
Multi-service	No	No	Yes	Yes	Yes
Capacity	Low	Medium	High	High	High
Cost/m^2 *	High	High	Medium	Medium	Low

* Indicates the cost for large area signal coverage per remote unit per service.

Table 1.1 gives a brief comparison among different indoor signal coverage solutions. Repeaters and stand-alone small cells are suitable for a single operator and small area coverage, such as

home use. Although RRU small cell and DDAS can be used for large area signal coverage, because of the DSP complexity, they are high cost and not suitable for wide bandwidth and multi-operator multi-service signal coverage. Especially when in the scenarios that MIMO RoF is required, the huge data rate generated in the DDAS occupies wide optical bandwidth and leads to high cost in digital signal processing and optical transceiver components. All these reasons the make analogue DAS be a potential solution for next-generation indoor broadband MIMO signal coverage.

In this thesis, the author will discuss the topics relating to transmitting broadband MIMO signals using analogue DAS.

1.2 Thesis Scope

The aim of this dissertation is to study the challenges and solutions to the transmission of MIMO signals over a single optical fibre in a low-cost and high-quality way for indoor analogue distributed antenna systems.

Chapter 2 introduces fundamentals of a MIMO radio over fibre system. From an intrinsic RoF link to the architecture of an analogue DAS, the implementation of a MIMO-enabled DAS is illustrated. Technical challenges to build such a system and state-of-the-art of current solutions are described.

Chapter 3 discusses a cost-effective MIMO radio over fibre system using double sideband (DSB) frequency translation multiplexing scheme. Models have been built to simulate the link performance and the origins of system noise, nonlinearity and crosstalk. Experiments have been carried out to exam the system characteristics.

Chapter 4 extends the narrowband implementation in chapter 3 into a broadband solution. Frequency bands of all the services to be transmitted over DAS have been investigated. In the experiment, system EVM performance has been tested using commercial LTE bands. The

throughput of an IEEE 802.11n 2x2 MIMO signal is measured, showing that the system can work under real-life conditions.

Chapter 5 theoretically and experimentally demonstrates that the DSB frequency translation system can effectively improve the system 3rd order SFDR. If the number of sidebands is increased, say to quadruple sidebands (QSB), the SFDR can be further improved. By using DSB and QSB frequency translation, the system SFDR can be higher than the intrinsic optical link itself. This research shows the potential to trade optical bandwidth for SFDR improvement.

Chapter 6 proposes a hybrid system using analogue and digital radio over fibre. By using the hybrid system, the dynamic range of the SISO LTE service can be improved, so that fewer number of RAUs are required for the LTE coverage. Compared with the pure analogue or pure digital system, the hybrid system can lower the system cost.

The conclusions and potential future works are discussed in Chapter 7.

1.3 Novel Contributions

The novel contributions in this thesis are included below:

- A simple power equaliser has been designed to make the DSB frequency translation system capable of transmitting wideband LTE MIMO service over MMF optical link.
- The broadband operation of a MIMO RoF system using DSB frequency translation technique has been proposed and investigated, showing that by selecting certain LO oscillator frequencies (for example, 2.2GHz in the UK), the original MIMO signal can always be translated into the free spectrum over the DAS, giving the DSB frequency translation system the capability to support broadband operation.
- It is shown that the optical bandwidth of a RoF system can be traded for the SFDR. The DSB frequency translation technique has been extended to a higher number of sidebands.

By using double sideband and quadruple sidebands frequency translation, it is shown that the SFDR of an RoF link can be improved beyond the intrinsic optical link.

- A hybrid analogue and digital radio over fibre system have been proposed and demonstrated. The low-cost hybrid system has higher dynamic range than the traditional analogue system and simpler DSP than the traditional system.

Chapter 2 Fundamentals of a Radio over Fibre Systems and Literature Reviews

2.1 Intrinsic Analogue RoF Link

2.1.1 Benefits of using radio over fibre

The idea of analogue radio over fibre was introduced in the 1990s [20]. The analogue radio over fibre system delivers the radio frequency (RF) microwave signals by modulating them onto the lightwave carrier and transmitted over optical fibres. In this sense, the RoF link is serving as an active RF waveguide. In recent decades, there has been an explosion in the number of applications of analogue optical links. Compared with traditional microwave cables, such as coaxial cables and twisted pairs, the optical fibre has many benefits, such as:

i) The smaller size and lighter weight: a conventional coated optical fibre has 250μm diameter [21]. This allows the optical fibre links much easier to be installed and maintained.

ii) Much wider bandwidth: The combination bandwidth of 850nm, 1310nm and 1550nm window is >50THz [22]. It allows systems' multi-service and wide bandwidth operation.

iii) Lower attenuation loss: The attenuation loss for a single mode fibre operating at the 1550nm wavelength is 0.2dBo/km [23], which is much lower than the coaxial cable loss. RG6 coaxial cable, for instance, has ~214dB/km loss at 1GHz frequency [24].

All these properties make the optical link suitable for wide bandwidth RF transmission, especially in long distance.

In the DAS, multiple wireless services from multiple operators are to be transmitted from the centralised hub to remote units. The transmitting range is a few hundred metres to 1 kilometre, depending on the size of the building. Compared with the passive DAS which uses coaxial cables, the DAS using radio over fibre has higher bandwidth and can cover larger areas. It is also easier to be installed and maintained.

2.1.2 The architecture of an intrinsic analogue RoF link

A. Detection of lightwave

To deliver RF signals over an optical link, the lightwave needs to be modulated and detected using one of its parameters, such as amplitude (power), frequency or phase. Direct detection of an intensity-modulated lightwave is straightforward using a photodiode [25]. The photodiode has a square law characteristic, producing a photocurrent (I_{pd}), which is proportional to the incident optical power (P) and its responsivity(R).

$$I_{pd} = RP$$

On the other hand, the detection of phase or frequency modulated lightwave needs a coherent optical receiver [26]. Although coherent detection has higher sensitivity than direct detection [27], it requires a much more complicated receiver structure than direct detection. Direct detection performance can satisfy the performance requirement for current commercial mobile services, as will be explained in the following chapters. Here, in this thesis, we use direct intensity detection in the optical receiver.

The PIN photodiodes and avalanche photodiodes (APD) are two types of commonly used photodiodes. A brief comparison between the InGaAs PIN photodiodes and the InGaAs APD is shown in Table 2.1. Here the Si photodiodes are not included because the 1310nm and 1550nm wavelength windows are more widely used in the radio over fibre systems for indoor DAS.

Table 2.1 Performance comparison between the PIN photodiode and the APD [28] [29]

	InGaAs PIN photodiode	InGaAs APD
Typical operating wavelength	1100 - 1700 nm	1100 - 1700 nm
Responsivity	0.5 – 0.8 A/W	0.5 – 0.8 A/W
Multiplication factor	1	20-400
RF bandwidth	Up to 40GHz	Up to 40GHz
Reverse bias voltage	5 – 10 V	25 – 400 V

Both the InGaAs PIN photodiode and the InGaAs APD have a wide optical bandwidth from 1100nm to 1700nm, meaning that if 1310 nm and the 1550 nm optical signals exist in the same optical link, both of them can be detected by the same photodiode. In the radio-over-fibre applications, the primary difference between the PIN photodiodes and APDs are the multiplication factor and the reverse bias voltage.

The avalanche effect does not happen in the PIN photodiode. However, in the APDs, the detected optical signal is converted into electrical signal and then amplified by the avalanche effect, in which additional carriers are injected into an area with a high electrical field. The carriers then collide with neutral semiconductor atoms generating other carriers. This collision process repeats, again and again, giving the effectively amplified number of carriers in the free carrier generation [30]. Therefore, compared with the PIN photodiode, the APD produces multiplication factor giving additional gain. It can be used various of applications with high sensitivity requirement [31].

However, the APDs require much higher reverse bias voltage than the PIN photodiodes [32], meaning harder to be implemented in the DAS remote units. Moreover, as the APD multiplication factor changes with the reverse bias voltage, the vibration in the power source may affect the output RF performance. Therefore, a higher cost power source is required in an APD system. The PIN photodiode, on the other hand, is much easier to be installed into a low power system and has a lower cost than the APD. In this thesis, because the application is for

indoor wireless communication, in which the typical transmission distance is in hundred metre range, we use the PIN photodiode in the intrinsic optical link.

B. Intensity modulation

Because direct intensity detection is used, the optical carrier must be modulated in intensity. Broadly the optical intensity modulation can be categorised into two means - direct modulation and external modulation [33], as shown in Figure 2.1.

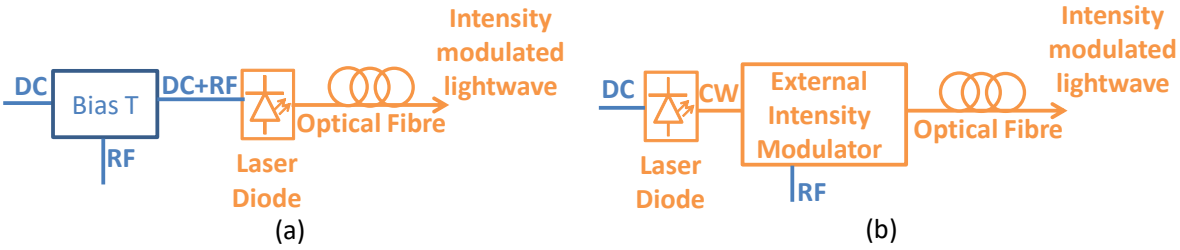

Figure 2.1 Intensity modulation of RF signal over optical link: (a) Direct Modulation; (b) External Modulation

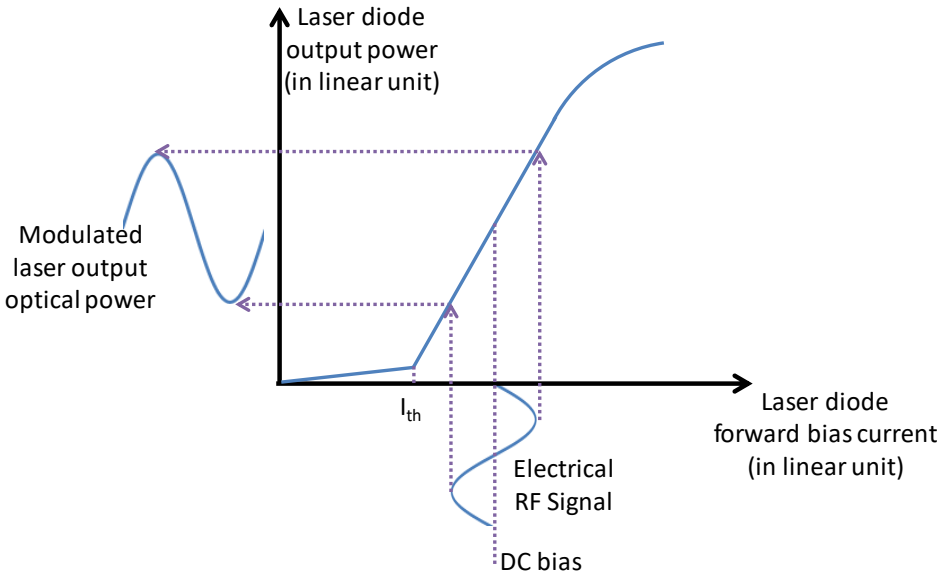

Figure 2.2 Concept of direct modulation of a laser diode

In **direct modulation** (Figure 2.1(a)), a DC bias current is applied to the laser diode to make it operate in the linear region, as shown in Figure 2.2. Usually, the highest dynamic range can be achieved when the laser diode is biased at the middle point of the linear region. As shown in Figure 2.2, in the linear region, laser diode output optical power follows to the variation of its driving current. The electrical RF modulation signal is inside the linear region and produces a modulated output optical signal. As the RF signal is directly applied to the laser diode, the modulation signal must be within the laser's modulation bandwidth, which can be limited by the relaxation oscillation frequency [27] and chirping [28].

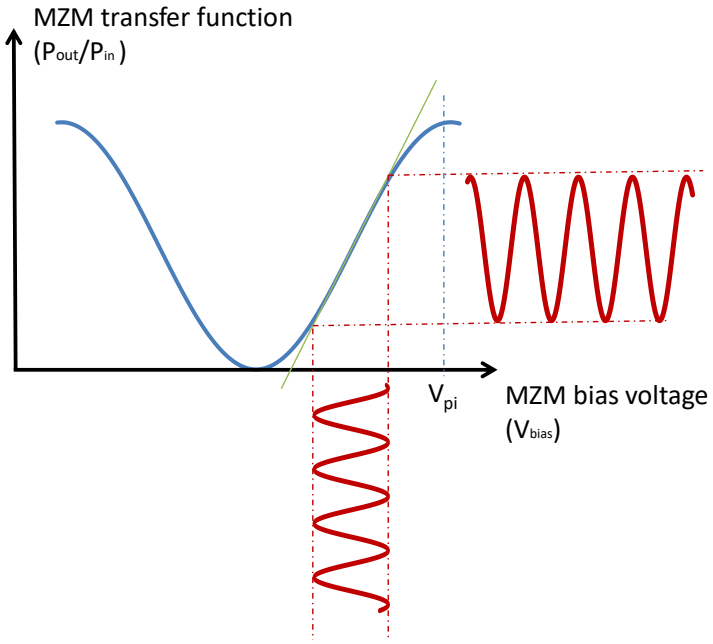

Figure 2.3 Concept of external intensity modulation

In **external modulation** (Figure 2.1(b)), the laser diode emits continuous wave (CW) light, and the modulation is done in an external optical modulation device, such as a Mach-Zehnder Modulator (MZM) or Electro-absorption (EA) modulator. As shown in Figure 2.4, if the MZM is biased at the Vpi/2, it has an approximately linear transfer function which does not rely on the laser diode modulation frequency. The output optical intensity follows the MZM driving voltage. In the external modulation, the modulation bandwidth is not limited by the laser diode

relaxation frequency. Therefore, compared with the direct modulation, the external modulation has higher modulation bandwidth.

A brief comparison between the direct modulation and the external modulation has been shown in Table 2.2. The external modulation has advantages over the direct modulation regarding RF noise figure, SFDR and bandwidth. However, in the external modulation, an additional optical component is required, so it has a higher cost than the direct modulation.

Table 2.2 Comparison between direct modulation and external modulation

	Direct Modulation	External Modulation
	Modulate in electric domain	Modulate in optical domain
Lowest Noise Figure	17.8 dB [34]	2.5 dB [35]
Greatest SFDR	128 dB*Hz$^{-2/3}$ [36]	132 dB*Hz$^{-2/3}$ [37]
Bandwidth	20GHz to 40GHz depends on laser [38] [39] [40]	MZM:70GHz [41] EA: 60GHz [42]
Complexity	Simple	Complex
Cost	Cheap	Expensive needs optical modulator

C. Laser diodes for direct modulation

Nowadays, the development of semiconductor lasers enables the direct modulation at high frequencies. It has been reported that the modulation bandwidth of a distributed feedback (DFB) laser can be 35GHz [40] and this is enough for current commercial wireless services. And the cost for a packaged DFB laser has been lowered to less than a hundred dollars in mass production [43].

A brief comparison among the DFB, Fabry-Perot and vertical-cavity surface-emitting (VCSEL) laser has been shown in Table 2.3 [44]. The DFB laser is a preferable type laser in

the directly modulated RoF link regarding the SFDR, relative intensity noise (RIN) and stable single-mode operation at high frequencies [16]. For some short-range RoF, or for the scenarios in which the noise and linearity performance is not critically required, the FP laser and the VCSEL can be a replacement.

Table 2.3 a brief comparison among DFB, F-P and VCSEL lasers [45]

	DFB Laser	FP Laser	VCSEL
Operating Wavelength	1300nm,1550nm	1300nm, 1550nm	800-1000nm (where fibre characteristics are less desirable)
Slope Efficiency (Greatest)	0.44 W/A [40]	0.38 W/A [46]	0.61 W/A [47]
Bandwidth (Greatest)	20 GHz [40]	40GHz [48]	36 GHz [38]
Slop Efficiency*BW (Greatest)	8.8(W/A) *GHz [40]	10(W/A) *GHz [46]	8.0 (W/A) *GHz [47]
SFDR	128 dB*Hz^2/3 [36] (temperature controlled) >104 dB*Hz^2/3 [49] (20GHz, uncooled)	107-117 dB*Hz^2/3 [50]	95-100dB*Hz^2/3 (5GHz) [50]
RIN (dBc/Hz)	-160— -150 dBc/Hz	-140— -130 dBc/Hz	<-130 dBc/Hz
Cost	High production cost, but <$100 each in mass production [43]	Lower than DFB	Lower than DFB

In this thesis, we focus on the RoF link with 500m to 1km distance range and the system dynamic range need to satisfy the standards requirements.

Thus, by considering the trade-off between cost and performance, we define the intrinsic optical link as an intensity-modulated-direct-detection (IM-DD) link using a direct modulated DFB laser, an SMF and a PIN photodiode, as shown in Figure 2.4.

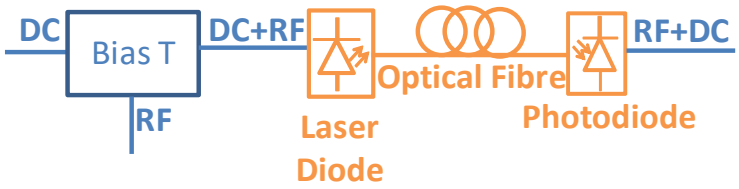

Figure 2.4 Intrinsic analogue radio over fibre link

D. Fibre Path

The single mode (SMF) fibre and the multi-mode fibre (MMF) are two commonly used types of optical fibres. Both types of fibres typically have 125 μm outer diameter which is similar to the size of the human hairs. The single-mode fibre has typically 9 μm core diameter which allows the light to be transmitted in only in the fundamental mode, while other modes are removed. However, the multi-mode fibre has a larger core (typically 50 μm or 62.5 μm) so that multiple modes can be transmitted [51].

Theoretically, the multimode fibre has better light gathering ability than the single mode fibre. However, the severe dispersion problem in the MMF make it hard to be used in the long-distance transmission, and the RF bandwidth can be limited by the dispersion effect. The MMFs are easier to be manufactured than the SMFs, so have a lower price, although compared with other parts of the system and the engineering cost, the price of the optical fibres is negligible. Historically, many buildings' ethernet backbones use MMFs, so it is still meaningful to do RoF over the MMF in some scenarios. Because of SMFs' higher bandwidth * distance product, the single mode fibres are preferred in the new infrastructures [52].

2.2 Performance Measurement of a RoF Link

2.2.1 Link intrinsic gain

The power of the intrinsic RoF link (the LD-Fibre-PD link) is defined as the ratio between the output RF power at the load following the photodiode and the input RF power to be modulated

at the RoF link input (direct modulated onto the laser diode). The intrinsic link power gain is usually negative and dominated by the electrical to optical (E/O) conversion loss and the optical to electrical (O/E) conversion loss. A comprehensive analysis can be carried out using the small signal model as shown in Figure 2.5.

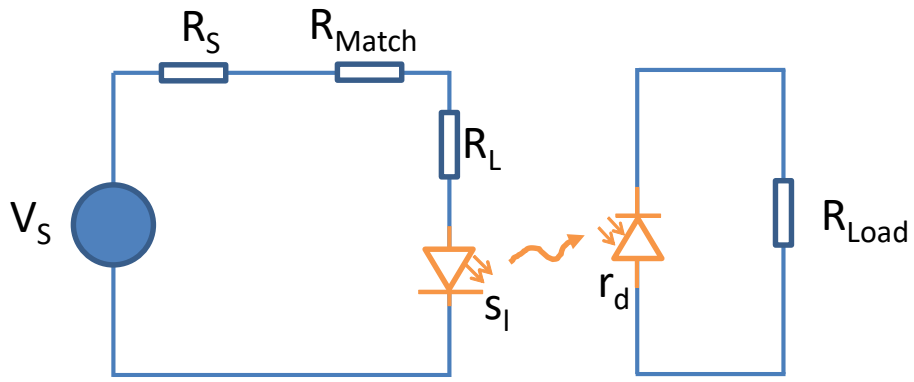

Figure 2.5 Small signal model of the intrinsic RoF link [16]

A DC-biased RF signal source (Vs) with impedance Rs is input into an impedance matching circuit and then to a laser diode. There is voltage loss, because of the impedance mismatch between R_L and R_S. Assuming the laser diode has slope efficiency S_l (W/A) and the photodiode has responsitivity r_d (A/W), the current and the voltage across the load are:

$$i_{out} = \frac{V_s}{R_s+R_{Match}+R_L} s_l r_d \tag{2.1}$$

$$v_{out} = \frac{V_s}{R_s+R_{Match}+R_L} s_l r_d R_{Load} \tag{2.2}$$

Considering the input side,

$$i_{in} = \frac{V_s}{R_s+R_{Match}+R_L} \tag{2.3}$$

$$v_{in} = V_s \tag{2.4}$$

The intrinsic power gain of the link yields,

$$g_i = \frac{v_{in} i_{in}}{v_{out} i_{out}} = \frac{s_l^2 r_d^2 R_{Load}}{R_S + R_{Match} + R_L} \tag{2.5}$$

It can be seen in (2.5) that $g_i \propto s_l^2 r_d^2$. When $R_{Load} = R_s + R_{Match} + R_L$,

$$g_i = s_l^2 r_d^2 \tag{2.6}$$

For a typical 1.3μm DFB laser, the diode laser fibre-coupled slope efficiency ranges from 0.035 to 0.32 W/A, and the photodiode responsivity ranges from 0.5 to 0.8 A/W [16]. Thus, from (2.6), the intrinsic link gain should be between -35 and -12dB.

Considering the components cascaded before and after the intrinsic optical link, the overall gain of the system follows the equation below:

$$g_{system} = \left(\prod_i g_{pre\,i}\right) * g_i * \left(\prod_i g_{post\,i}\right) \tag{2.7}$$

in which, g_{pre} is the gain of the components before the intrinsic optical link and $g_{post1}$is the gain the components after the intrinsic optical link. The gain of the intrinsic optical link is g_i.

2.2.2 Error Vector Magnitude

The quadrature amplitude modulation (QAM) is a commonly used modulation scheme in mobile wireless networks. It takes digital data and separates it into in-phase (I) and quadrature (Q) data streams. The I and Q signals are then modulated onto a passband carrier (fc) in quadrature by a QAM transmitter, as shown in Figure 2.6.

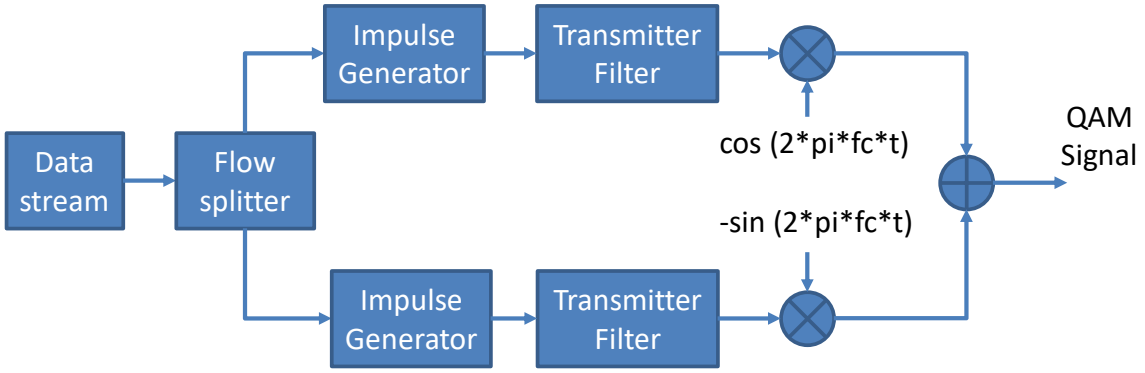

Figure 2.6 Typical layout for a QAM transmitter

The QAM receiver (Figure 2.7), takes the QAM signal and demodulates it by multiplying it with two sine waves with the 90-degree phase difference. A low-pass filter is then used to obtain the baseband information.

Because the QAM uses the phase of the signal, it has high spectrum efficiency, and it is included in many wireless standards, such as IEEE 802.11 series and 3G/4G cellular standards.

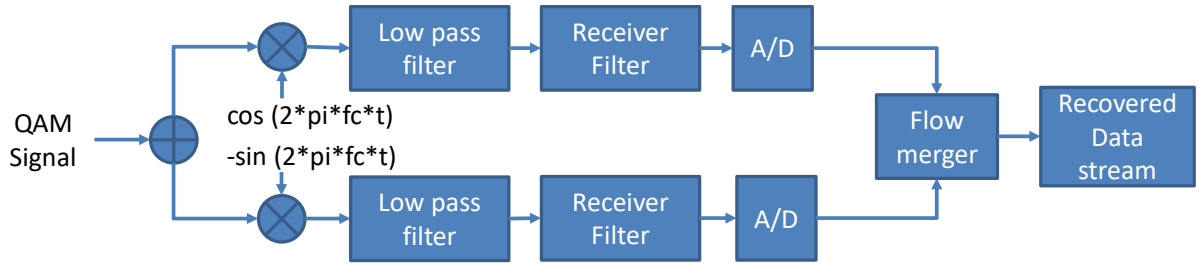

Figure 2.7 Typical layout for a QAM receiver

The demodulated QAM signal can be shown in a constellation diagram. Because of the noise and interference, the demodulated signal does not necessarily locate to the position of the reference constellation point. The shift between the demodulated QAM signal and the ideal constellation point results in an error vector. The average amplitude of the error vector (normalised to the ideal symbol vector) is the EVM (Figure 2.8), which can be expressed in the equation below:

$$EVM(\%) = \sqrt{\frac{1}{N}\sum_{n=1}^{N}\frac{|Error\ Vector|^2}{|Ideal\ Symbol\ Vector\ |^2}} \times 100\% \qquad (2.8)$$

In an analogue RoF system, the signal's EVM directly relates to the signal to noise and interference ratio (SNIR) at the receiving end [49]:

$$EVM(\%) = \sqrt{\frac{1}{snir(1)}} \tag{2.9}$$

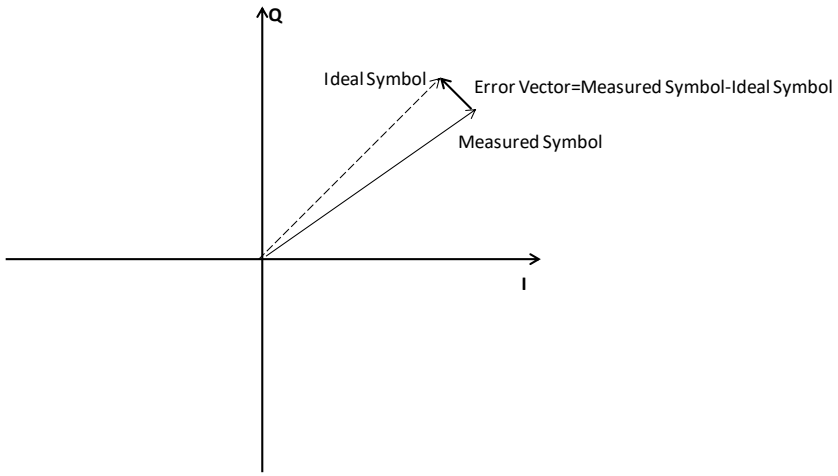

Figure 2.8 Error vector magnitude

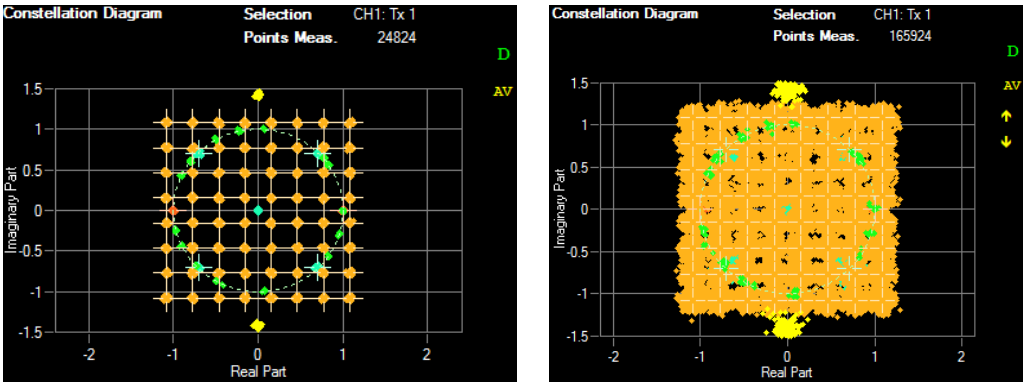

(a) (b)

Figure 2.9 Constellation diagrams with (a) low EVM; (b) high EVM (measured by a vector signal analyser in the experiment)

As shown in Figure 2.9, when the system has low EVM, the constellation points can be clearly distinguished. On the other hand, when the EVM is high, each of the constellation diagrams can no longer be distinguished. The EVM requirement has been described in various of standards. 3GPP, for example, has defined EVM requirement for the LTE PDSCH as shown in Table 2.4. IEEE has defined the EVM requirement for Wi-Fi devices as shown in Table 2.5 The EVM requirement depends on the modulation schemes and coding rate. In a higher modulation scheme, the relative distance between each of the reference constellation points to the signal power is smaller than that of the lower dimension modulation scheme. Therefore, the EVM requirement for higher dimension modulation scheme is lower, for example, in the LTE PDSCH, the EVM requirement for the QPSK is 17.5%, but it is only 8% for the 64QAM. In modern wireless communication standards, such as 3GPP LTE and IEEE 802.11 series, if the communication environment is not suitable for the dimension high modulation scheme, the system will be forced to operate in a lower dimension modulation scheme, so that the EVM requirement can be satisfied.

Table 2.4 3GPP defined EVM requirement for QAM in LTE PDSCH [53] [54]

Modulation Scheme for PDSCH	EVM requirement (%)
QPSK	17.5%
16QAM	12.5%
64QAM	8%

Table 2.5 EVM requirement for IEEE 802.11a/g legacy devics and 802.11n devices [55]

Modulation	Coding Rate	EVM (dB) for legacy devices	EVM (dB) for 802.11 devices
BPSK	1/2	-5	-5
BPSK	3/4	-8	-8
QPSK	1/2	-10	-10
QPSK	3/4	-13	-13
16QAM	1/2	-16	-16
16QAM	3/4	-19	-19
64QAM	2/3	-22	-22
64QAM	3/4	-25	-25
64QAM	5/6	--	-28

2.3 Architecture of an Analogue SISO DAS

An analogue single-input-single-output(SISO) DAS can be built by combining multiple optical links. They distribute basestation signals to each of the RAUs and also collect users' signal from the RAUs to the basestation. Figure 2.10 shows two downlink layouts for inbuilding analogue DASs. To save the cabling cost, many DASs use multi-stage splitting. Taking the Zinwave® UNItivity solution as an example, two stages of DAS hubs are implemented, as shown in Figure 2.10(a). The primary hub separates the basestation signal into n ways, and each of the secondary hubs further amplifies and split the signal into m ways. Therefore, n*m RAUs can be supported by the system. Compared with the active secondary hub (Figure 2.10(a)), the passive secondary hub (Figure 2.10(b)) saves the cost of active components.

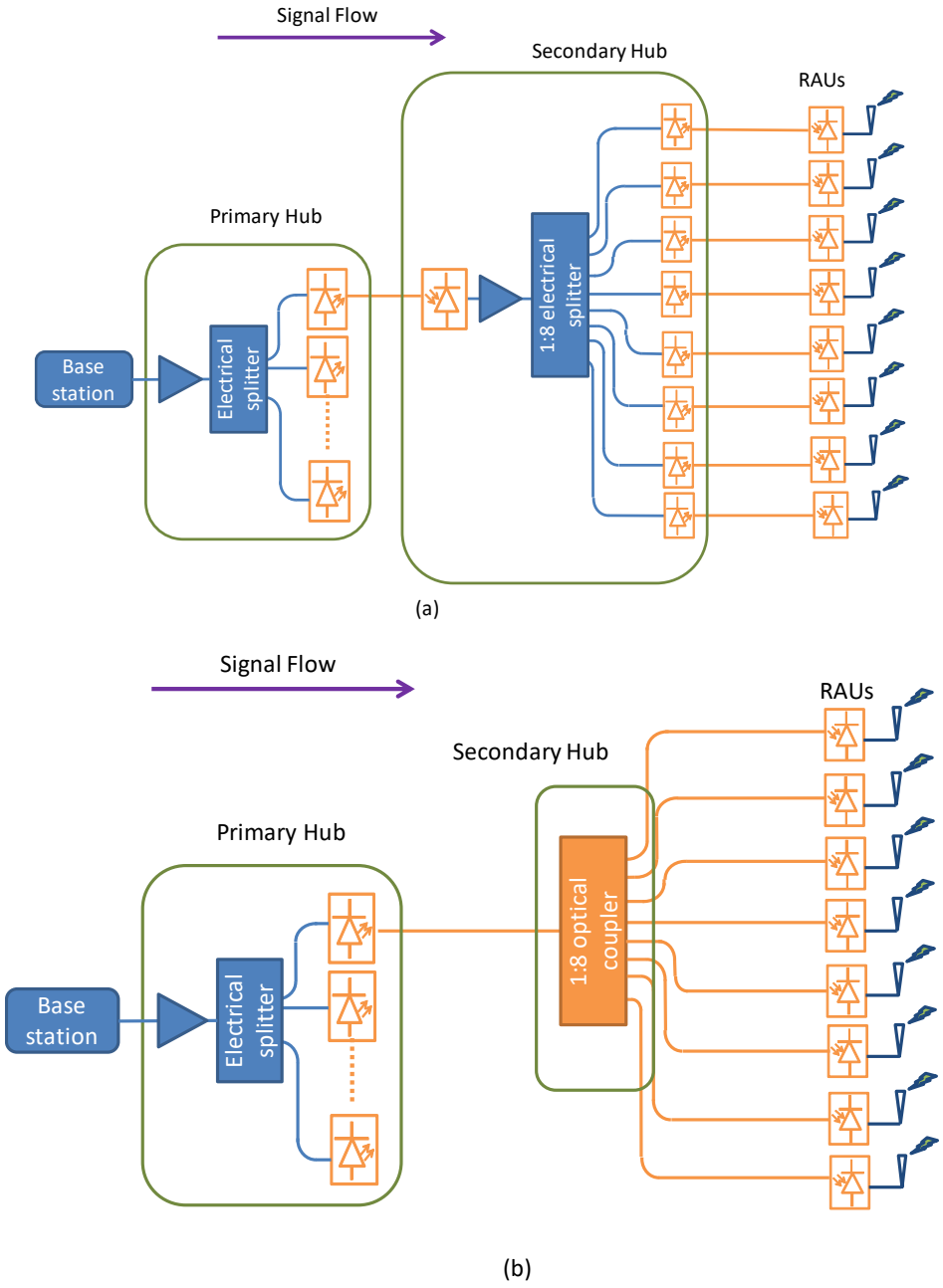

Figure 2.10 Typical downlink layout of an in-building analogue DAS: (a) active secondary hub; (b) passive secondary hub

2.4 Challenges to Implement DAS and Integrate MIMO Services into an Analogue DAS

Currently, the DAS has been one of the most commonly used solutions to cover and extend wireless services in large venues like shopping malls, stadiums, undergrounds, airports. Soon, the DAS will be more implemented in areas such as universities, healthcare, multi-functional buildings, and in urban areas for offloading data traffic.

As a service-agnostic system, the DAS needs to transmit all different services to users within one infrastructure. Nowadays, there is a range of wireless services and services providers, such as 3G/4G cellular services (O2, 3, Vodafone, …), Wi-Fi, public safety and others. All these services and service providers use different standards and occupy different frequency bands. Delivering these various things together to users become one of the key challenges to the DAS. To do this, the DAS needs to be broadband, covering all frequency bands from 700MHz to 3.5GHz [56]. In a future 5G network, this frequency range may be extended up to 80GHz [57].

From a business perspective, the cost and complexity is a challenge to DAS deployment. The installation of a DAS requires long optical fibres and power supplies at each of the RAUs. The cabling from the central unit to the RAUs is complicated (as shown in Figure 2.11) and the installation cost can be enormous. Due to the complicity of the system and the lack of ready solutions for rack elevation drawings, cabling installation guidance, and other system design elements, the installation of a DAS needs experienced RF engineers and technicians.

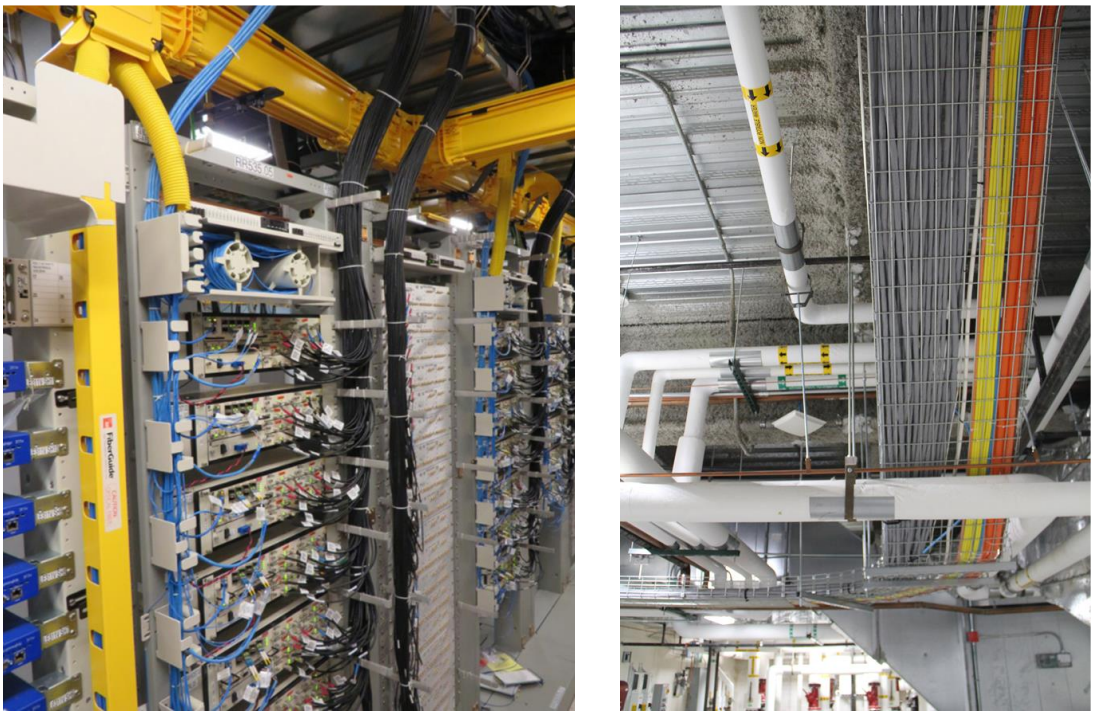

(a) (b)

Figure 2.11 Cabling of a Commscope® DAS: (a) central hub; (b) inbuilding cabling [58]

As mentioned in Chapter 1, the MIMO technology has now been widely included in many wireless standards. There is a strong driver to upgrade traditional SISO DAS to MIMO DAS. However, the MIMO-type signals overlap in frequency bands, which makes them not able to be transmitted directly on the traditional SISO DAS infrastructure. A straightforward solution is to build parallel systems to transmit MIMO signals over DAS. This makes the system components increase linearly with the MIMO channel number and results in a high upgrade and maintenance cost. Therefore, a solution which can upgrade existing DAS to MIMO DAS without installing additional optical fibres will be very much needed.

2.4.1 Nonlinearity

A. The 2nd and the 3rd order intermodulation products

The linearity of the RoF is a critical parameter, which influences the system dynamic range. The nonlinearity of a RoF link can cause intermodulation distortion (IMD), and unwanted RF harmonics will be generated. Nonlinear products can make the system RF performance degrade significantly [59].

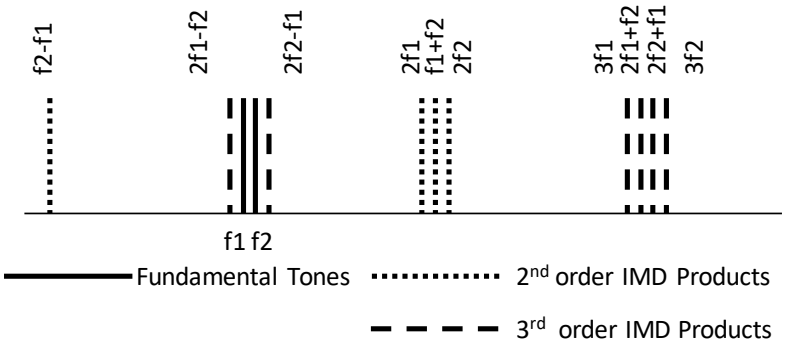

Figure 2.12 Frequency distribution of 2nd and 3rd order IMD products

Assuming there are two pure sine waves (f1 and f2) at the input of a nonlinear system, at the system's output, the spectrum consists of fundamental tones (f1, f2) and high order IMD products.

Figure 2.12 shows the frequency spectrum at the output of the nonlinear system with fundamental tones and the second order and the third order distortion harmonics. The fundamental tone appears at the same frequency as the input signals, but the 2nd order and 3rd order harmonics appear at the following frequencies, as shown in Table 2.6.

Table 2.6 Frequency distribution of IMD harmonics

Harmonic order	m	n	frequencies
2	-1	1	-f1+f2
	0	2	2f2
	1	1	f1+f2
	2	0	2f1
3	-1	2	-f1+2f2
	0	3	3f2
	1	2	f1+2f2
	2	-1	2f1-f2
	2	1	2f1+f2
	3	0	3f1

Now consider the input signal has bandwidth Δf, as shown in Figure 2.13. At the output of the nonlinear system, some of the 3rd order intermodulation distortion harmonics (IMD3) creates inband interference. Therefore, IMD3 can affect the performance of a RoF even if it is operating in the single-service mode. Thus, IMD3 becomes one of the most significant nonlinearity factors needs to be considered in the RoF link design.

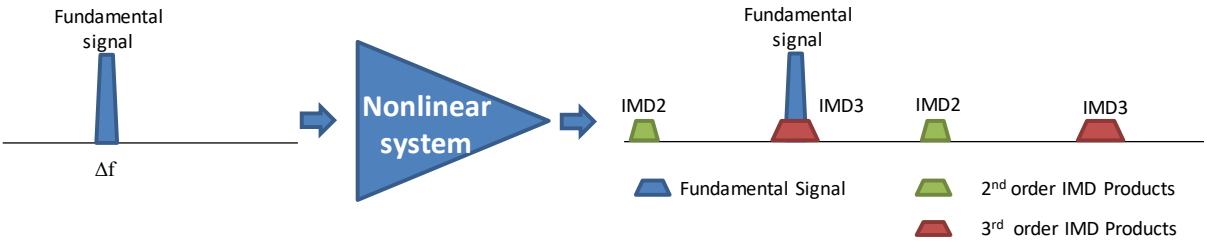

Figure 2.13 Passband signal going through a nonlinear system

However, the 2nd order intermodulation distortion harmonics do not overlap with the fundamental signal and can be filtered out. If filters have been properly installed, the IMD2 does not influence the performance of a single service RoF link. On the other hand, if multiple

services need to be supported in the RoF link, the 2nd order harmonics of one service can overlap with the frequency bands of the other services.

As many RoF systems are designed for multiple-service operation, the linearity requirements need to be satisfied in a wide range of frequencies [60].

B. nth order interception point and SFDR

The nth order intermodulation distortion (IMDn) product of an RoF link can be estimated by nth order interception point (IPn) and nth order spurious-free dynamic range (SFDRn). The nth order interception point determines the system's nth order nonlinearity, and the SFDRn takes both the nonlinearity and system signal to noise ratio (SNR) into account.

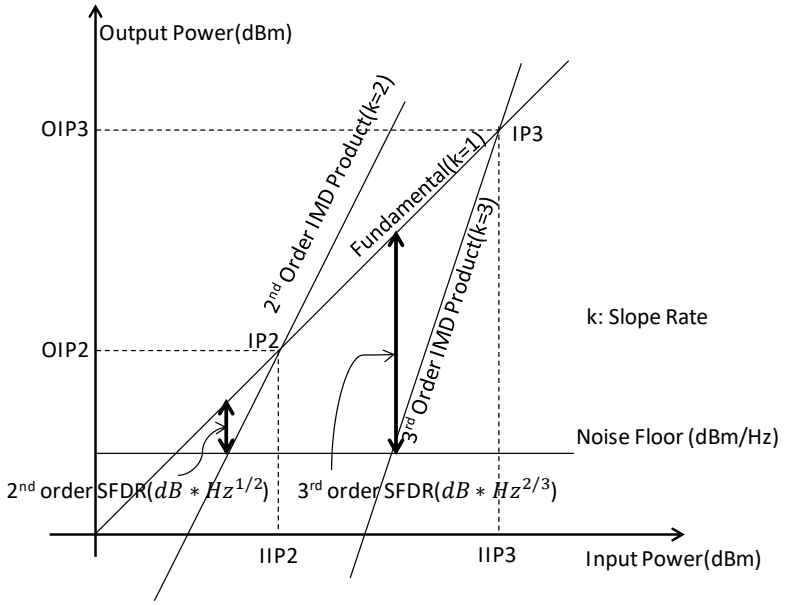

Figure 2.14 nth order IMD, IIP, OIP and SFDR

Figure 2.14 shows a plot of the output power vs input power in log scale. The output power of the fundamental signal and nth order IMD product increase proportionally with input signal power, and the slope rate (k) equals to the order numbers. For example, the slop rate for the 3rd order IMD product is equal to 3.

IPn is defined as the crossing point between the n^{th} order IMD product curve and the fundamental signal power curve. IIPn and OIPn are respectively defined as the input power and the output power at the n^{th} order interception point.

SFDRn is defined as the power difference between the fundamental signal and the n^{th} order IMD product when the power of the n^{th} order IMD product equals to system output noise floor (per Hz).

2.5 State-of-the-Arts of MIMO-enabled RoF System

2.5.1 Interleaved MIMO DAS and co-located MIMO DAS

The MIMO DAS can be broadly categorised into interleaved MIMO DAS and co-located MIMO DAS. The interleaved DAS (Figure 2.15(a)) separates MIMO antennas by relatively large distance (at least a few metres), and each of the MIMO antennas work with each other. The MIMO services can achieve nearly full MIMO performance at the overlapped areas among MIMO antennas [61]. The Co-located MIMO DAS (Figure 2.15(b)), on the other hand, place MIMO antenna from each channel at every RAU, so that MIMO service can be achieved in all signal coverage areas.

Because there is only one signal channel to be transmitted to the interleaved MIMO DAS RAUs, while there are multiple MIMO signal channels to be transmitted to the co-located DAS RAU, the interleaved DAS has relatively lower cost than the co-located DAS. However, previous research [62, 63] have shown that the co-located MIMO DAS has better QoS than interleaved DAS. Practically, the co-located MIMO DAS can offer better MIMO signal coverage than the interleaved DAS. Moreover, in the future mobile wireless network, large scale MIMO is desirable to provide users with large capacity [64]. It is meaningful to investigate the methods to deliver MIMO signals over co-located DAS. Therefore, the co-located DAS is the structure we discuss in this thesis.

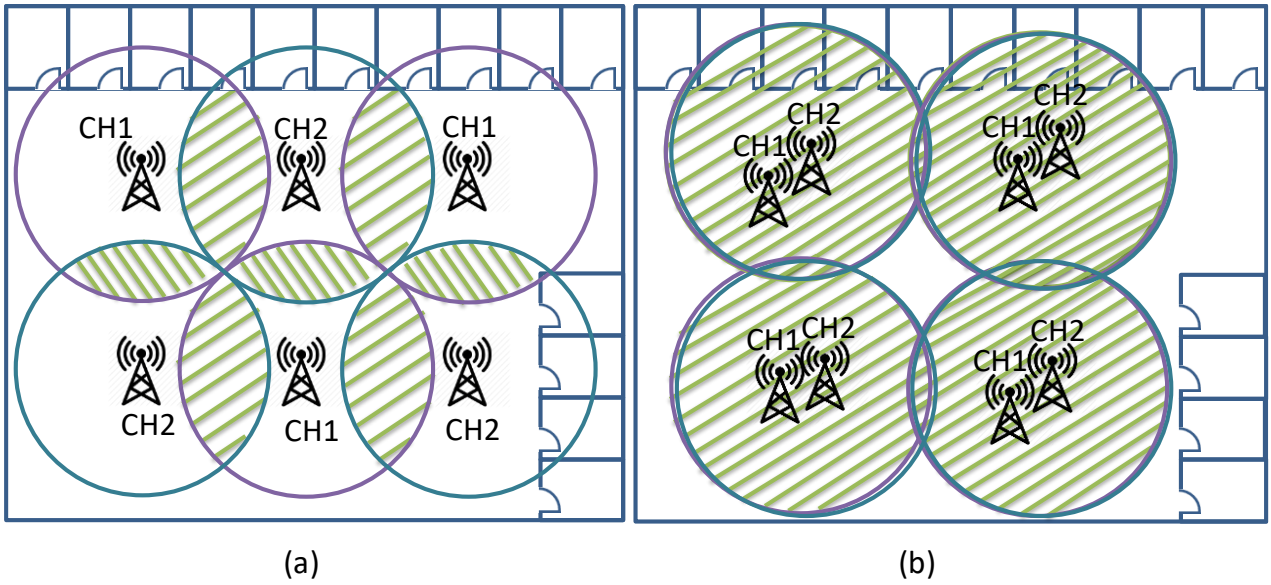

Figure 2.15 Interleaved 2x2 MIMO DAS and co-located 2x2 MIMO DAS

(green lines indicate MIMO coverage areas)

2.5.2 Multiplexing Schemes

As MIMO signal channels overlap in the frequency domain, a multiplexing scheme is required to transmit them together. A straightforward solution to tackle the problem is to install as many optical fibres as the number of MIMO channels (spatial multiplexing), as mentioned in Section 2.4. However, this leads to high optical component and fibre installation cost.

Some solutions, including wavelength division multiplexing (WDM) [65], subcarrier multiplexing (SCM) [66] and mode division multiplexing (MDM) [67], are capable of transmitting MIMO signals over a single optical fibre. However, they can be expensive and complicated to implement.

In a WDM system, as shown in Figure 2.16, an optical source and photodetector are required for each MIMO channel. And additional optical multiplexer and demultiplexers have to be used to combine and separate each of the lightwave channels [68, 69].

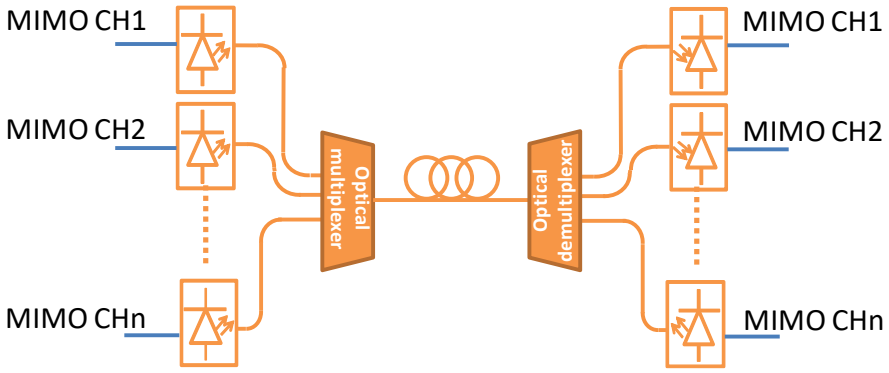

Figure 2.16 Typical Layout for a WDM RoF system

In an SCM system [66], as shown in Figure 2.17, each of the MIMO channels is shifted into different frequency bands by local oscillators (LO) and mixers. n-1 LOs are required for n MIMO signal channels.

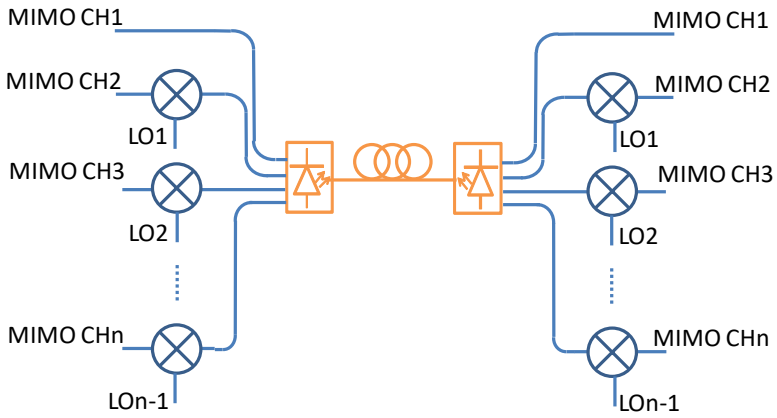

Figure 2.17 Typical layout of an SCM RoF system

In other words, the number of optical or electrical components increases linearly with the number of MIMO signal channels in WDM systems and SCM systems. In an MDM system, an expensive spatial light modulator is required.

Digital time division multiplexing (TDM) can also be a potential solution. However, here radio frequency signals need to be digital before transmission and this requires high-speed digital signal processing modules, which add cost and significant power consumption. Although some

research has been done on lowering the digital RoF bit rate [70], the high-cost components, such as analogue-to-digital and digital-to-analogue converters, are unavoidable.

To reduce the cost of MIMO-enabled RoF system, two alternative analogue RoF systems using double sideband (DSB) frequency translation [71] and single sideband (SSB) frequency translation [72] techniques have been proposed by researchers. The operating principle of these two systems is similar to a traditional SCM system, but here two MIMO channels share the same LO so that the number of LOs can be halved. However, in [71] and [72], the authors find that the DSB system does not have such good performance as the SSB system and cannot work when the upper band and the lower band of the translated signal are widely separated. Moreover, a narrow band notch filter is required in the DSB frequency translation system which results in the system only carry a single service.

Some researchers have improved the SSB system to support multiple services by translating signals to different bands [73] and lower its cost using directly modulated lasers and MMF [74, 75, 76]. However, due to the filtering process required by the SSB frequency translation system, it unavoidably wastes the power of one of the upper sideband and the lower sideband of the signal, and it requires many filters at the basestation side and the RAU side of the system.

There are also researchers working on low-cost MDM systems [67], WDM systems [65], as well as polarisation-multiplexing systems [77]. Although all these systems can support multiple-service, none of them is likely to fundamentally be lower cost than the system using frequency translation technique.

Some of the previous literatures about the multiplexing schemes for the MIMO-RoF have been shown in Table 2.7.

Table 2.7 Previous researches in commercial analogue MIMO-enabled RoF systems

Year	Technique	Transmitted Signals	Carrier Frequency	Channel bandwidth or throughput or data rate	Fibre	Limitations	Ref
2008	DSB Freq Translation, Direct Mod	PRBS, QAM16, 3×3	2.4GHz	1 MSymb/s	SMF 2.2km	Cannot multiple services, narrow band filter	[71]
2010	SSB Freq Translation, Direct Mod	PRBS, QAM16, 3×3	2.44GHz	11 MSymb/s	MMF 550m	Power of lower sideband is lost	[72]
2010	SSB Freq Translation, External Mod	PRBS, AM, 3×3	0.5GHz-3GHz & 60 GHz	100Mb/s	SMF 10km	Power of lower sideband is lost	[73]
2011	WDM-PON, VCSEL, Direct Mod	PRBS, QAM4, 2×2	5.6GHz	198.5Mb/s	SMF 20km	High cost	[75]
2012	WDM, Direct Mod	802.11n, 2×2	2.4GHz	~15 Mbit/s for single channel to ~22 Mbit/s max for MIMO	MMF 5.4km	High cost	[76]
2013	SSB Freq Translation, Direct Mod	802.11n, 2×3	2.4 GHz	~22 Mbit/s	MMF 100m	Power of upper sideband is lost	[74]
2014	MDM	802.11n, 3×3	2.4GHz	20MHz channel, 43.3Mbps	MMF 30m	High cost	[78]
2014	Polarization-Multiplex	LTE-A, 2×2	0.8GHz, 2.6GHz	10MHz, 20MHz channel	SMF 10km-50km	High cost	[77]
2016	DSB Freq Translation, Direct Mod	LTE, 2×2, 802.11g,	0.7GHz & 2.4GHz	20MHz LTE channel, 54Mbps 802.11g	MMF 300m	Limited by the speed of laser, original carrier frequency cannot be very high.	[79]

2.6 Summary and Conclusion

In this chapter, we have defined the intrinsic analogue RoF link in this thesis as a directly modulated DFB laser followed by a short single mode fibre and a PIN photodiode with direct detection.

The e/o and o/e conversion gain contributes to the most to the gain of an intrinsic RoF link, which is typically -35 to -12 dB. Other performance measurement terms, such as nonlinearity and EVM are also introduced in this chapter.

By extending the intrinsic RoF link, typical layouts of an analogue SISO DAS are described in this chapter, showing that using a passive secondary DAS hub is a more cost-effective solution than the active secondary hub when the number of RAUs is <64.

Because MIMO-type signals overlap in the frequency domain, a multiplexing scheme has to be used to implement a co-located MIMO-enabled DAS. The SSB and DSB frequency translation systems are considered to be relatively low-cost solutions among state-of-the-art technologies.

Chapter 3 2x2 MIMO RoF System using DSB Frequency Translation Technique

3.1 Introduction

This chapter introduces the modelling of the SISO RoF optical link and then extends it to the SSB and the DSB MIMO RoF system. Experiments are then carried out to demonstrate the feasibility of transmitting MIMO type signals to remote units.

3.2 SISO RoF System

3.2.1.1 Basic modelling of a general cascaded system

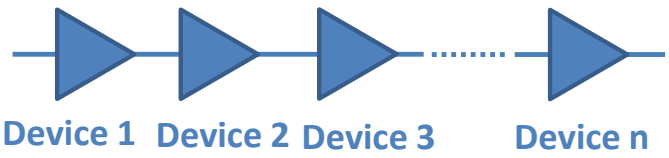

Figure 3.1 Layout for a general cascaded system

Consider a general cascaded system, as shown in Figure 3.1. The gain, noise factor and ip3 (in linear units) of a cascaded system can be expressed as below [80]:

$$g_{system} = g_1 * g_2 * \cdots * g_n \tag{3.1}$$

$$nf_{system} = nf_1 + \frac{nf_2 - 1}{g_1} + \frac{nf_3 - 1}{g_1 * g_2} + \cdots + \frac{nf_n - 1}{g_1 * g_2 * \cdots * g_{n-1}} \tag{3.2}$$

$$iip3_{system} = \left(\frac{1}{iip3_1} + \frac{g_1}{iip3_2} + \frac{g_1 g_2}{iip3_3} + \cdots + \frac{g_1 * g_2 * \cdots g_{n-1}}{iip3_n} \right)^{-1} \tag{3.3}$$

$$oip3_{system} = iip3_{system} * g_{system} \tag{3.4}$$

Assuming system input noise is the thermal noise, system output noise floor follows the equation below:

$$System\ Output\ Noise\ Floor = Thermal\ Noise * g_{system} * nf_{system} \tag{3.5}$$

The system 3rd order SFDR in dB can be expressed as below:

$$SFDR3_{System}(dB) = \frac{2}{3}\big(OIP3(dBm) - Output\ Noise\ Floor(dBm)\big) \tag{3.6}$$

To compensate the loss in a RoF link, a pre-amplifier and a post-amplifier are installed in a SISO RoF system, as shown in Figure 3.2. It can be considered as a cascaded system, in which the intrinsic RoF link has the dominant noise figure.

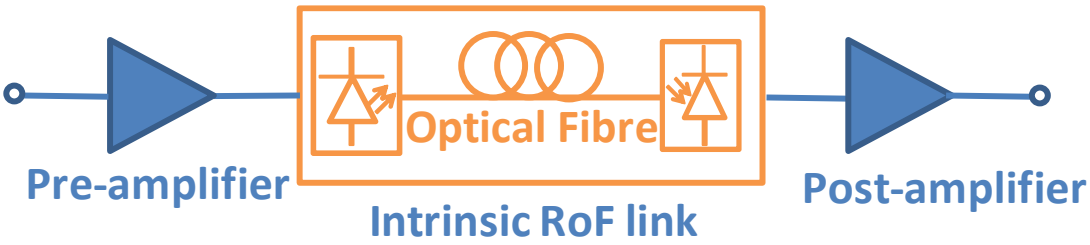

Figure 3.2 SISO RoF System

3.2.2 Pre-amplifier and post-amplifier in a SISO RoF system

A simulation has been performed to show the contributions of the pre-amplifier and the post-amplifier to the performance of the SISO RoF link. It is assumed that the intrinsic optical link

has -33dB gain, 37.5dBm IIP3 and 57.3dB noise figure. These values are the same as those in the experimental measurement as described in Section 3.2.3.

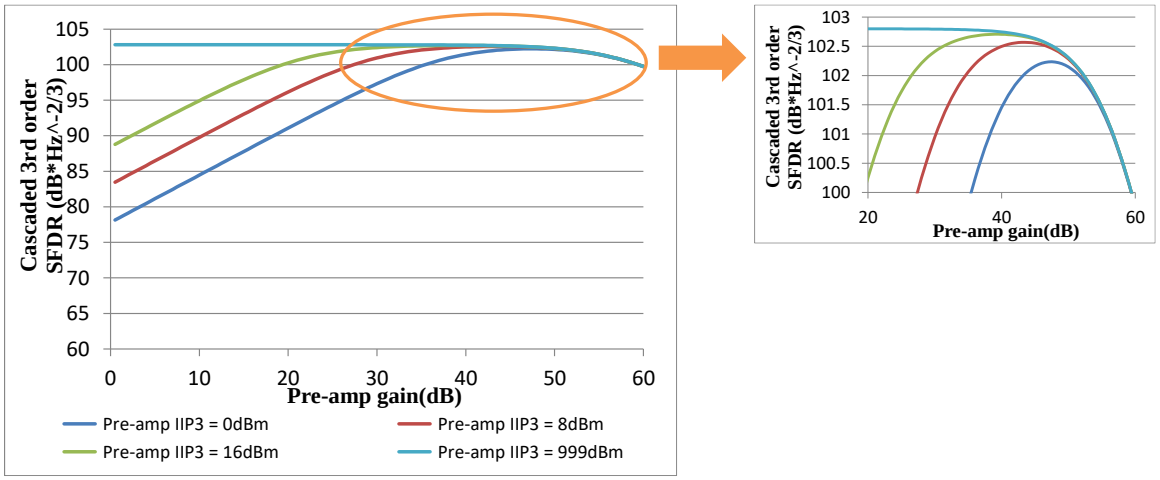

Figure 3.3 3rd order SFDR vs pre-amplifier gain for a SISO RoF system when pre-amplifier noise figure=0dB

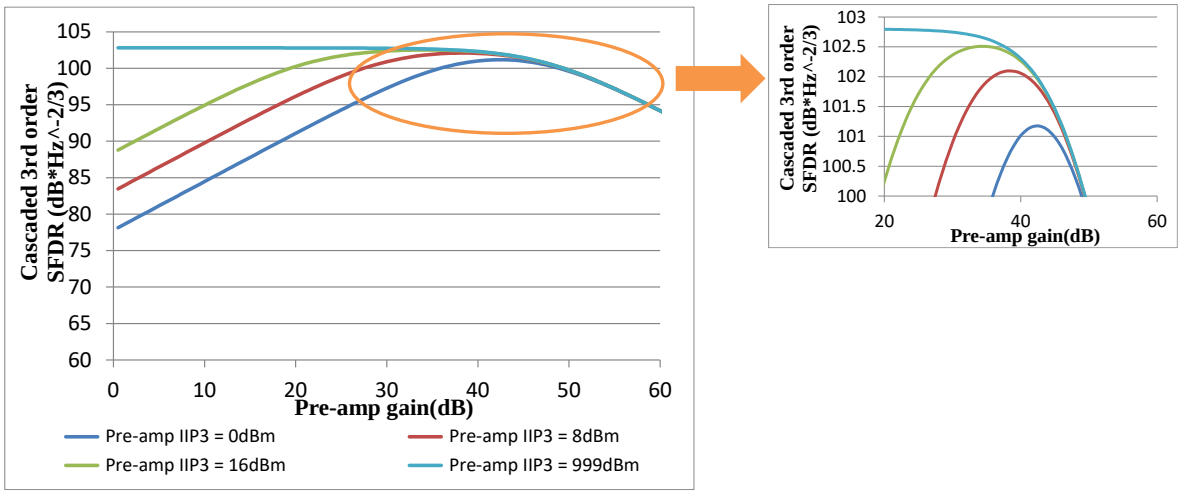

Figure 3.4 3rd order SFDR vs pre-amplifier gain for a SISO RoF system when pre-amplifier noise figure=10dB

Figure 3.3 shows the 3rd order SFDR of a SISO RoF system with different pre-amplifier gain and IIP3. The 3rd order SFDR of the intrinsic optical link used in the simulation is 102.8dB*Hz$^{-2/3}$. The system 3rd order SFDR raises with the pre-amplifier gain until it reaches the SFDR of the intrinsic optical link (without amplifier). This is because the intrinsic optical link has the dominant noise figure. When the pre-amplifier gain is higher than the optimum value, the noise

from the pre-amplifier overshoots the noise from the intrinsic optical link, and thus the system SFDR drops.

Typically, commercial RF amplifiers have IIP3>0dBm [81]. Without considering the noise figure of the pre-amplifier, the IIP3 of the pre-amplifier decreases the maximum system SFDR3 by <1dB, as shown in the zoomed-in figure in Figure 3.3.

However, if the noise figure of the pre-amplifier is considered, the pre-amplifier has a greater influence on the system maximum 3rd order SFDR as shown in Figure 3.4. In the simulation, the pre-amplifier noise figure = 10 dB, which is a typical value for a high gain RF amplifier. If a low noise amplifier is used, the noise figure can be as low as ~2 dB [82], but the bandwidth and gain can be limited. Figure 3.5 describes the influence of the pre-amplifier IIP3 and the NF on the system optimum SFDR. Both parameters lower the system optimum SFDR.

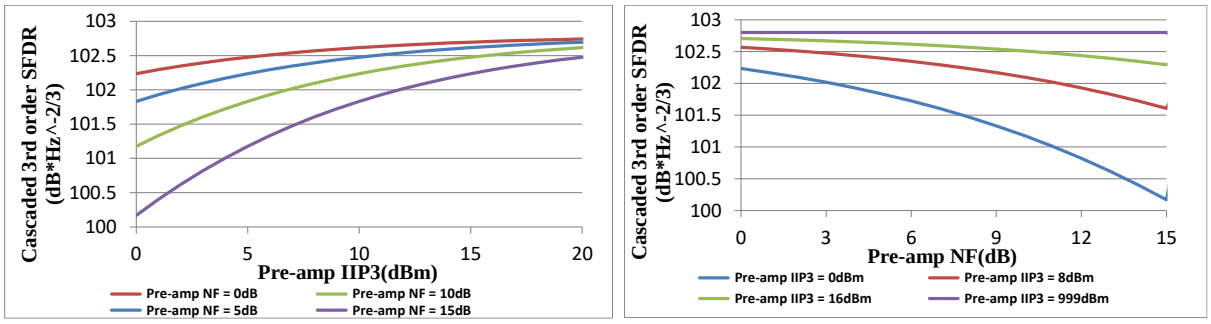

(a) (b)

Figure 3.5 Influence of the pre-amplifier on the cascaded 3rd order SFDR of a SISO RoF link: (a) cascaded SFDR3 vs Pre-amplifier IIP3; (b) cascaded SFDR3 vs pre-amplifier noise figure

Different from the pre-amplifier case, the effect of the post-amplifier nonlinearity on the system overall performance is more straightforward. As shown in Figure 3.6, the system's 3rd order SFDR does not rely on the post-amplifier gain, but increases with its IIP3 (Figure 3.7(a)) and drops with its NF (Figure 3.7(b)). Whilst the post-amplifier IIP3 plays a major role in the system SFDR3, the post-amplifiers noise figure does not significantly reduce the system's SFDR3 when it is lower than 15dB. This is because, for a component with noise figure = nf_{comp} and input noise = n_{in}, its output noise follows:

$$n_{out} = [n_{in} + n_{th}(nf_{comp} - 1)]g_{comp}$$

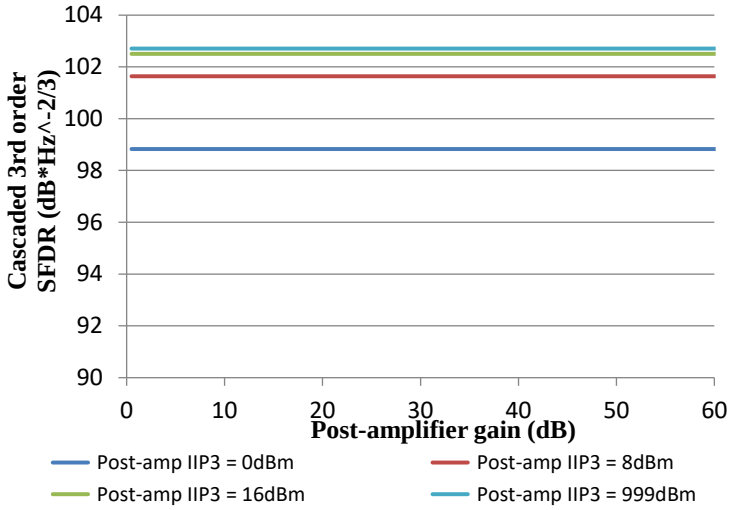

Figure 3.6 3rd order SFDR vs post-amplifier gain for a SISO RoF system when post-amplifier noise figure=10dB

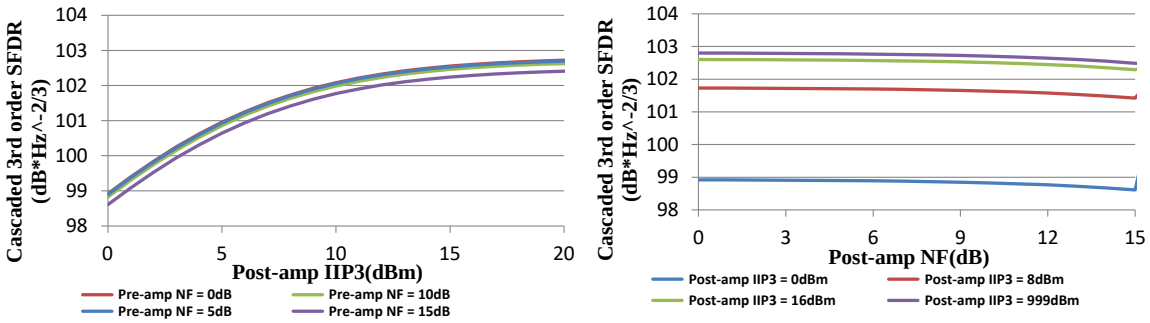

Figure 3.7 Influence of the post-amplifier on the cascaded 3rd order SFDR of a SISO RoF link: (a) cascaded SFDR3 vs post-amplifier IIP3; (b) cascaded SFDR3 vs post-amplifier noise figure

In the SISO RoF link, the input noise of the post-amplifier is much greater than the thermal noise, and therefore, its noise figure does not critically raise the system's output noise floor until it reaches a certain level (30dB in this case). Normally, the noise figure of a high gain amplifier is much smaller than 30dB.

3.2.3 Basic experimental measurements of a SISO RoF system

A. Laser diode L-I characteristic

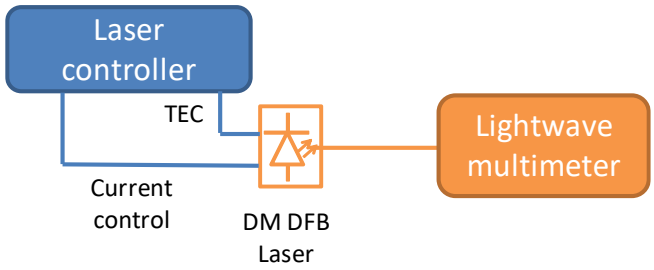

Figure 3.8 Experiment setup for laser diode L-I characteristic test

The light-current characteristic of the Mitsubishi® FU-68-PDF Direct modulated DFB laser at 20 °C has been tested using a lightwave multimeter as shown in Figure 3.8. The laser diode temperature is controlled by a thermoelectric cooler (TEC) inside the laser diode's package. In the experimental results in Figure 3.9, the slope rate for the L-I curve is ~0.2W/A. And the curve starts to be nonlinear when laser diode bias current >80 mA. The laser diode threshold current ~10 mA. Therefore, if the laser diode is biased at the ~45 mA point, the RoF link will have the best linearity performance in direct modulation. Moreover, if this laser is directly modulated, severe distortion will happen when the RF signal peak current >35 mA, which is ~15dBm in power if it is 50 ohms matched.

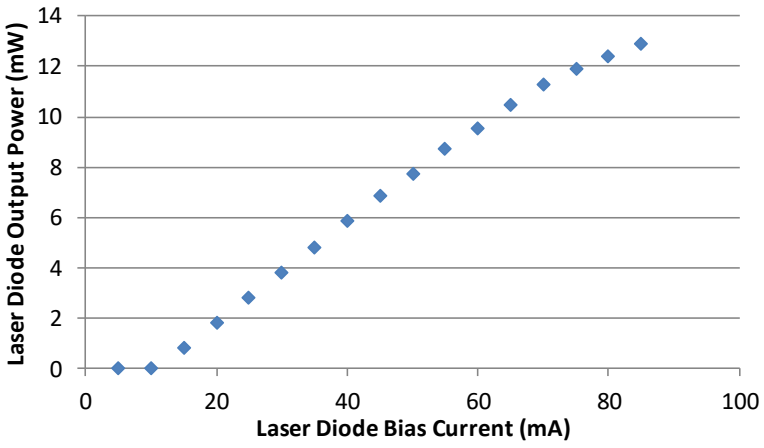

Figure 3.9 L-I characteristic of the Mitsubishi® FU-68-PDF DFB laser

B. S21 parameter of the optical link

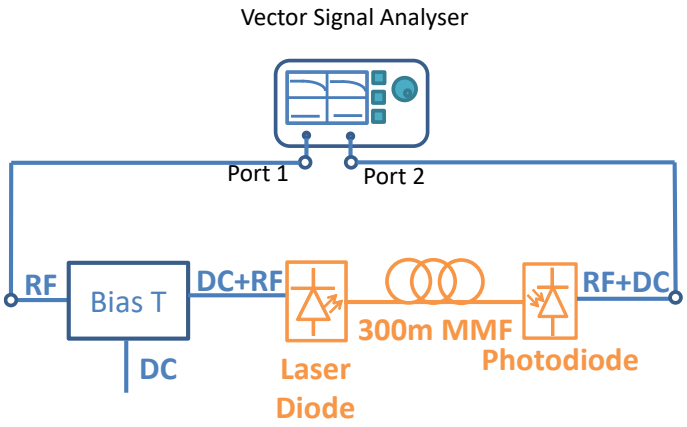

Figure 3.10 Experimental layout for 300m MMF link S21 parameter test

The S21 parameter of the 300m MMF optical link has been tested using an Anritsu® 37347A vector signal analyser (VNA), as shown in Figure 3.10. The VNA is calibrated from 40MHz to 4GHz

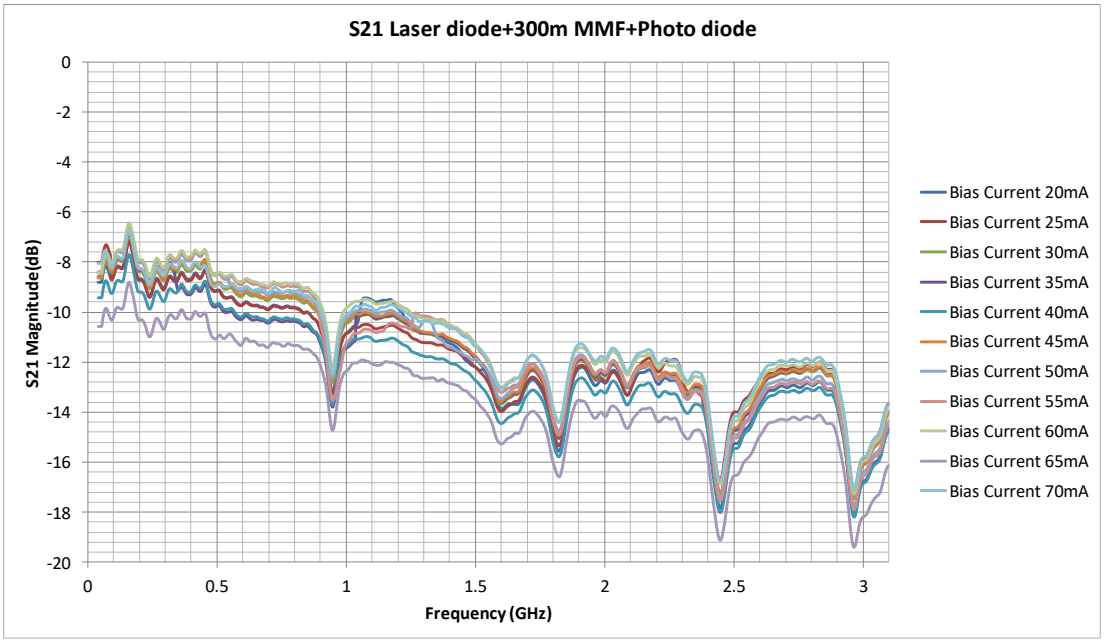

Figure 3.11 S21 amplitude-frequency response of the optical link using Mitsubishi® FU-68-PDF DFB laser

It is shown in Figure 3.11 that for the direct modulated DFB laser under test (Mitsubishi® FU-68-PDF DFB), the 6dB RF bandwidth of the optical link is ~2.5GHz. RF resonance in the laser diode package causes the dips in the plot.

C. SFDR

The 3rd order SFDR of the system can be measured by the two-tone test (Figure 3.12). Two signal generators generate two sine waves with respectively 800MHz and 801MHz carrier frequencies. A power coupler then combines signals from two signal generators, and the comobined signals are directly modulated to a DFB laser. The power of the fundamental tones and 3rd order tones at the output of the intrinsic optical link have been measured using a spectrum analyser, as plotted in Figure 3.13. The interception point between the fundamental tone and the 3rd order harmonics (IP3) shows the optical link has 37.5dBm IIP3 and 8dBm OIP3. The output noise floor of the optical link is measured -145dBm/Hz. Therefore, the 3rd order SFDR can be calculated using equation (3.6): 102dBm/Hz$^{2/3}$.

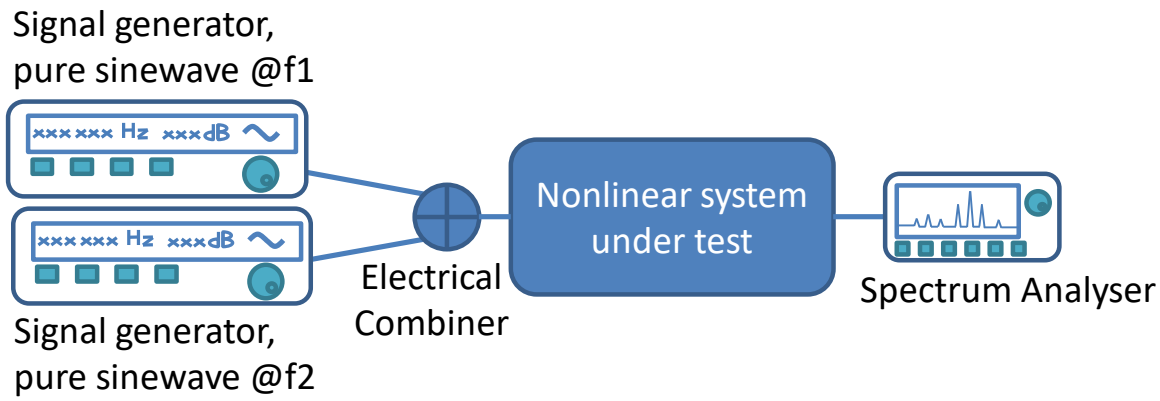

Figure 3.12 General layout of the two-tone test to measure the SFDR of a nonlinear system

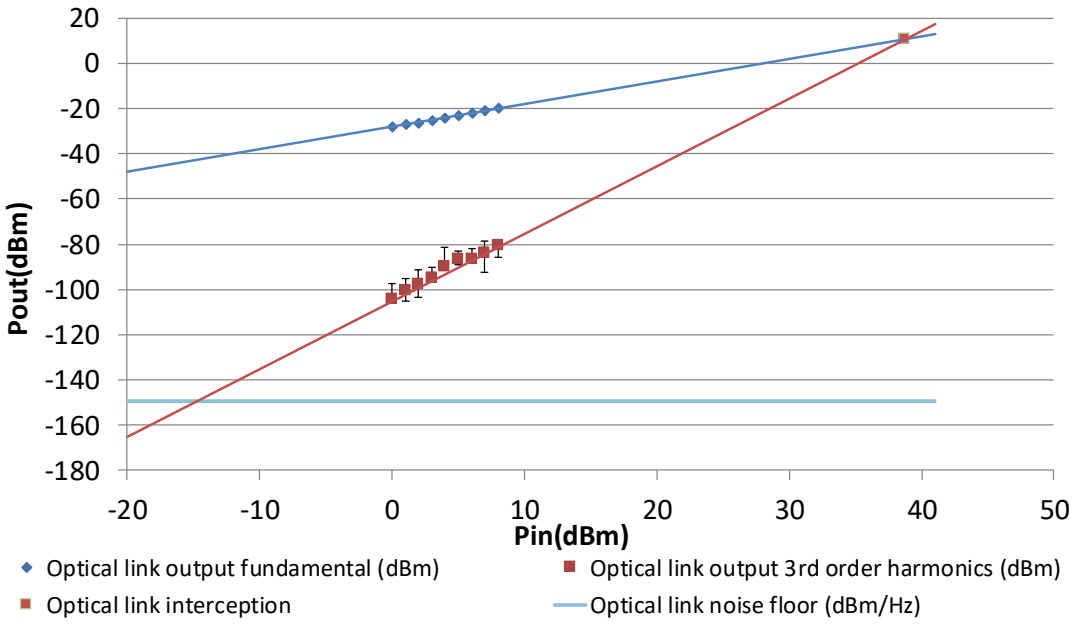

Figure 3.13 3rd order SFDR test result for intrinsic optical link

3.3 Modelling of SSB and DSB MIMO-enabled RoF System

The single sideband (SSB) and double sideband (DSB) frequency translation systems convert original MIMO signals into different electrical sidebands as shown in Figure 3.14 and Figure 3.15. The two MIMO channels share the same local oscillator. Therefore, half the number of local oscillators are required than the number of channels. In both systems, the local oscillator translates the original MIMO signals into upper and lower sidebands, respectively at $f_{low} = |f_{LO} - f_c|$ and $f_{up} = f_{LO} + f_c$.

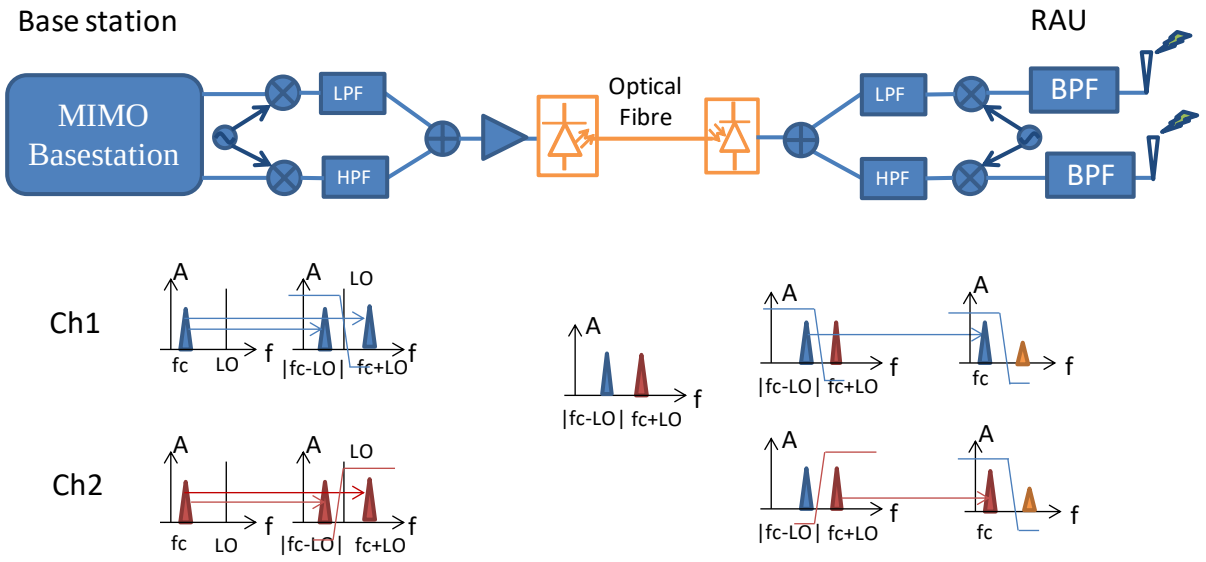

Figure 3.14 Schematic of a single sideband frequency translation system for 2x2 MIMO RoF [72]

In an SSB frequency translation system, one of the sidebands of each MIMO channel is filtered out. As shown in Figure 3.14, after the mixers, the upper sideband of channel 1 has been filtered out, while the lower sideband of channel 2 has been filtered. Both channels are then combined by an electrical coupler and transmitted through the optical link. Each of sidebands contains the information from only one of the MIMO channels. At the RAU side, another pair of low pass/high pass filters is required to de-multiplex the MIMO signals.

In a DSB frequency translation system, as illustrated in Figure 3.15, each of the MIMO channels is mixed with the same local oscillator frequency, but with a 90-degree phase shift. Therefore, both MIMO channels can be multiplexed with each other in quadrature and power in both sidebands can be kept. Two pairs of high-pass and low-pass filters at the base station and RAU sides are avoided.

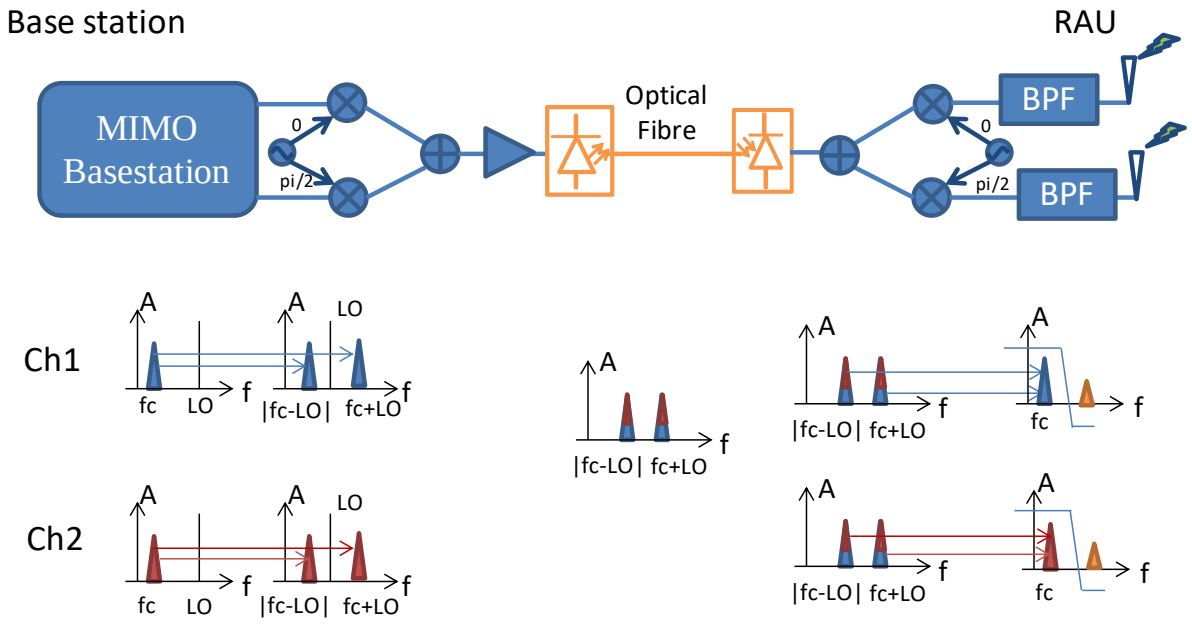

Figure 3.15 Schematic of a double sideband frequency translation system for 2x2 MIMO RoF [71]

3.3.1 Third order SFDR of the SSB and the DSB frequency translation system

Different from the SISO RoF link, the SSB and DSB frequency translation system involves RF mixers, which usually have poor IIP3 and high conversion loss. For example, the frequency mixer used in the experiment and simulation has ~25dBm IIP3 and ~8dB conversion loss. This will influence the system's overall performance.

In the SSB frequency translation system, if the input noise of the mixer is thermal noise, the noise figure of a mixer equals to its conversion loss. In a DSB frequency translation system, at the RAU side, when the mixer translates upper and lower sidebands back to the original frequency, the signal power adds coherently but the noise power adds in-coherently, giving the DSB system higher SNR than the SSB system (if two systems use the same optical link and the same pre-amplifier).

Simulations have been performed in spreadsheet model by calculating the link power budget as shown in Figure 3.16. Detailed mathematical theory will be described in Chapter 5.

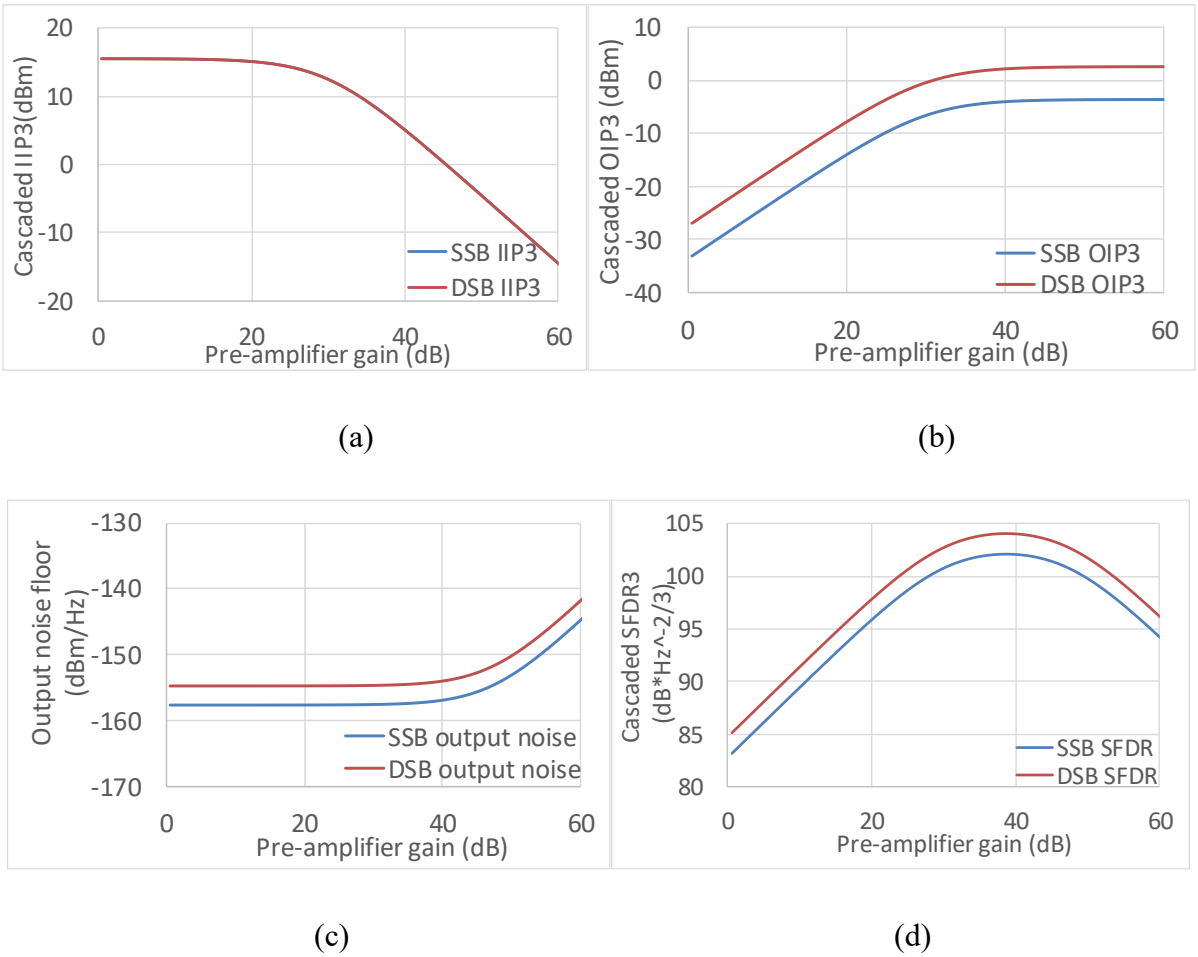

Figure 3.16 Simulation results comparing DSB with SSB frequency translation system: (a)IIP3; (b) OIP3; (c)output noise floor; (d) 3rd order SFDR.

The SSB and DSB system have the same IIP3 (Figure 3.16(a)). However, as the double sideband system uses the power from both sidebands, its OIP3 is 6dB higher than the SSB system (Figure 3.16(b)). In the DSB system, the noise from both sidebands adds in-coherently, thus the output noise floor is 3dB higher than the SSB system (Figure 3.16(c)).

Thus, overall, the DSB system has 2/3*(6dB-3dB) = 2dB higher 3rd order SFDR than the SSB system (Figure 3.16 (d)). This property makes the DSB system's dynamic range superior to the SSB system and means that the optical bandwidth can be traded for the electrical SFDR.

3.3.2 Crosstalk in the DSB frequency translation system

Two major factors contribute to the crosstalk between the two MIMO channels in a DSB frequency translation system – phase error of the 90-degree hybrid coupler and the amplitude imbalance between the upper sideband and the lower sideband.

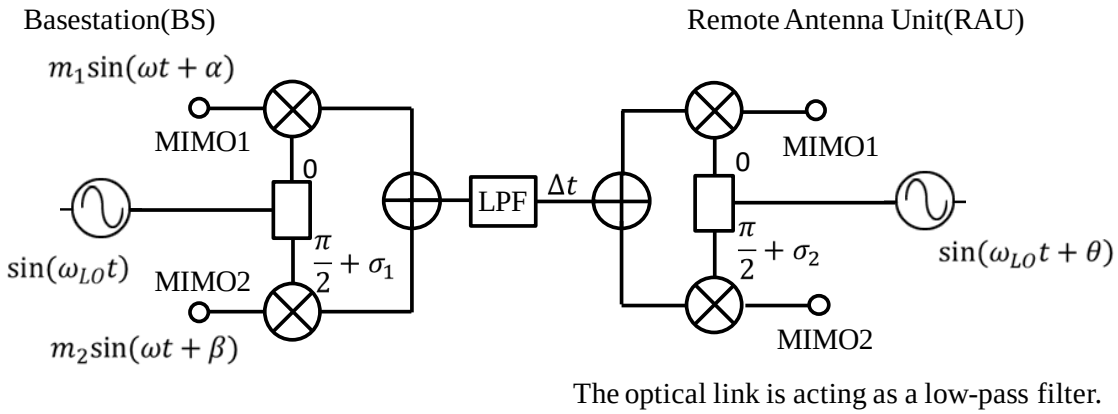

Figure 3.17 Schematic of the model of MIMO-enabled RoF system using DSB frequency translation.

To simplify the model, we model the optical link as a low-pass filter and time delay (Δt), as shown in Figure 3.17. Assuming there are two MIMO channels, they respectively contain information m_1 and m_2. And they are modulated to the same carrier angle frequency ω, but the initial phases are different – respectively α and β. The 90-degree hybrid couplers have σ_1 and σ_2 phase error. The local oscillators at the basestation side and the RAU side are not synchronised and they have phase difference θ, but with the same angle frequency θ. It is assumed that the phase of the local oscillator at the BS side is the reference phase.

The multiplexing and de-multiplexing process can be expressed as the equations shown below:

$$\begin{aligned} M_{mux} &= m_1 \sin(\omega t+\alpha)\sin(\omega_{LO}t) + m_2 \sin(\omega t+\beta)\cos(\omega_{LO}t+\sigma_1) \\ &= M_{pre,\omega-\omega_{LO}}(t) + M_{pre,\omega+\omega_{LO}}(t) \end{aligned} \tag{3.7}$$

in which,

$$M_{pre,\omega-\omega_{LO}}(\mathrm{t}) = \frac{1}{2}\{m_1 \cos[(\omega-\omega_{LO})t+\alpha] + m_2 \sin[(\omega-\omega_{LO})t+\beta-\sigma_1]\} \quad (3.8)$$

$$M_{pre,\omega+\omega_{LO}}(t) = \frac{1}{2}\{-m_1 \cos[(\omega+\omega_{LO})t+\alpha] + m_2 \sin[(\omega+\omega_{LO})t+\beta+\sigma_1]\} \quad (3.9)$$

After the RoF link,

$$M_{post,\omega-\omega_{LO}}(\mathrm{t}) = G_{\omega-\omega_{LO}} M_{pre,\omega-\omega_{LO}}(\mathrm{t}+\Delta\mathrm{t}) \quad (3.10)$$

$$M_{post,\omega+\omega_{LO}}(\mathrm{t}) = G_{\omega+\omega_{LO}} M_{pre,\omega+\omega_{LO}}(\mathrm{t}+\Delta\mathrm{t}) \quad (3.11)$$

then, the de-multiplexed signal,

$$M_{demux1} = \left[M_{post,\omega-\omega_{LO}}(\mathrm{t}) + M_{post,\omega+\omega_{LO}}(\mathrm{t})\right] \cdot \sin(\omega_{LO}\mathrm{t}+\theta) \quad (3.12)$$

$$M_{demux2} = \left[M_{post,\omega-\omega_{LO}}(\mathrm{t}) + M_{post,\omega+\omega_{LO}}(\mathrm{t}) \cdot \cos(\omega_{LO}\mathrm{t}+\theta+\sigma_2)\right] \quad (3.13)$$

Considering only the components at ω in channel 1,

$$M_{demux1} = M_{signal1} + M_{crosstalk1} \quad (3.14)$$

$$M_{signal1} = \frac{m_1 G_{\omega-\omega_{LO}}}{4}\sin(\omega t+\alpha+\delta_1+\theta) + \frac{m_1 G_{\omega+\omega_{LO}}}{4}\sin(\omega t+\alpha+\delta_2-\theta) \quad (3.15)$$

$$M_{crosstalk1} = -\frac{m_2 G_{\omega-\omega_{LO}}}{4}\cos(\omega t+\beta-\sigma_1+\delta_1+\theta) + \frac{m_2 G_{\omega+\omega_{LO}}}{4}\cos(\omega t+\beta+\sigma_1+\delta_2-\theta) \quad (3.16)$$

If no crosstalk, $M_{crosstalk1} = 0$. Then,

$$G_{\omega-\omega_{LO}} = G_{\omega+\omega_{LO}} \quad (3.17)$$

and

$$\beta-\sigma_1+\delta_1+\theta = \beta+\sigma_1+\delta_2-\theta+2n\pi \quad (3.18)$$

(3.18) can be rearranged into:

$$\theta = \sigma_1 + \omega_{LO}\Delta t + n \tag{3.19}$$

Similarly, if we consider channel 2, when no crosstalk,

$$\theta = \omega_{LO}\Delta t - \sigma_2 + n\pi \tag{3.20}$$

and $G_{\omega-\omega_{LO}} = G_{\omega+\omega_{LO}}$

All the symbols used from (3.7) to (3.20) are shown in

Table 3.1 Symbols used from (3.7) to (3.20)

Symbol	Quantity
$\mathbf{m_1, m_2}$	Message contained in MIMO channel 1 and channel 2
$\boldsymbol{\omega}$	Angle frequency of MIMO signals
$\boldsymbol{\omega_{LO}}$	Angle frequency of LO signal
$\boldsymbol{\alpha, \beta}$	Initial phase of MIMO channel 1 and channel 2 signal
$\boldsymbol{\sigma_1, \sigma_2}$	Phase error of the 90-degree splitter at the BS and the RAU side
$\boldsymbol{\theta}$	Phase difference between two LOs
$\boldsymbol{\Delta t}$	Delay time between the BS side and RAU side
$\boldsymbol{\delta_1, \delta_2}$	Respectively $(\omega - \omega_{LO})\Delta t$ and $(\omega + \omega_{LO})\Delta t$
$\mathbf{M_{mux}}$	Multiplexed signal, before the laser, but after the power combiner at the BS side.
$\mathbf{M_{pre,\omega\pm\omega_{LO}}}$	Frequency component at $\omega \pm \omega_{LO}$ of M_{mux}
$\mathbf{M_{post,\omega\pm\omega_{LO}}}$	Frequency component at $\omega \pm \omega_{LO}$ of the signal after the optical link (low-pass filter)

$\mathbf{G_{\omega\pm\omega_{LO}}}$	Gain of the optical link (low-pass filter) at $\omega \pm \omega_{LO}$
$\mathbf{M_{demux1}}$	De-multiplexed signal of channel 1 and channel 2 after the frequency mixer at RAU side
$\mathbf{M_{signal1}}$	Effective signal contained in M_{demux1}
$\mathbf{M_{crosstalk1}}$	Crosstalk contained in M_{demux1}

Equations (3.17) to (3.20) show that three major factors contribute to the crosstalk: (i) phase mismatch caused by the microwave transmission time (Δt); (ii) phase error of the 90-degree hybrid couplers (σ_1, σ_2); (iii) amplitude imbalance between two bands ($G_{\omega-\omega_{LO}}, G_{\omega+\omega_{LO}}$). To eliminate the crosstalk between two channels, Equations (3.17) to (3.20) have to be satisfied.

Due to the group delay of the link (Δt), the upper band and the lower bands arrive at the frequency mixers with different phases ($\delta_1$and δ_2). If there is no phase error in the 90-degree hybrid couplers ($\sigma_1 = 0, \sigma_2 = 0$), the effect of $\delta_1$and δ_2 can be eliminated by adjusting the phase difference between the mux and demux LOs via a delay line, which sets the value of $\theta = \omega_{LO}\Delta t + n\pi$.

However, if there is a phase error in the 90-degree hybrid couplers, Equation (3.19) and (3.20) can never be fully satisfied at the same time, and this becomes one of the major factors which results in the system crosstalk.

The amplitude imbalance between the upper band and the lower band is another important factor that causes crosstalk. As shown in equation (3.17), when the signals are demultiplexed at the RAU side, the signal from the unwanted channel has to be cancelled which requires that the two sidebands of the DSB signal have the same amplitude.

The simulation results in Figure 3.18 show the crosstalk caused by the phase error of the 90-degree hybrid coupler and the amplitude imbalance between two frequency bands. Typically, the phase error of a 90-degree hybrid coupler can be within 2°, but the amplitude imbalance of

the two sidebands caused by the variation in the S21 frequency response of the optical link can be >1dB.

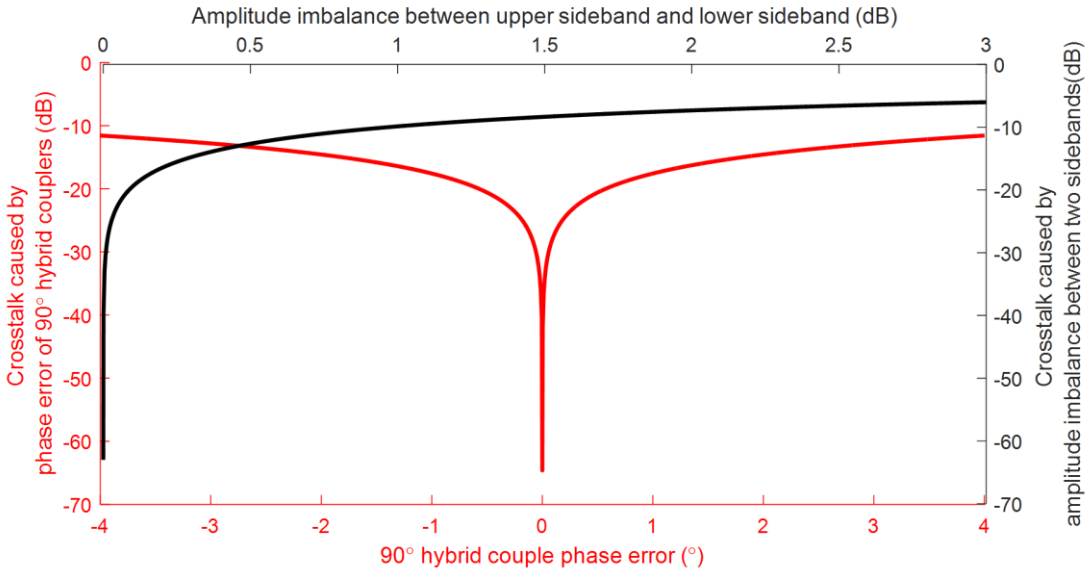

Figure 3.18 Simulation of the crosstalk caused by the phase error of 90-degree hybrid couplers, and amplitude imbalance between two sidebands.

3.3.3 EVM simulation for a DSB frequency translation system

A simulation is performed to show the EVM performance of a DSB frequency translation system in VPItransmissionMaker® as shown in Figure 3.19. Two channels each of 20MHz bandwidth 64QAM signal at 800MHz carrier bandwidth have been used at the input of the system. The input signal power is -20dBm. The mixer is modelled as an ideal multiplier followed by a nonlinear component, whose IIP3 has been defined the same as the mixer used in the experiment. An attenuator represents the mixers' conversion loss. The phase error of the 90-degree hybrid coupler is <2°, which is a typical value for a commercial product [83]. The optical link used in the simulation consists of a direct modulated DFB laser and a PIN photodiode. The optical fibre is a 300m MMF.

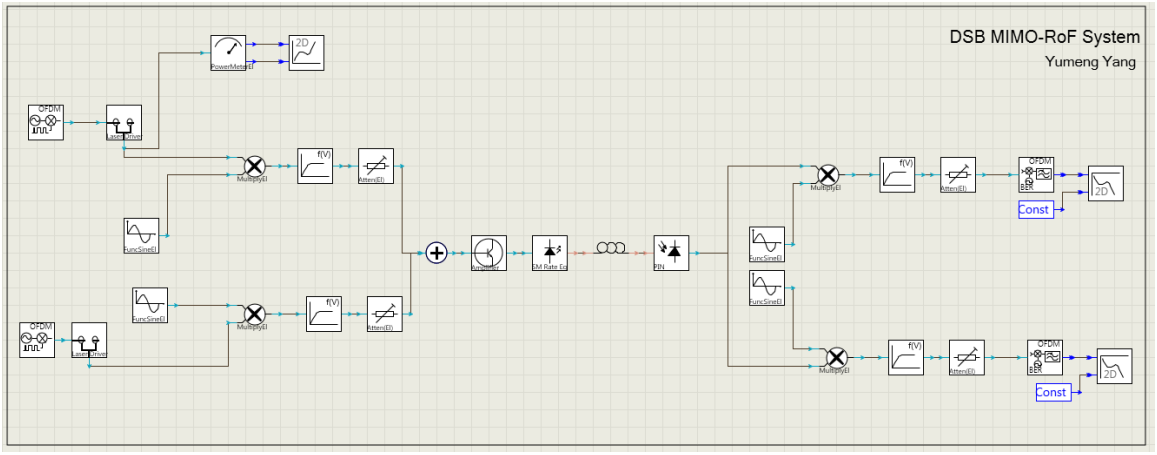

Figure 3.19 Simulation layout for 2x2 DSB MIMO RoF system in VPItranmissionMaker®

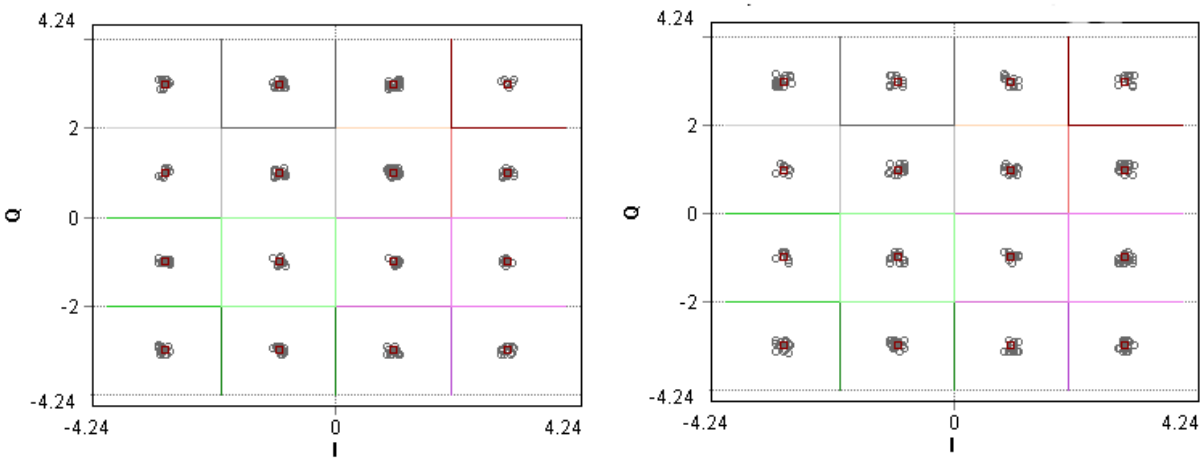

Figure 3.20 Simulation result: constellation diagram of two channels of 64QAM 20MHz BW signal transmitted over 300m MMF link using DSB frequency translation. Left: channel 1 EVM=3.1%; right: channel 2 EVM = 3.8%

The model has included the noise and the crosstalk in the system. The constellation diagrams of two channels at the receiving ends are shown in Figure 3.20. It can be seen that the signals from both channels can be demodulated and EVM is around ~3.5%.

3.4 Experiments for MIMO-enabled RoF using DSB frequency translation

3.4.1 Experimental Setup

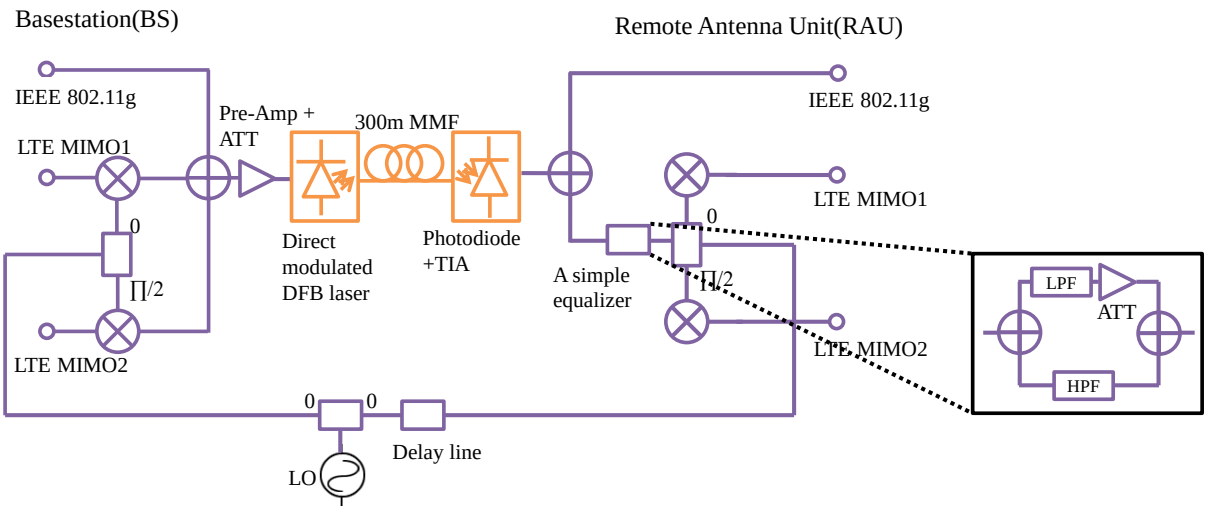

Figure 3.21 Experimental layout of MIMO-enabled RoF system using DSB frequency translation technique (local oscillator frequency = 2.2GHz and LTE carrier frequency = 800MHz).

Figure 3.21 shows the experimental layout of the MIMO-enabled RoF system using the DSB frequency translation technique. At the BS side two MIMO signal channels are mixed using the same local oscillator but with a 90° phase difference. In order to show the multi-service operation of the system, the mixed signals are summed with an independent IEEE 802.11g signal by a power combiner and then directly modulated onto a DFB laser (3dB RF bandwidth=2GHz), emitting at 1550 nm. In most of the building backbones, the MMF is a commonly pre-installed type of optical fibre for Ethernet communication [84]. Making use of the existing MMFs to transmit base station signals to each RAU can be a cost-effective way to build a DAS. Here, we use a 300m length of MMF in the optical link, because it is a typical length for the in-building wireless signal coverage.

At the RAU side, after the photodiode, followed by a trans-impedance amplifier (TIA), a simple equaliser is used to equalise the amplitude of the upper band and the lower band of the mixed

signals. Here, the filters in the equaliser also prevent the leakage of IEEE 802.11g signal to the frequency mixers. Following the equaliser, a symmetry layout as the transmitting side is used to de-multiplex the MIMO signals.

In this experiment, the BS side and the RAU side share the same LO to save one test device. In reality, there should be two phase-locked LOs, one for each side of the link. To show the difference between two LOs and to provide the necessary phase shift (θ, explained in Section 3.3.2), a delay line is used.

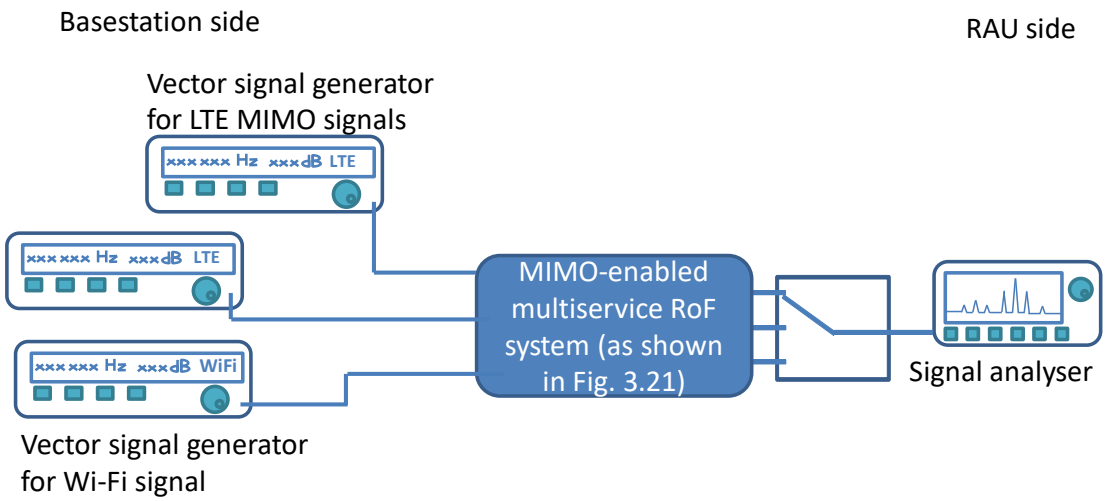

Figure 3.22 EVM test layout for MIMO-enabled multi-service RoF system

Figure 3.22 shows the experimental layout for the EVM test. Rohde & Schwarz® vector signal generators and an Anritsu® signal generator are used to generate two channels of LTE signals (centred at 700MHz) and a channel of an IEEE 802.11g signal (centred at 2.4GHz). A Rohde & Schwarz® vector signal analyser is used to analyse the de-multiplexed LTE MIMO signals and received Wi-Fi signal at the RAU side separately. MIMO processing, which can lower the EVM by doing EVM compensation, is not used. The system is tested for 5MHz, 10MHz and 20MHz LTE channel bandwidths.

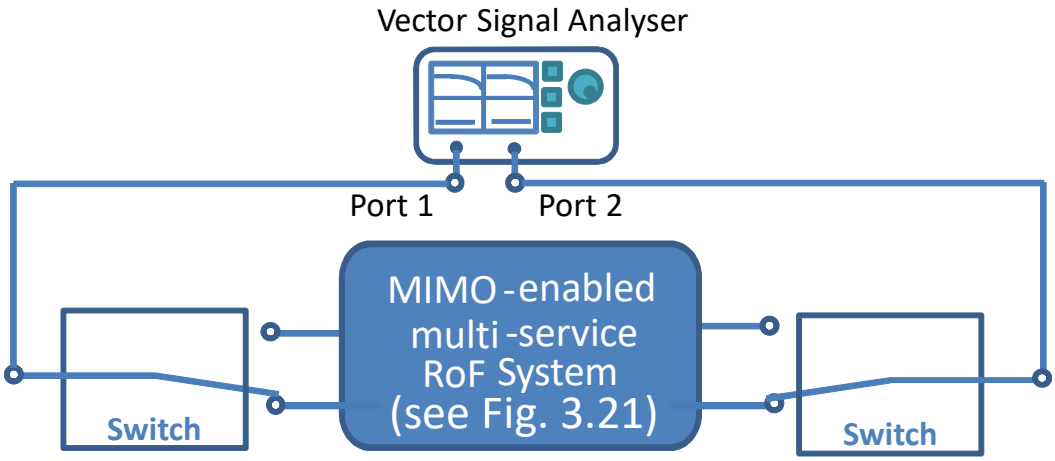

Figure 3.23 Experimental setup for condition number test.

The experimental setup for condition number measurement is shown in Figure 3.23. A vector network analyser (VNA) is scanning from 600MHz to 1GHz, and 1600 points are taken in this range. The S21 parameters are logged to measure each element of the channel matrix individually.

3.4.2 Experimental Results

A. 2×2 LTE along with IEEE 802.11g over RoF Link Test

The system is tested using LTE channels at a 700MHz carrier frequency, and 3MHz, 10MHz and 20MHz channel bandwidths. In the experiment, two LTE channels are independently transmitted over 300m OM1 MMF using a temperature controlled DFB laser (RF bandwidth=2GHz). Due to limitations of the test and measurement equipment, the EVM of each channel can only be measured independently, meaning that the recorded results are pessimistic compared to a full MIMO EVM since MIMO processing compensation is not employed. Figure 3.24 shows EVM vs carrier frequency curves and constellation diagrams. The average EVM measurement for 3MHz, 10 MHz and 20 MHz channel bandwidths are respectively 1.7%, 2.3% and 5.1%. These values are well within the 8% EVM requirement for

64QAM in LTE Physical Downlink Shared Channel (PDSCH) standard. It can be seen in Figure 3.24(a) that for the 3MHz channel bandwidth, the EVM vs carrier frequency curve remains relatively flat, while at the 20MHz channel bandwidth, the EVM at two sides of the band increases. This is due to the crosstalk caused by the amplitude mismatch. As illustrated in Section 3.3.2, the power equaliser needs to be changed to make the upper band, and the lower band has the same amplitude. However, the frequency response of optical link changes with frequency. In the experiment, the power equaliser can only equalise the amplitude at a particular carrier frequency (700MHz). At frequencies around it, the amplitudes of two bands no longer match with each other. It is intended in future that the crosstalk caused by this be compensated by MIMO EVM compensation, which will be illustrated in the next section.

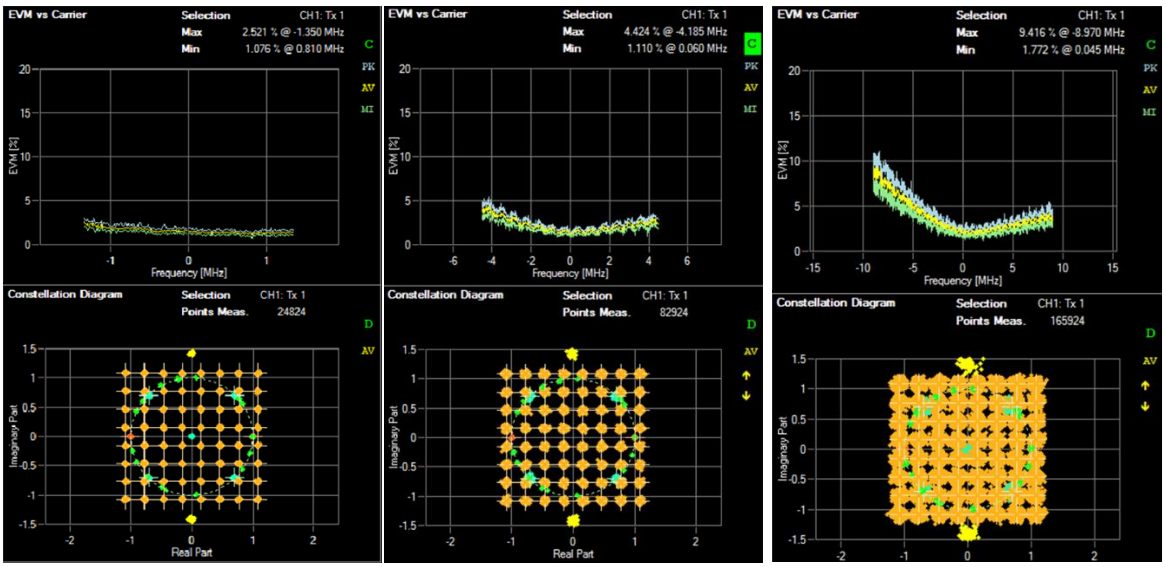

(a) (b) (c)

Figure 3.24 Experimental test result for 2×2 LTE MIMO-enabled radio over 300m MMF, using double sideband frequency translation technique. Central carrier frequency=700MHz Upper: EVM vs. carrier frequency (normalized); Lower: constellation diagram. (a) channel bandwidth=5MHz; (b) channel bandwidth=10MHz; (c) channel bandwidth= 20MHz

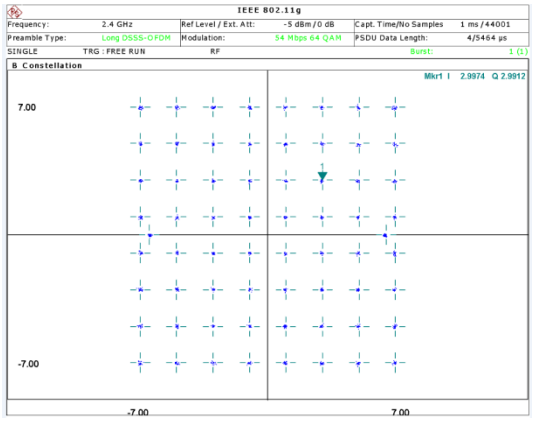

Figure 3.25 Experimental test result for IEEE 802.11g signal (54Mbps) transmitting along with 2×2 LTE MIMO signals. Mean EVM=1.16%.

Simultaneously with the LTE channels, a channel of a 64QAM IEEE 802.11g signal is transmitted. It can be seen in Figure 3.25 that when the system input power (at the system input as shown in Figure 3.21) is at the optimum level which is -5dBm, the received Wi-Fi signal has a very low EVM (~1.2%) and the MIMO signals can exhibit the same EVM both with and without the 802.11g signal, showing that the 802.11g signal and the MIMO signals do not influence each other. However, when the signal input power is high (>3 dBm for LTE in this case), intermodulation distortion between the Wi-Fi channel and the MIMO channels can occur due to nonlinear effects in the RoF link. The experiment shows that this effect can be minimised by carefully controlling the input power of the Wi-Fi signal. In the experimental layout, an attenuation of 10dB is required to compensate the conversion loss of frequency mixer. In a practical system, an automatic gain control (AGC) unit could fulfil this function.

The RoF signals over MMF suffer from dispersion and distortion effects. Thus the link performance of an MMF RoF link should be worse than for an SMF link. An EVM performance comparison for four different types of optical fibres is shown in Figure 3.26. It can be seen that the proposed system is also suitable for both 1km SMF and 600m OM1 MMF. EVM results for both are within LTE PDSCH standard requirement.

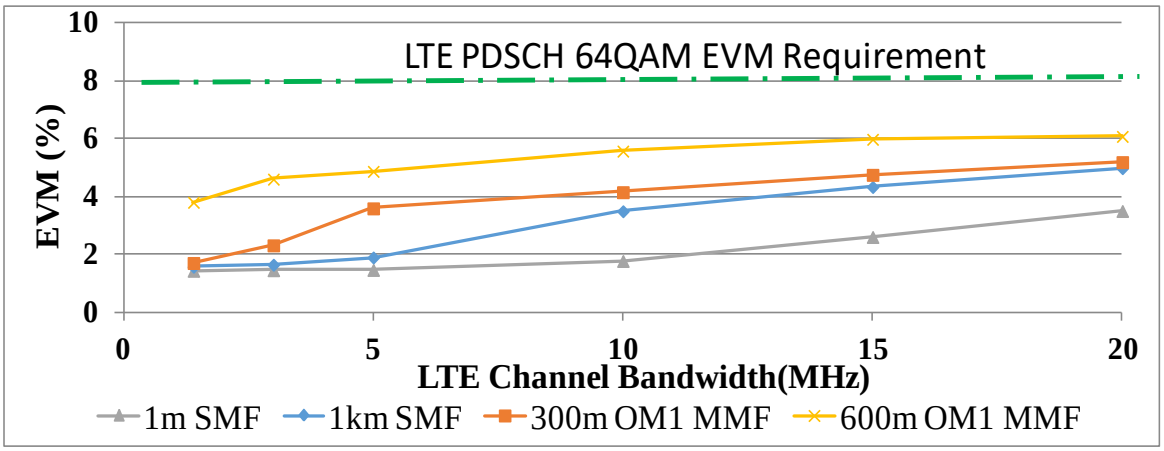

Figure 3.26 EVM comparison for four different types of optical fibres (carrier frequency = 700MHz)

B. Condition number test

The unitary of the channel matrix can be measured by the condition number, which is expressed as

$$\text{Condition number} = \frac{\sigma_{max}(H)}{\sigma_{min}(H)} = \|H^{-1}\|\|H\|$$

in which $\sigma_{max}(H)$ and $\sigma_{min}(H)$ represents the maximum and minimum singular values of the channel matrix H.

Figure 3.27 shows the measured channel matrix elements and the calculated condition numbers shown in dB. The system is adjusted to operate at a carrier frequency of 700MHz. It can be seen that at frequencies from 610MHz to 750MHz, the condition number is lower than 10dB, which shows the system is well-conditioned and the EVM will be compensated in a 140MHz bandwidth if MIMO signal processing is used [85]. This bandwidth is enough to support intra-band carrier aggregation. For the case of inter-band carrier aggregation, multiple power equalisers need to be used.

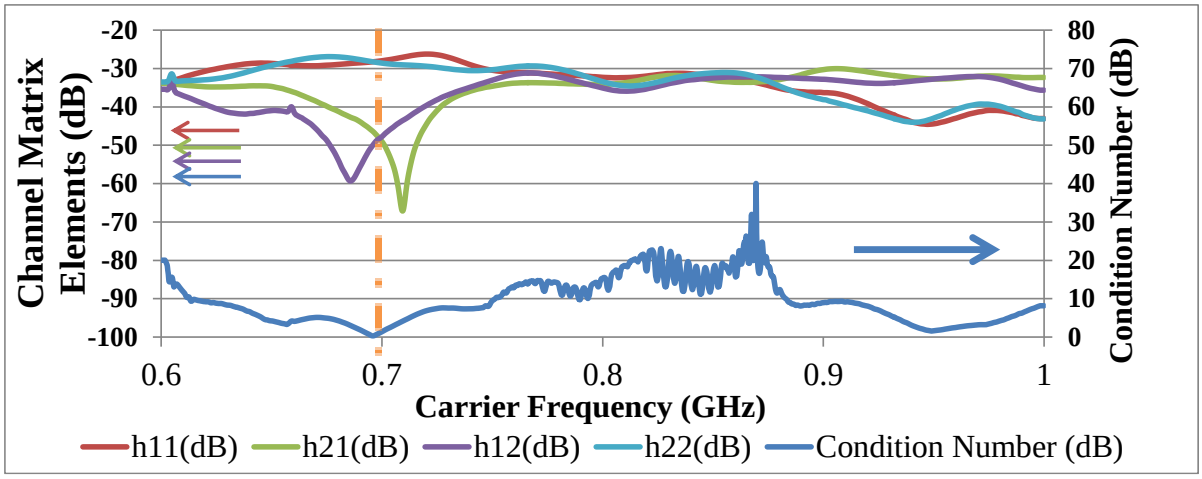

Figure 3.27 Measurement of channel matrix elements (phase is not shown) and calculated condition number vs carrier frequency.

Limited by the phase error of the 90-degree hybrid couplers, the minimum value of the h12 and h21 parameters are not at the same frequency (Figure 3.27). The minimum points for both the h12 and h21 curves occur when one of the equation (11) and (13) is satisfied, and the intersection of the two curves occurs when θ is chosen to be an optimum value between $\sigma_1 + \omega_{LO}\Delta t + n\pi$ and $\theta = \omega_{LO}\Delta t - \sigma_2 + n\pi$, such that h12 and h21 are both small. At this point, the condition number is the lowest (0.27dB) and the EVM can be well compensated by MIMO processing.

At the frequencies out of the bandwidth of the power equaliser, which is 610MHz to 750MHz in this experiment, the condition number increases and the system become ill-conditioned. In this case, the power equaliser needs to be adjusted.

C. Noise Figure, SFDR and EVM Dynamic Range Test

In the DSB system, when the upper and lower band signals are translated back to their original frequency, they sum in the field. Thus there will theoretically be a 6dB signal power increase over an SSB system. In contrast, the independent noise power will only be increased by 3dB. Experimentally, it is shown that, compared with the SSB system, the DSB system can increase

the output signal power by 5.8dB and output noise power by only 3.0dB, and thus the system NF is lowered from 46.0dB to 43.2dB. This approximately agrees with theory and the 0.2dB impairment can be attributed to the phase mismatch of the 90° hybrid coupler.

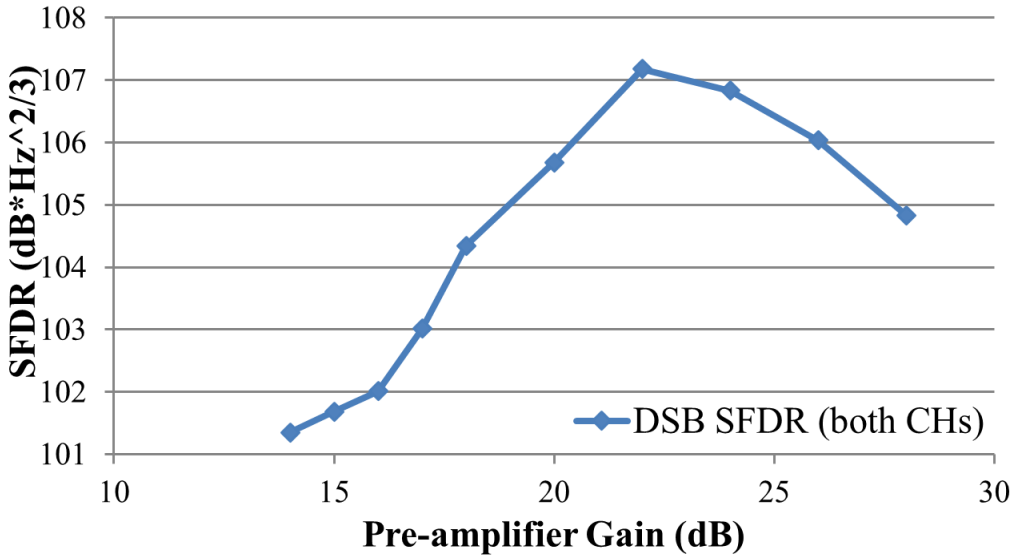

Figure 3.28 SFDR test for MIMO-enabled RoF system using DSB frequency translation

The SFDR of the MIMO-enabled DSB frequency translation system is measured. In Figure 3.28, it is shown that by adjusting the pre-amplifier gain, the system SFDR increases from 101 $dB \cdot Hz^{2/3}$ to above 107 $dB \cdot Hz^{2/3}$. This is because when pre-amplifier gain <22dB, the optical link has the dominant noise figure in the whole system. Higher pre-amplifier gain can give system higher OIP3 without significantly increasing output noise floor. When the pre-amplifier gain >22dB, the noise introduced by the amplifier becomes dominant, thus the SFDR drops. The detailed illustration will be shown in Chapter 5.

In Figure 3.29, a comparison between the system using DSB frequency translation and conventional SSB frequency translation is made when using 3.84MHz channel bandwidth. A variable attenuator is added at the output of the pre-amplifier to adjust the system dynamic range. In the SSB system, two MIMO channels always have different EVM curves. This is due to the bandwidth of the optical link – the upper band of the translated signal suffers from a

much higher RF loss than the lower band, which results in a lower SNR. However, in the DSB system, as the two MIMO channels are orthogonally multiplexed, they occupy the same spectrum and thus in principle have the same EVM performance. This leads to a much larger effective EVM dynamic range.

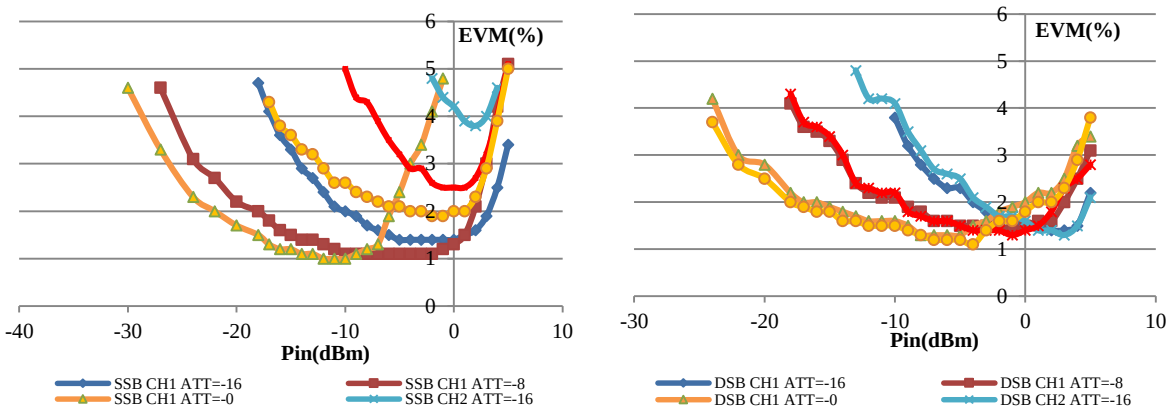

Figure 3.29 EVM dynamic range improvement of DSB frequency translation from SSB frequency translation

3.5 Summary and Conclusion

In this chapter, a SISO RoF system was modelled and then extended into a MIMO RoF system.

The SISO RoF system can be modelled as a cascaded system, consisting of a pre-amplifier, an optical link and a post-amplifier. The pre-amplifier's gain needs to be chosen to be a suitable value to get optimum system SFDR, but the gain of the post-amplifier does not significantly affect system SFDR.

The DSB frequency translation system is an effective solution to transmit MIMO signals over a single optical link. Compared with SSB frequency translation system, theoretically, the DSB system has 2dB higher 3rder order SFDR. However, there are two major factors that contribute to the crosstalk in the DSB frequency translation system, which can reduce the performance: i. the phase error in 90-degree hybrid couplers; ii. the amplitude imbalance between the upper and lower sidebands of the mixing products. In the simulation, if the crosstalk between two

MIMO channels is required to be <-10dB, the amplitude variation in the S21 response of the optical link should be <1dB and the phase error of the 90-degree hybrid coupler should be <4°.

Experimentally, a power-equaliser is installed to overcome the problem of the amplitude imbalance between two sidebands of the mixing products. Therefore, 20MHz bandwidth LTE MIMO radio over fibre system can be demonstrated beyond optical link's 3dB RF bandwidth.

An IEEE 802.11g (Wi-Fi) and a 2x2 LTE MIMO service are transmitted together using the DSB frequency translation. The optimum average EVM test result for the Wi-Fi service is 1.16% and for LTE service is 1.7% (for 3MHz channels), 2.3% (for 10MHz channels) or 5.1% (for 20MHz channels). All these values are within the standard requirement.

The experimental results show the DSB frequency translation system has improved effective dynamic range than the SSB frequency translation system because both of the MIMO channels are symmetric and have the same EVM performance.

Chapter 4 Broadband Implementation for MIMO RoF using DSB Frequency Translation

4.1 Introduction

There is a range of wireless services that we transmit over distributed antenna systems, and all these wireless services have different service providers. A service agnostic DAS needs to be broadband and each of the services should not influence the others.

In a DSB frequency translation system, all services are transmitted through the same optical link. Two major factors may cause crosstalk among services – i) the upper sideband and the lower sideband after frequency translation may overlap with other services over the optical link; ii) the second order harmonic of the service may influence the others.

In this chapter, the broadband implementation of a 2x2 MIMO RoF system using DSB frequency translation technique will be investigated.

4.2 Services to be transmitted over a DAS

For a commercial DAS, various wireless services are required to be transmitted to users, including 2G, 3G, 4G and Wi-Fi. On the other hand, not all the spectral regions need to be transmitted over DAS, for example, the spectral regions for space to earth communication, aeronautical mobile and aeronautical radio navigation. In a DSB frequency translation system, the original MIMO signal is translated into the upper sideband and the lower sideband. The system designer needs to make sure the sidebands after frequency translation occupy the regions that are not used for other services on the DAS.

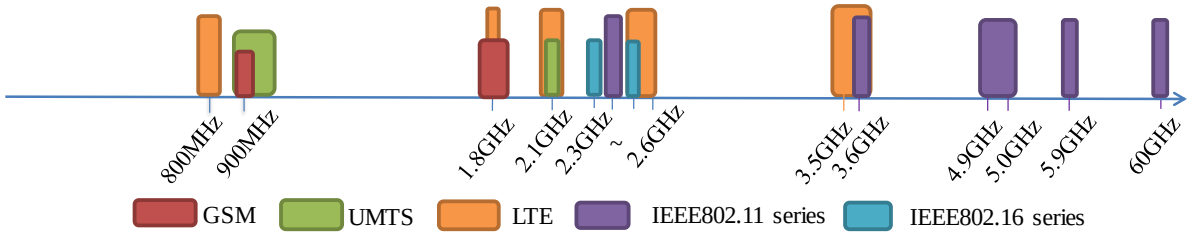

Figure 4.1 Typical services to be transmitted over a DAS in the UK

Figure 4.1 shows the frequency spectrum allocation for the 2G/3G/4G, Wi-Fi and WiMax services in the UK. These services are typically required to be transmitted over a DAS. In the UK, the LTE frequency bands are occupied by four major service providers – 3 mobile, EE, O_2, and Vodafone. They occupy 800MHz, 1800MHz, 2100MHz, 2600MHz and 3500MHz frequency bands. For the UMTS services, the UK service providers are in 900MHz and 2100MHz bands. For the GSM services, the standard has defined several frequency bands, such as GSM450, GSM800, GSM900, GSM1800, but only GSM900 and GSM1800 are used in the UK [86, 87, 88, 89, 90].

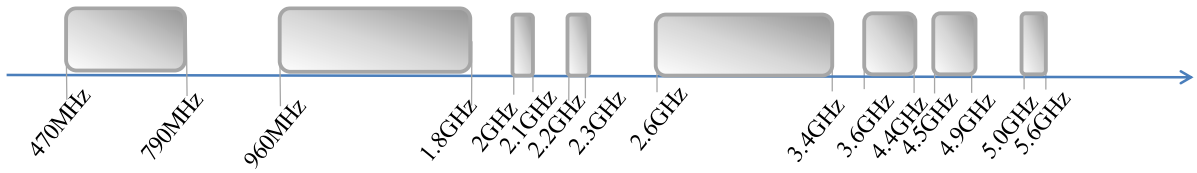

Figure 4.2 Typical frequency bands that are not occupied in the DAS in the UK (reserved for space to earth communication and aeronautical communication)

Although these services occupy many frequency bands, there are still empty spectral regions on the DAS. These empty regions are usually occupied by military communication, satellite communication and aeronautical communication [91], as shown in Figure 4.2. For example, the spectrum from 470MHz to 790MHz cannot be assigned to civilian use, but "Ofcom may agree to the use of these frequencies for military purposes with the Ministry of Defence" [91]; the wide band from 960MHz to 1350MHz is reserved for aeronautical mobile, aeronautical radio navigation, radio navigation satellite, earth exploration satellite and space research [91].

These empty spectral regions can be used to transmit the frequency translated MIMO signals over the DAS. Detailed frequency spectrum allocation in the UK can be found in [91] and is not listed here.

4.3 Local oscillator frequency selection

In a DSB frequency translation system, to translate original MIMO signals into unoccupied frequency bands in a DAS, the local oscillator frequency needs to be carefully selected.

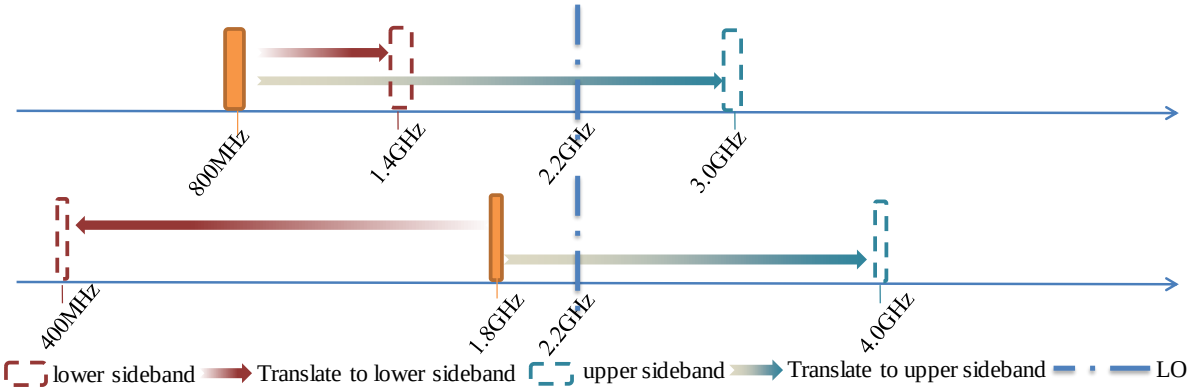

Figure 4.3 Example frequency translation map to translate 800MHz and 1.8GHz LTE channels into unoccupied frequency bands on a DAS

Figure 4.3 shows an example frequency translation map. The 800MHz LTE channel, for instance, can be translated into 1.4GHz and 3.0GHz bands by a 2.2GHz local oscillator and both sidebands are then in the empty spectral region as shown in Figure 4.2.

As shown in Table 4.1 and Figure 4.3, by using a 2.2GHz local oscillator, the LTE services in the UK can always be translated into unused spectral regions over the DAS. For the case outside the UK, similar situations can be found. The 2.2GHz local oscillator frequency can be used in many major countries in the world. The frequency translation maps using 2.2GHz LO for the US and China are shown in

Table 4.2 and Table 4.3. For some special cases, the same principle can be applied, but different local oscillator frequency needs to be used. In Japan, for instance, a 2GHz local oscillator can be used.

Table 4.1 Detailed LTE frequency translation table in the UK when using DSB frequency translation and 2.2GHz LO frequency [92]

LTE band	Mobile operators	FDD/TDD	LTE band frequency	LO frequency	Upper sideband	Lower sideband
3	3, EE, O2, Vodafone	FDD Uplink	1710 – 1785MHz	2200MHz	3910 – 3985MHz	415 – 490 MHz
		FDD Downlink	1805 - 1880MHz		4005 – 4080 MHz	320 – 395 MHz
7	EE, Vodafone	FDD Uplink	2620 – 2690MHz	2200MHz	4620 – 4890 MHz	420 – 490 MHz
		FDD Downlink	2500 – 2570MHz		4700 – 4770 MHz	300 - 370MHz
20	3, EE, O2, Vodafone	FDD Uplink	832 – 862 MHz	2200MHz	3032 – 3062 MHz	1338 - 1368
		FDD Downlink	791 – 821 MHz		2291 – 3021 MHz	1379 – 1409 MHz
38	Vodafone	TDD	2570 – 2620 MHz	2200MHz	4770 – 4820 MHz	370 – 400MHz
42	3	TDD	3400 – 3600 MHz	2200MHz	5600 – 5800 MHz	1200 – 1400 MHz
43	3	TDD	3600 – 3800 MHz	2200MHz	5800 – 6000 MHz	1400 – 1600 MHz

Table 4.2 Detailed LTE frequency translation table in the USA when using DSB frequency translation and 2.2GHz LO frequency

LTE band	Mobile operators	FDD/TDD	LTE band frequency	LO frequency	Upper sideband	Lower sideband
2	AT&T, iWireless, T-Mobile, C Spire [93]	FDD Uplink	1850-1910 MHz	2200MHz	4050 - 4110MHz	350 - 290MHz
		FDD Downlink	1930 -1990 MHz		4130 - 4190MHz	270 - 210MHz
5	AT&T, U.S. Cellular, C Spire, T-Mobil [94]	FDD Uplink	824 – 849 MHz	2200MHz	3024 - 3049MHz	1376 - 1351MHz
		FDD Downlink	869 – 894 MHz		3069 - 3094MHz	1331 - 1306MHz
12	AT&T (via MFBI), T-Mobile, U.S. Cellular [95]	FDD Uplink	699 – 716 MHz	2200MHz	2899 - 2916MHz	1501 - 1484MHz
		FDD Downlink	729 – 746 MHz		2929 - 2946MHz	1471 - 1454MHz
13	Verizon	FDD Uplink	777 – 787 MHz	2200MHz	2977 - 2987MHz	1423 - 1413MHz
		FDD Downlink	746 – 756 MHz		2946 - 2956MHz	1454 - 1444MHz
17	AT&T, Adams Networks, Evolve Broadband	FDD Uplink	704 – 716 MHz	2200MHz	2904 - 2916MHz	1496 - 1484MHz
		FDD Downlink	734 – 746 MHz		2934 - 2946MHz	1466 - 1454MHz

24	Ligado Networks	FDD Uplink	1626.5 – 1660.5 MHz	2200MHz	3826.5 - 3860.5MHz	573.5 - 539.5MHz
		FDD Downlink	1525 – 1559 MHz		3725 - 3759MHz	675 - 641MHz
25	Sprint	FDD Uplink	1850 – 1915 MHz	2200MHz	4050 - 4115MHz	350 - 285MHz
		FDD Downlink	1930 – 1995 MHz		4130 - 4195MHz	270 - 205MHz
26	Sprint	FDD Uplink	814 – 849 MHz	2200MHz	3014 - 3049MHz	1386 - 1351MHz
		FDD Downlink	859 – 894 MHz		3059 - 3094MHz	1341 - 1306MHz
30	AT&T	FDD Uplink	2305 – 2315 MHz	2200MHz	4505 - 4515MHz	105 - 115MHz
		FDD Downlink	2350 – 2360 MHz		4550 - 4560MHz	150 - 160MHz
41	Sprint	TDD	2496 – 2690 MHz	2200MHz	4696 - 4890MHz	296 - 490MHz
71	T-Mobile	FDD Uplink	663 – 698 MHz	2200MHz	2863 - 2898MHz	1537 - 1502MHz
		FDD Downlink	617 – 652 MHz		2817 - 2852MHz	1583 - 1548MHz

Table 4.3 Detailed LTE frequency translation table in P. R. China when using DSB frequency translation and 2.2GHz LO frequency [96, 97, 98]

LTE band	Mobile operators	FDD/TDD	LTE band frequency	LO frequency	Upper sideband	Lower sideband
3	China Mobile, China Unicom	FDD Uplink	1710 – 1785 MHz	2200MHz	3910 – 3985 MHz	490 – 415 MHz
		FDD Downlink	1805 - 1880 MHz		4005 – 4080 MHz	395 – 320 MHz
38	China Mobile	TDD	2570 - 2620 MHz	2200MHz	4770 – 4820 MHz	370 – 420 MHz
39	China Mobile	TDD	1880 - 1920 MHz	2200MHz	4080 – 4120 MHz	320 – 280 MHz
40	China Mobile, China Telecom, China Unicom	TDD	2300 - 2400 MHz	2200MHz	4500 – 4600 MHz	100 – 200 MHz
41	China Mobile, China Telecom, China Unicom	TDD	2496 - 2690 MHz	2200MHz	4696 – 4890 MHz	296 – 490 MHz

4.4 Experiment for broadband EVM test

4.4.1 Experimental setup

The broadband performance of a DSB frequency translation 2x2 MIMO RoF system is tested using an optical link with >10GHz RF bandwidth. A directly modulated DFB laser emitting at 1310nm wavelength and a 500m SMF link is used. The pre-amplifier used in the system has been chosen to be a broadband amplifier, which can provide the system with a relatively flat S21 amplitude-frequency response.

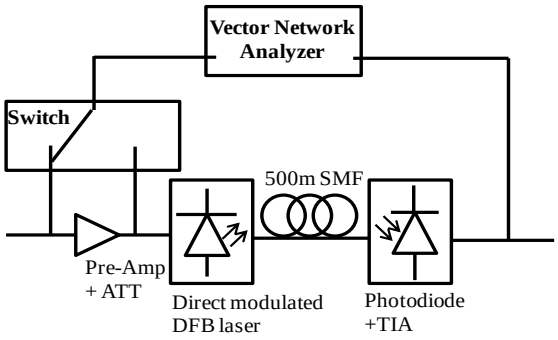

Figure 4.4 Experiment setup for S21 parameter measurement for broadband RoF optical link

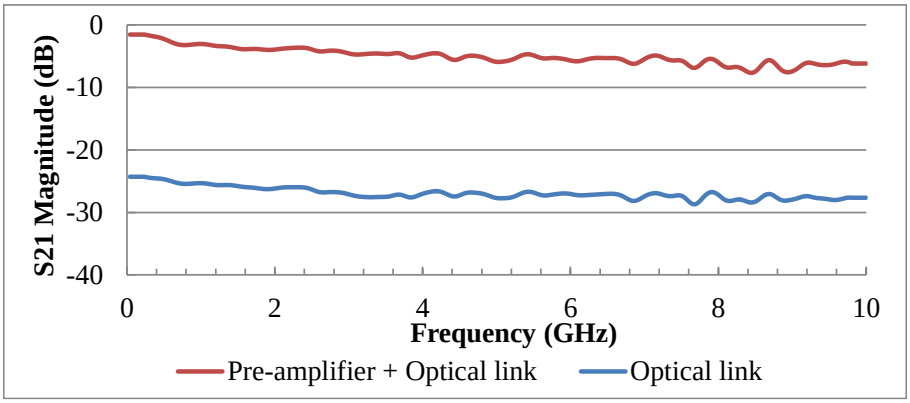

Figure 4.5 S21 magnitude response for broadband optical link and pre-amplifier+optical link

The system S21 amplitude-frequency response has been tested using the setup shown in Figure 4.4. As shown in Figure 4.5, the S21 magnitude slowly decays with some fluctuation in the required frequency bands (0.1GHz to 5.8GHz). The roll off at high frequencies is <5dB.

As illustrated in Section 3.3.2, to lower the crosstalk in the DSB frequency translation system, a power equaliser needs to be used to balance the amplitude difference of the lower sideband and the upper sideband after the frequency translation.

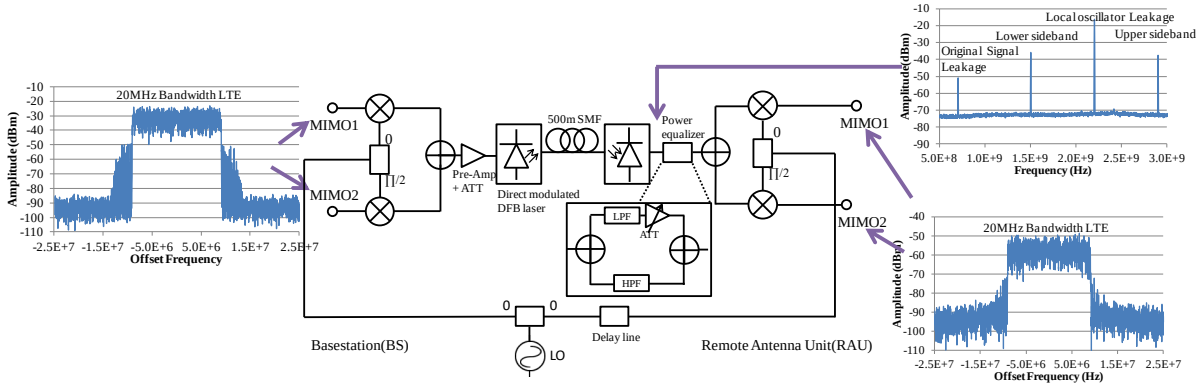

Figure 4.6 Experimental layout for 2×2 MIMO-enabled broadband RoF using DSB frequency translation technique and frequency spectrum (700MHz carrier frequency LTE shown by way of example).

As shown in Figure 4.6, a power equaliser consisting of a low-pass filter and a high-pass filter with 3dB cut-off frequencies at 2.2GHz and a variable attenuator is employed to compensate any imbalance between the upper and lower bands of the signal after the optical link. A 2.2GHz cut-off frequency is chosen to allow the upper and the lower bands to be separated without affecting any of the frequency-translated LTE signals shown in Table 4.1. LTE MIMO-type signals with 20MHz channel bandwidths are presented to the system input. The electrical spectrums at different positions in the system are shown in Figure 4.6.

Figure 4.7 shows the experimental layout for the error vector magnitude (EVM) measurement. A Rohde & Schwarz® SMW200A vector signal generator is used to generate an LTE channel, while another Rohde & Schwarz® FMQ06B vector signal generator is used to generate a 64QAM signal with the same bandwidth and centre frequency to create an LTE-like signal at the same RF frequency due to the availability of only one LTE signal source. A Rohde & Schwarz® FSQ26 vector signal analyser (VSA) is used to receive and analyse the signal at the RAU side.

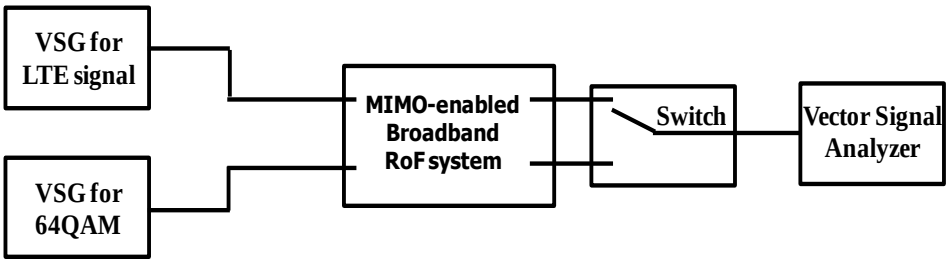

Figure 4.7 2x2 LTE MIMO EVM measurement setup

The system has been tested using LTE carrier frequencies from 700MHz to 2.6GHz, covering most of the commercial LTE bands, other than 3.5 and 3.6GHz bands. This is because the Rohde & Schwarz® SMW200A vector signal generator used in the experiment has a maximum RF frequency of 3GHz, so it was not possible to generate test signals in these bands. If the original carrier frequency is 3.5-3.6GHz, when using 2.2GHz LO, the upper sideband of the signal after translation is at 5.7-5.8GHz respectively. As shown in Figure 4.5, these frequencies are within 6dB RF bandwidth of the pre-amplifier + optical link. Therefore, the system can be expected to also work for 3.5 and 3.6GHz bands.

4.4.2 Experimental results

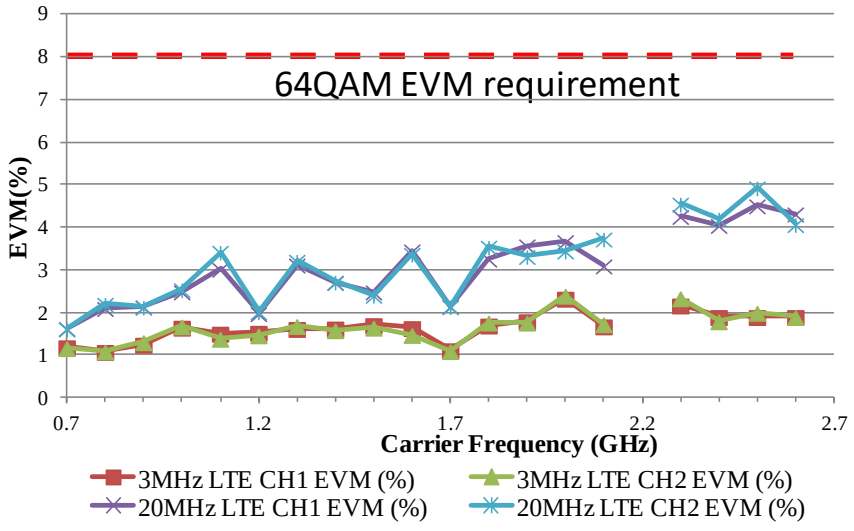

Figure 4.8 Broadband EVM test result for 2×2 LTE MIMO-enabled RoF using DSB frequency translation.

Figure 4.8 presents the experimental results for a broadband EVM test when the channel bandwidths are 3MHz and 20MHz. Both channels have similar EVM performance. When the channel bandwidth was 3MHz, the EVM remains around 2%; and was 5% for the 20MHz channel bandwidth. Crosstalk between two channels is the dominant factor, which contributes to the elevated EVM. When the bandwidth increases from 3MHz to 20MHz, the power equaliser is less able to match the amplitude of the side, so the EVM has been increased.

The EVM vs input signal power curve is shown in Figure 4.9. The EVM input power dynamic range for 20MHz bandwidth LTE test model E-TM3.1 (64QAM) is ~30-35dB at two typical UK mobile operator frequency bands (800MHz and 1800MHz) without automatic gain control (AGC). If AGC were to be applied, the system dynamic range is expected to be further improved.

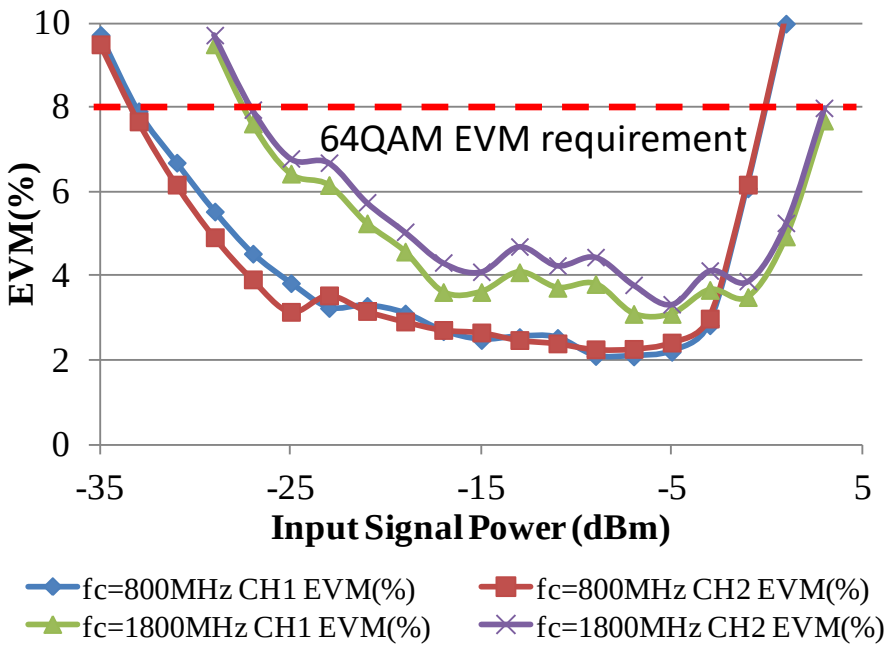

Figure 4.9 EVM input power dynamic range tested at 800MHz and 1800MHz

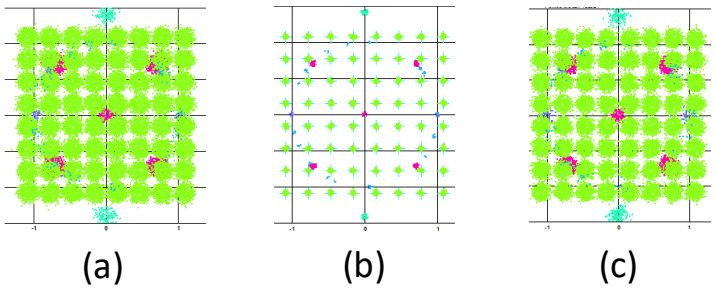

Figure 4.10 Constellation diagrams for 800MHz carrier frequency 20MHz BW LTE: (a) input power = -27dBm; (b) input power =-11dBm; (c) input power = 3dBm

4.5 Demonstration for local oscillator signal remote delivery and real-life 2x2 MIMO RoF

In the experimental setup in Section 4.4.1 and Figure 4.6, the base station side and the RAU side share the same local oscillator. In a real system, however, the local oscillator signal needs to be remotely delivered to each RAU. Limited by the available equipment, the MIMO signal processing is not included in the experiments in the previous sections. In this section, a real-life 2x2 MIMO radio over fibre system will be demonstrated using an IEEE 802.11n 2x2 MIMO Wi-Fi signal.

4.5.1 Local oscillator signal remote delivery.

First of all, a simple experiment has been performed in the laboratory environment. As shown inFigure 4.11, before the optical link, a local oscillator is split, and half of the signal power is used to translate a 700MHz LTE signal into another carrier frequency (here 1.5GHz); the other half of LO signal is combined with the LTE signal after the frequency translation and then transmitted together via the optical link. The electrical spectrum after the photodiode is shown in Figure 4.11, the LO signal and the LTE signal can be clearly seen in the diagram. After the

photodiode, the LO signal is filtered out then fed back to translate the LTE signal back to the original frequency using the mixer.

The EVM performance of the transmitted signal by using LO remote delivery is compared with the ideal case (both the mixers from both sides of the optical link share the same local oscillator source), as shown in Figure 4.12. The EVM performance of the system using remote LO delivery is comparable to the ideal case.

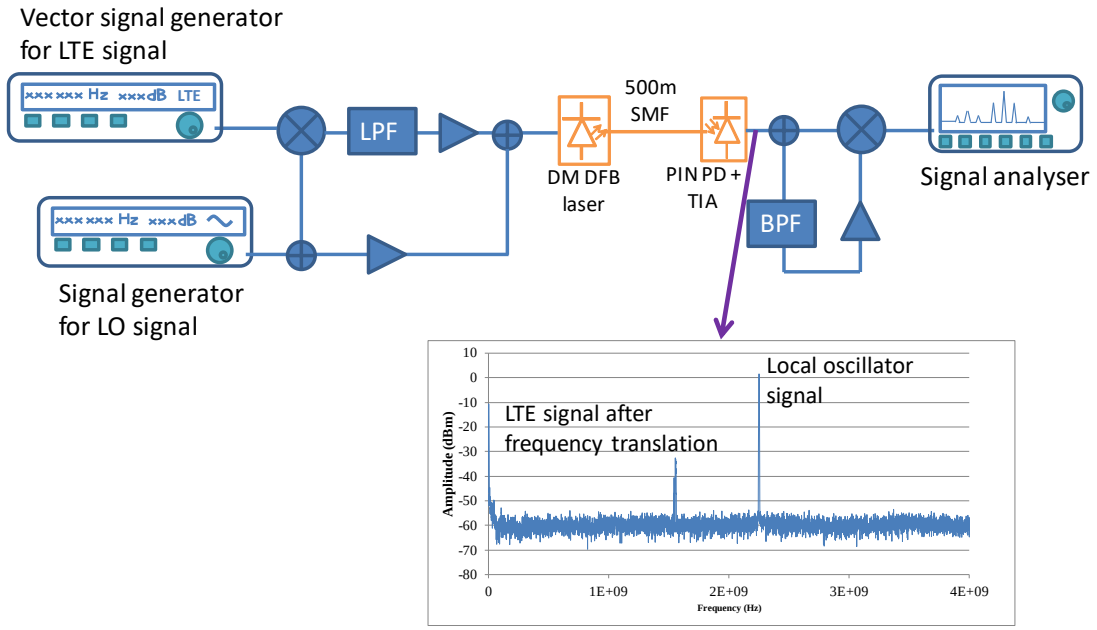

Figure 4.11Experimental setup for LO remote delivery in an SCM system.

Because the LO is transmitted at relatively high RF power on the optical link, the high order harmonics of the LO signal occur in the received spectrum. Because the LO signal used here is 2.2GHz, as illustrated in Section 4.3, the LO high-order harmonic products (at 4.4GHz, 6.6GHz…) do not overlap with any of the other services to be transmitted over DAS. However, it is still possible that the beating products of the LO and service signals on the optical link influence the system performance. Therefore, the LO signals need to be attenuated before the optical link to reduce or prevent distortion.

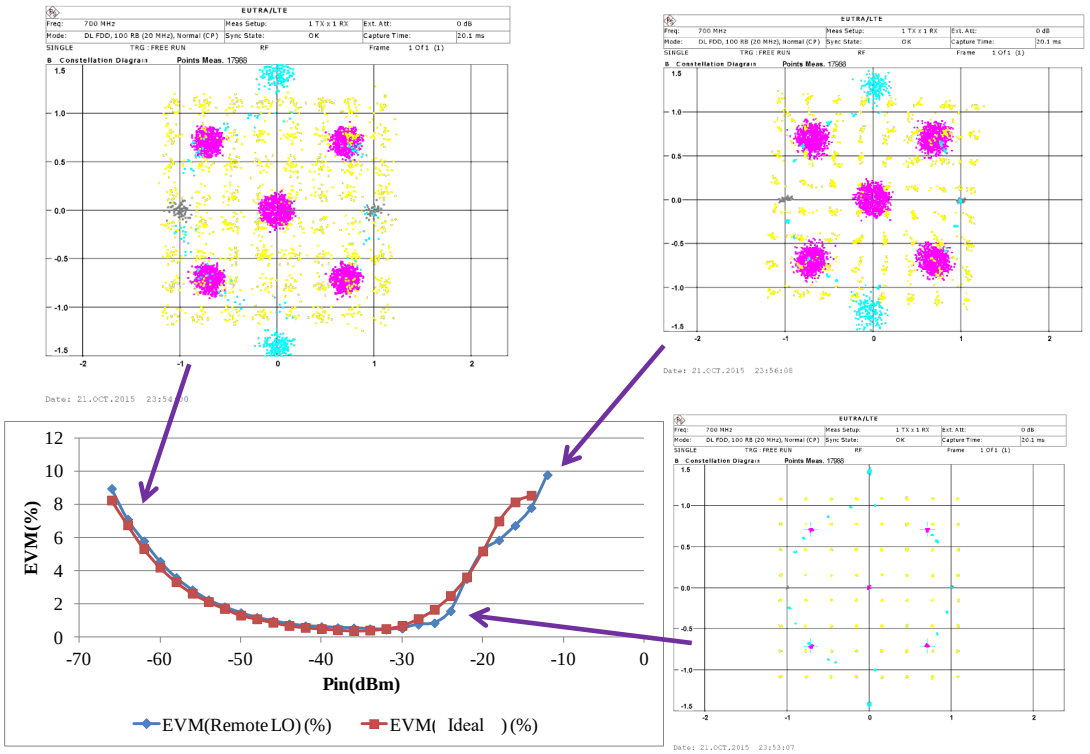

Figure 4.12 EVM performance comparison between the LO remote delivery and the ideal case when using SCM

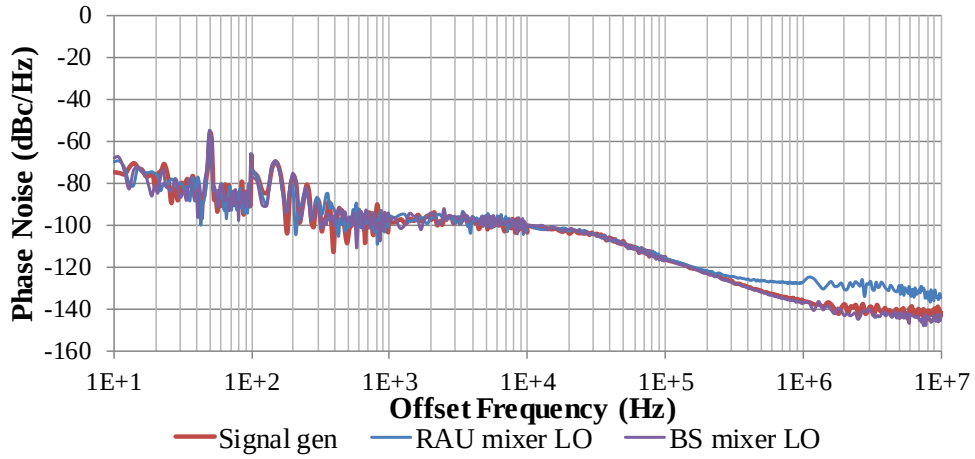

Figure 4.13 LO oscillator phase noise in LO remote delivery

The LO phase noise has been tested for the LO remote delivery as shown in Figure 4.13.The local oscillator signal at the RAU side (after the optical link) has 10dB higher phase noise when offset frequency >1MHz.

Now we extend the system into a 2x2 MIMO RoF system using the DSB frequency translation technique. As shown in Figure 4.14, two vector signal generators are used at the system input for two channels of MIMO type signals at the 700MHz carrier frequency, and they are multiplexed together using the DSB frequency translation technique. A sine wave at 2.2GHz frequency and 18dBm electrical power is generated as the LO signal at the base station side (before the optical link). A power splitter follows the LO signal generator to split the LO signal two ways – one is used to feed the mixers at the base station side, the other is attenuated by 20dB and then transmitted to the RAU side. At the RAU side, the LO signal from the optical link is filtered out and amplified to feed the mixers.

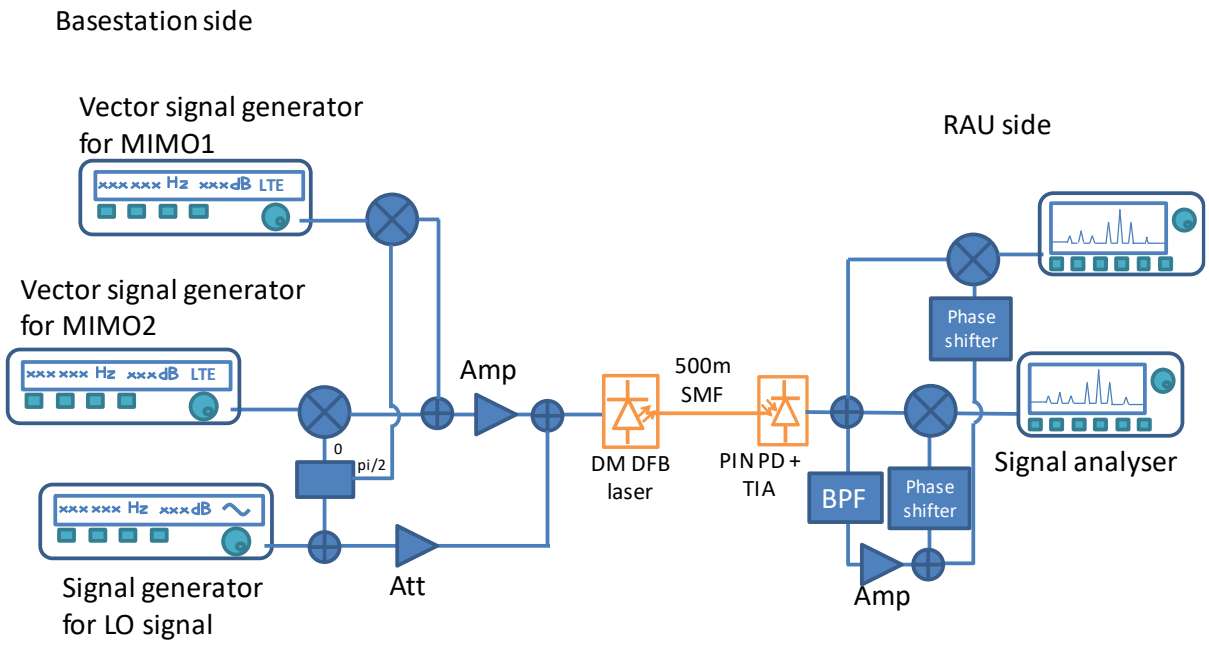

Figure 4.14 Experimental layout for DSB 2x2 MIMO RoF system using LO remote delivery.

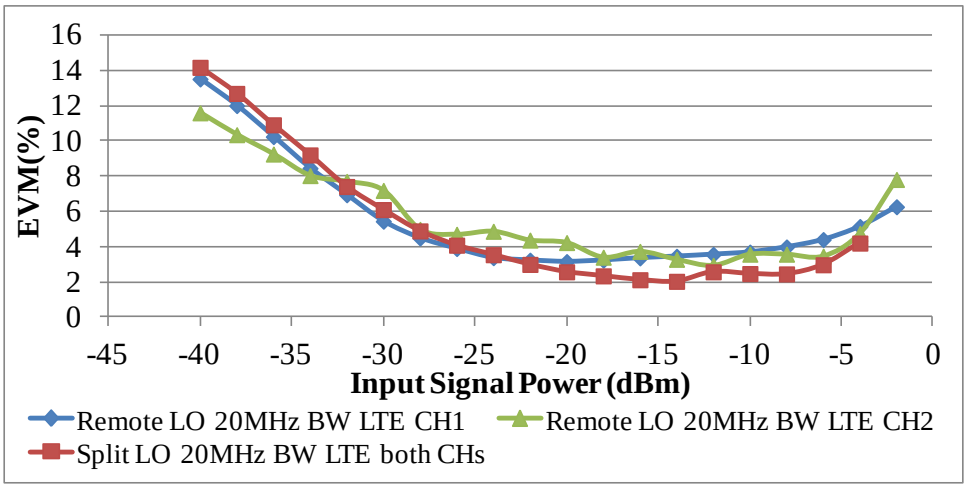

Figure 4.15 EVM test result for both MIMO channels when using LO remote delivery

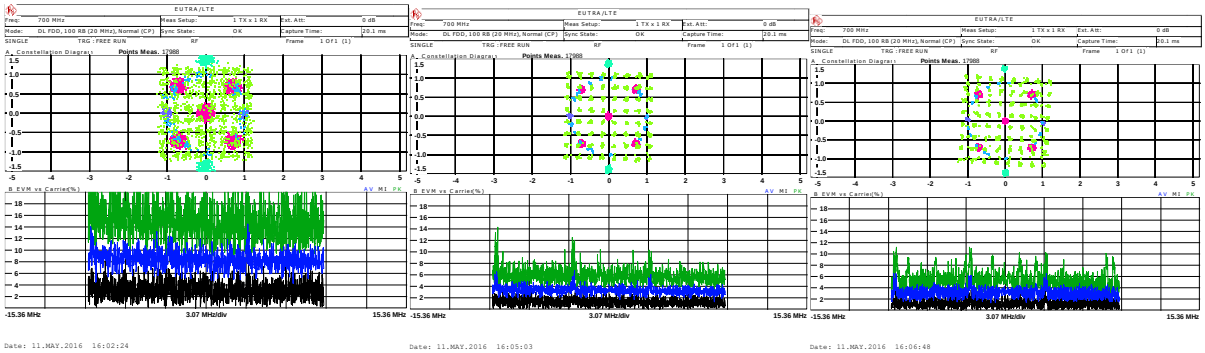

Figure 4.16 Constellation and EVM vs. carrier frequency diagrams for the LO remote delivery in 2x2 DSB MIMO RoF system: (a) at -35dBm input signal power; (b) at -12dBm input signal power; (c)at -3dBm input signal power

Figure 4.15 shows the EVM test result for both MIMO channels. As both channels have identical EVM performance, only one curve has been presented here. It can be seen that the LO has been effectively delivered to the RAU. The EVM result is well below the standard requirement for 64QAM in ~35dB range, and if an AGC is used, the dynamic range can be further improved. Also, the EVM performance for using LO remote delivery is comparable to

the ideal case (when the BS side and the RAU side share the same LO). The constellation diagrams at -35dBm, -12dBm and -3dBm input power are shown in Figure 4.16.

4.5.2 Real-life Wi-Fi 2x2 MIMO RoF test with free-space propagation

In the previous sections, the MIMO signal processing and the free-space propagation has not been included. Although the MIMO signal processing can improve the previous EVM test results, a real-life 2x2 MIMO RoF system test is done to show the feasibility of using the DSB frequency translation RoF system.

Limited by the equipment, an experiment has been carried out using IEEE 802.11n MIMO signal. As shown in Figure 4.17, a computer with an IEEE 802.11n 2x2 MIMO wireless card with has been used as a server, which is shielded inside a metal cupboard and no signal leak out. The downlink MIMO signal from the server is transmitted to the remote antennas using SSB and DSB frequency translation via a 500m SMF link. The layout of the SSB and the DSB systems are as shown in Figure 3.14 and Figure 3.15. Another computer with an IEEE802.11 MIMO wireless card and antennas are used as a client to receive MIMO signals from the free space. The uplink is connected directly using coaxial cables with gain control to maintain the same gain with the downlink.

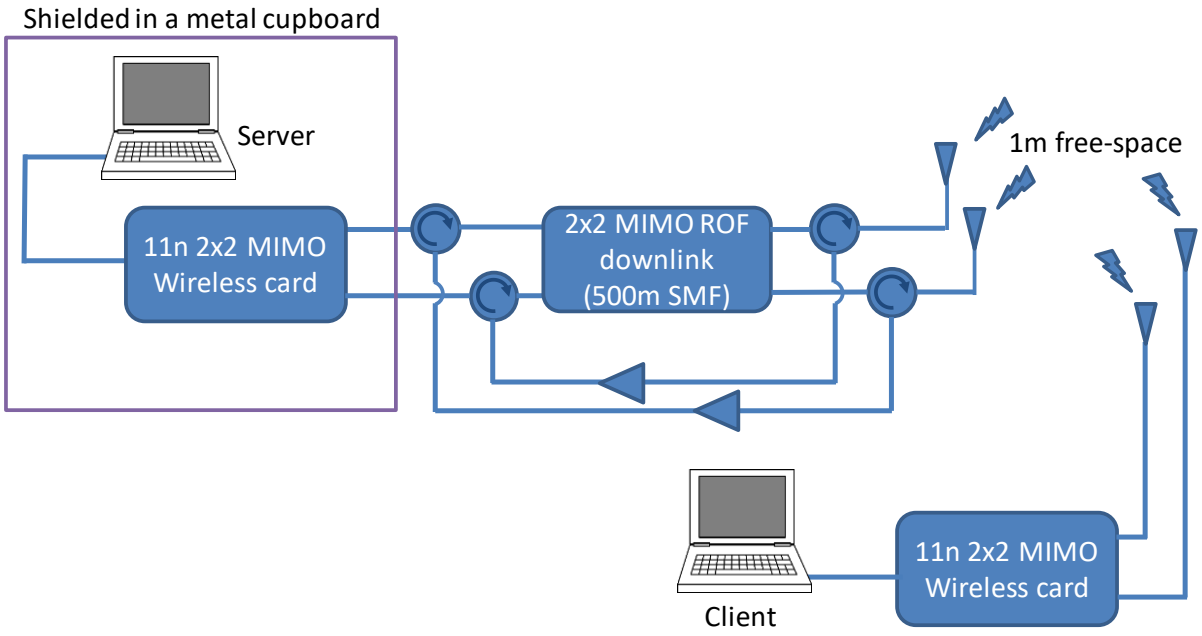

Figure 4.17 Experiment setup for Wi-Fi 2x2 MIMO RoF throughput test

The throughput test is done by TamoSoft® Throughput Test software using UDP and IPv4 protocols. The downlink throughput is tested and 100 data points have been collected respectively for the SISO back-to-back and SSB/DSB frequency translation system. The throughput cumulative distribution function is as shown in Figure 4.18. It can be seen that the Wi-Fi MIMO signal can be delivered to the client. When the DSB 2x2 MIMO RoF system is used the system can achieve ~1.5 times throughput as the SISO back-to-back result. There are some points in the SSB/DSB frequency translation system that has low throughput. This is because the Wi-Fi transceiver used here is operating in the EVM margin, some degradation in the optical link can cause the system in operation in the lower dimension modulation scheme.

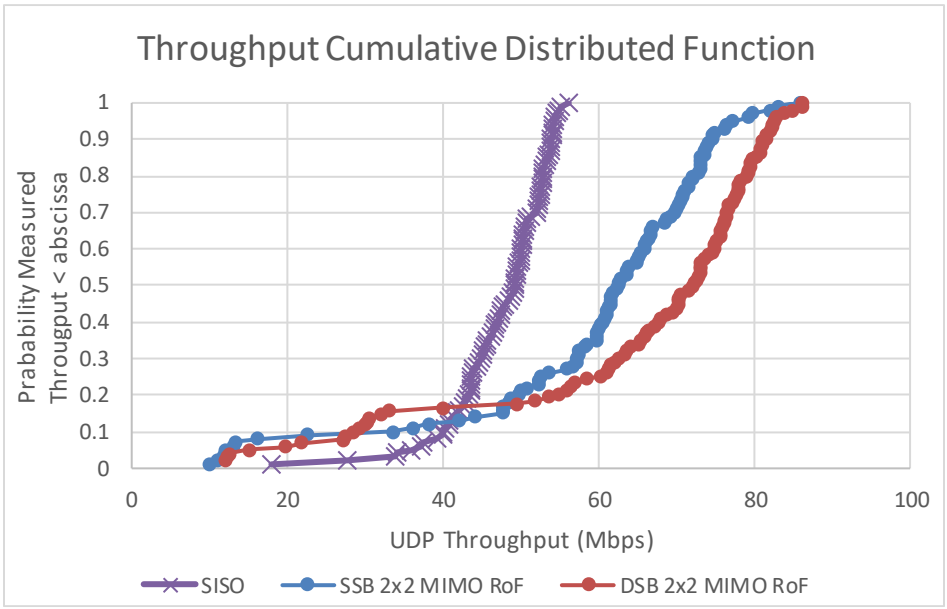

Figure 4.18 Throughput cumulative distribution function for MIMO RoF system using SSB/DSB frequency translation

4.6 Summary and Conclusion

To use the DSB frequency translation system in a service-agnostic DAS, it should be able to have a broadband operation. In this chapter, we have investigated the frequency bands that are to be transmitted over DAS in the UK, showing that there are many empty spectral regions in the DAS. Most of these empty spectral regions are reserved for aeronautic radio or space-to-earth communication, which are not usually required to be transmitted over a DAS. The upper and lower sidebands in the DSB frequency translation system can occupy these spectrums so that they do not overlap with other services on the DAS. In many major countries, such as the UK, the US and China, using a 2.2GHz LO can translate all LTE bands into unoccupied spectral regions on the DAS. Although there are some individual cases, such as Japan, different LO frequencies need to be chosen, but the same principle can be applied.

The LO signal can be delivered to the RAUs via the analogue optical link, but the LO signal power needs to be carefully adjusted to prevent additional high order distortion products.

Experimentally, the LO signal at the base station side needs to be attenuated by ~10dB before the optical link. The EVM performance of the LO remote delivery in the DSB frequency translation system is <2% higher than the ideal LO delivery (using the LO signal is split to feed the BS side and the RAU side). A real-life WiFi MIMO radio over fibre system has been demonstrated using LO remote delivery, showing that the system can successfully deliver Wi-Fi MIMO signal from the central unit to the client. The throughput is tested using the SSB and DSB frequency translation for 2x2 MIMO RoF. The SSB system gives >60 Mbps throughput, and the DSB system offers >70 Mbps throughput.

Chapter 5 SFDR improvement using multiple-sideband frequency translation

5.1 Introduction

In the previous sections, we have described a DSB frequency translation system; two MIMO channels are multiplexed onto sidebands with a 90° phase shift. At the RAU side, the signals are de-multiplexed back to the original frequency. The noise from the upper and lower sidebands adds incoherently, but the wanted signals add coherently at the output. As a result, the DSB system can theoretically have a 2dB higher SFDR than the SSB system. The SFDR is a particularly important metric and one of the performance limiting factors for RF services on RoF links.

In this chapter, we extend this concept to a general quadrature-multiplexed frequency translation system and show that if the original RF signal is translated into more than two sidebands, for instance, quadruple sidebands (QSB), the system is not only MIMO-capable but can also exceed the 3rd order SFDR limit of the intrinsic optical link. This shows that in a general radio over the fibre system, the RF bandwidth in the optical link can be traded for electrical SFDR by increasing the number of sidebands onto which the original RF signal is modulated.

5.2 Theory of 3rd order SFDR improvement in a quadrature-multiplexed frequency translation system

A model has been built to analyse the 3rd order SFDR performance when original MIMO signal has been translated into different numbers of sidebands by using multiple frequency mixers. In a DSB frequency translation system, at the base station side, the original signal is translated into two sidebands using a frequency mixer. In the case for more than two sidebands, multiple mixers are cascaded. After the optical link, the frequency mixers combine all the sidebands back together, making the signal add coherently, but the noise adds incoherently. Figure 5.1 shows the layout for translating the RF signal into double sidebands (DSB), quadruple sidebands (QSB) and octuple sidebands (OSB). In the QSB system, two pairs of frequency mixers are used at each side of the optical link, while in the OSB system, three pairs are used.

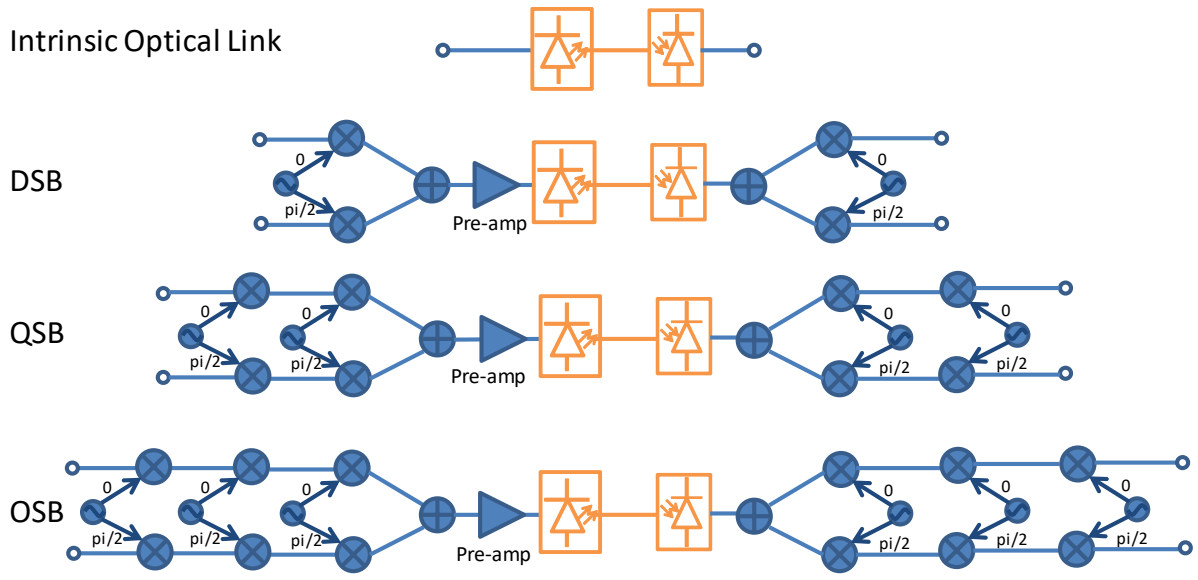

Figure 5.1 Translate signal into different numbers of sidebands, DSB: two sidebands; QSB: four sidebands; OSC: eight sidebands

Mathematically, we consider a radio over fibre system has thermal noise as input noise (n_{th}). The total cascaded output noise floor can be represented as,

$$n_{out} = n_{th} g_{opt} g_{mix2} (nf_{opt} - 1 + g_{amp} nf_{amp} - g_{amp})/m \tag{5.1}$$

where n_{th} is thermal noise; g_{opt}, g_{mix2} and g_{amp} are respectively the gains of the optical link, the mixers at the RAU side and the pre-amplifier; nf_{opt} and nf_{amp} are the noise factors of the intrinsic optical link and pre-amplifier; m is the number of sidebands that the system uses, for example, $m = 4$ if it is a quadruple sideband system.

The total cascaded iip3 is,

$$iip3_T = \left(\frac{1}{iip3_{mix1}} + \frac{g_{mix1}}{iip3_{amp}} + \frac{g_{mix1} g_{amp}}{iip3_{opt}} + \frac{g_{mix1} g_{amp} g_{opt}}{iip3_{mix2}}\right)^{-1} \tag{5.2}$$

Therefore, the total 3rd order sfdr is,

$$sfdr3 = \left(\frac{oip3_T}{n_{out}}\right)^{2/3} = \left(\frac{g_T * iip3_T}{n_{out}}\right)^{2/3} \tag{5.3}$$

in which,

$$g_T = g_{mix1} * g_{amp} * g_{opt} * g_{mix2} \tag{5.4}$$

$mix1$ and $mix2$ respectively represents the overall effect of the mixers at the basestation side and the RAU side.

Combining equations (5.1), (5.2) and (5.3)

$$\frac{oip3_T}{n_{out}} = m/\left[n_{th}\left(A + \frac{B}{g_{amp}}\right)(C + Dg_{amp})\right]$$

$$= m/\left[n_{th}(ADg_{amp} + \frac{BC}{g_{amp}} + AC + BD)\right] \quad (5.5)$$

in which, $A = \frac{1}{iip3_{opt}} + \frac{g_{opt}}{iip3_{mix2}}$; $B = \frac{1}{iip3_{mix1}g_{mix1}} + \frac{1}{iip3_{amp}}$; $C = nf_{opt} - 1$; $D = nf_{amp} - 1$

System 3rd order SFDR has the maximum value when equation (5.3) is at a maximum, and this happens when,

$$g_{amp} = \sqrt{\frac{BC}{AD}} = \sqrt{\frac{\left(\frac{1}{iip3_{mix1}g_{mix1}} + \frac{1}{iip3_{amp}}\right)(nf_{opt}-1)}{\left(\frac{1}{iip3_{opt}} + \frac{g_{opt}}{iip3_{mix2}}\right)(nf_{amp}-1)}} \quad (5.6)$$

and,

$$sfdr3(max) = \left[\frac{m}{n_{th}\left(\sqrt{AC}+\sqrt{BD}\right)^2}\right]^{\frac{2}{3}} \quad (5.7)$$

Because $nf_{opt} \gg nf_{amp}$, so C>>D,

$$sfdr3(max) \approx \left[\frac{m}{ACn_{th}}\right]^{\frac{2}{3}}$$

$$\approx \left[\frac{n_{th}}{m}\left(\frac{1}{iip3_{opt}} + \frac{g_{opt}}{iip3_{mix2}}\right)nf_{opt}\right]^{-\frac{2}{3}} \quad (5.8)$$

In (5.8), if $m \geq 2$ and $\frac{1}{iip3_{opt}} > \frac{g_{opt}}{iip3_{mix2}}$, (5.9)

$$sfdr3(max) > \left(n_{th} * \frac{nf_{opt}}{iip3_{opt}}\right)^{-\frac{2}{3}} = sfdr3\ of\ intrinsic\ optical\ link \quad (5.10)$$

It can be seen from (5.10) that if the conditions in (5.9) can be satisfied by selecting suitable frequency mixers and pre-amplifier, the 3rd order SFDR of the system using quadrature-

multiplexed multiple sideband frequency translation technique can be higher than the intrinsic optical link.

5.3 Simulation results and link trade-offs

Using the layout as shown in Figure 5.1, simulations have been performed, assuming the intrinsic optical link has -33dB gain, 57.3 dB noise figure and 37.5dBm IIP3; each frequency mixer has 22dBm IIP3 and -8dB conversion gain. These values are the same with the experimental measurements in previous sections.

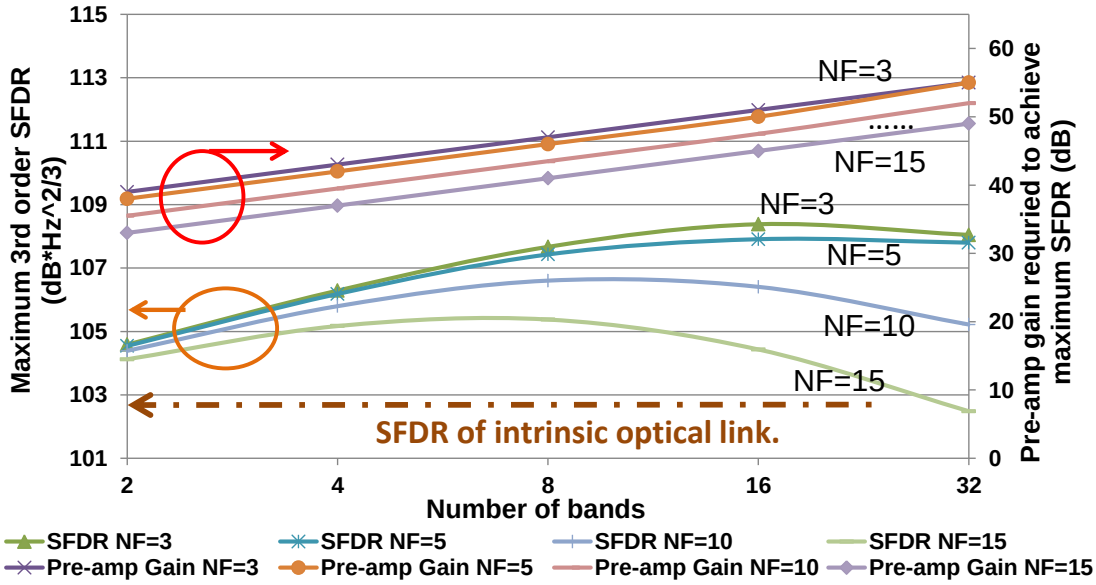

Figure 5.2 Simulation result: the system maximum possible 3rd order SFDR and pre-amplifier gain required to achieve maximum SFDR [99]

As shown in Figure 5.2, when the pre-amplifier has low noise figure, the system has to increase SFDR with the number of frequency bands. This is because the original MIMO signal has been spread into more frequency sidebands in the optical domain. And when these bands are combined back, the noise adds incoherently, but the signal adds coherently. As shown in equation (5.8), $sfdr3(max)$ rises with the number of sidebands (m).

On the other hand, to achieve the maximum SFDR, the required gain of pre-amplifier becomes higher with the number of frequency bands. This is because the overall mixers' conversion loss increases with the number of mixers used in the system and higher pre-amplifier gain is required to compensate the conversion loss of the mixers before the optical link. As shown in equation (5.6), because of using multiple frequency mixers, the mixers' overall conversion gain (g_{mix1} and g_{mix2}) and IIP3 ($iip3_{mix1}$ and $iip3_{mix2}$) will be lowered, meaning higher pre-amplifier gain (g_{amp}) will be required.

It can also be seen in Figure 5.2 that the pre-amplifier noise figure affects the maximum system SFDR. If the pre-amplifier noise figure>10dB, the maximum system SFDR does not increase much when there are more than eight bands. This is because, if the pre-amplifier has high noise figure, the output noise of the amplifier overtakes the optical link's noise floor in lower gain.

5.4 Experiment on the 3rd order SFDR improvement by trading optical bandwidth

A proof-of-principle experiment has been carried out using DSB and QSB frequency translation. A two-tone test has been performed at the 800MHz centre frequency, with a 1MHz frequency separation on one of the input channels with the other terminated, as shown in Figure 5.3. If both MIMO channels are occupied, the optimum pre-amplifier gain is lower so that the same composite power is presented to the optical link. However, the maximum SFDR is only slightly reduced since the optical ink is the most significant noise source, so the output noise is largely unaffected by the change in amplifier gain.

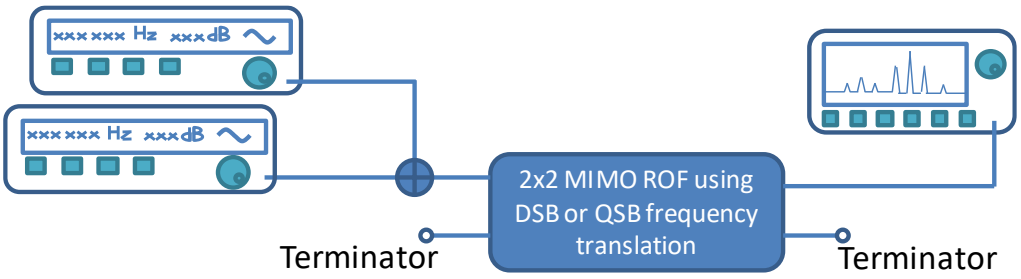

Figure 5.3 Experiment layout: two-tone test for 3rd order SFDR measurement of a 2x2 MIMO RoF system

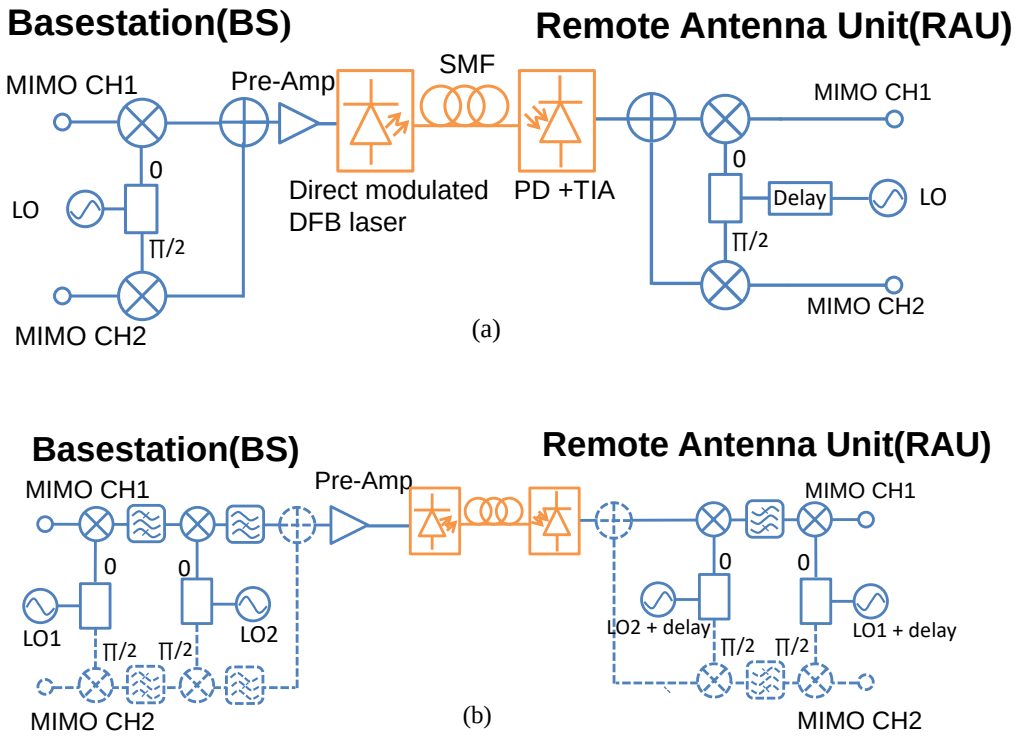

Figure 5.4 Layout for quadrature-multiplexed frequency translation system.

(a)DSB system (b)QSB system (dash line part is not used in SFDR test)

The layouts for the DSB and QSB systems are as shown in Figure 5.4 (a)(b). The optical link in the experiment uses a directly modulated DFB laser, a 500m SMF link and a PIN photodiode

with a transimpedance amplifier (TIA). The RF pre-amplifier has 40dB maximum gain and 10dB NF.

The experimental results for the SFDR measurement are shown in Figure 5.5. The 3rd order SFDR of the DSB and the QSB systems are 104.5 dB·Hz$^{-2/3}$ and 105.5 dB·Hz$^{-2/3}$ respectively, while the 3rd order SFDR of the intrinsic optical link is 102.8 dB·Hz$^{-2/3}$. Therefore, by using DSB and QSB frequency translation, the system 3rd order SFDR has been improved by 1.7dB and 2.7dB beyond that of the intrinsic optical link respectively. The results are achieved using a pre-amplifier gain of 30dB for the DSB system and 35dB for the QSB system. These results are in line with the theory presented above.

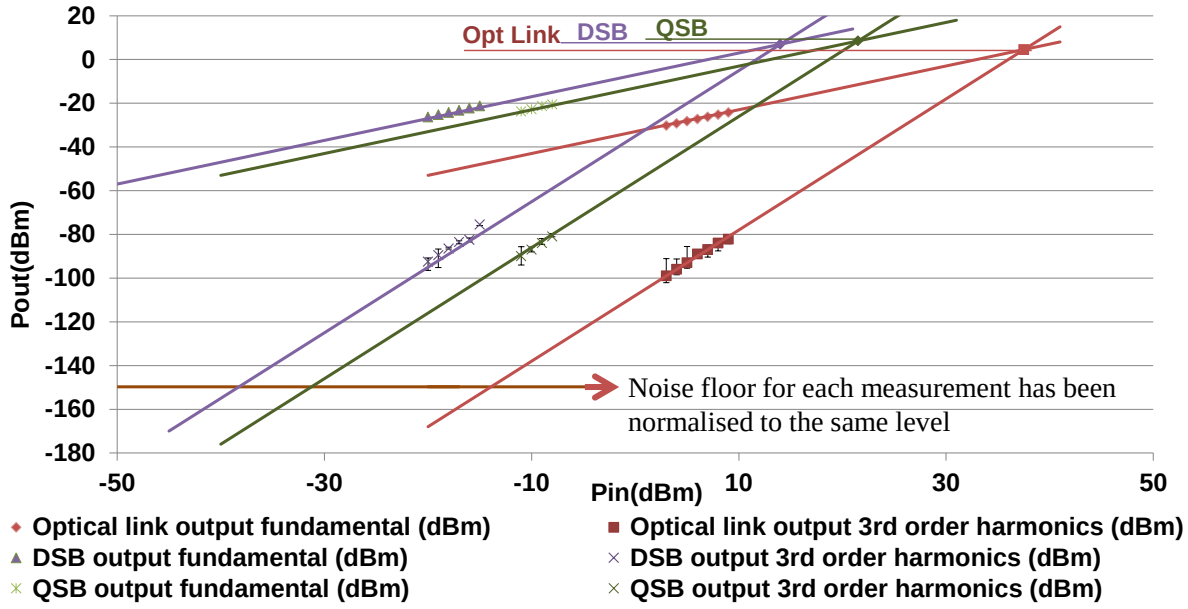

Figure 5.5 Experimentally measured 3rd order SFDR of DSB and QSB system at 800MHz centre frequency, comparing with intrinsic optical link

5.5 Simulation on the capability to transmit MIMO-type signals using QSB frequency translation

To show the system's MIMO capability, a simulation has been performed in VPItransmissionMaker^{TM} with the same QSB system layout as in Figure 5.4(b). The optical

link used in the simulation is identical to the experimental parameters in the SFDR measurement.

Two MIMO channels, with 20MHz bandwidth at the 800MHz carrier frequency and with 0dBm power have been simulated at the system input. The preamplifier gain has been chosen to be 30dB in the simulation. The mixer nonlinearity has been considered in the simulation by using nonlinear components with the same IIP3 (22dBm) as in the experiment. By selecting LO1 = 50MHz, LO2 = 1.0GHz, two MIMO channels are orthogonally multiplexed into four frequency bands, respectively centred at 150MHz, 250MHz, 1.75GHz and 1.85GHz. The 90° hybrid couplers used in the simulation have 3° phase error, which is a typical worst value in a commercial product [83]. Figure 5.6 shows the constellation diagram of the received 64QAM signals. The optimum EVM for both channels are ~1%, which is well below requirement in the LTE standard.

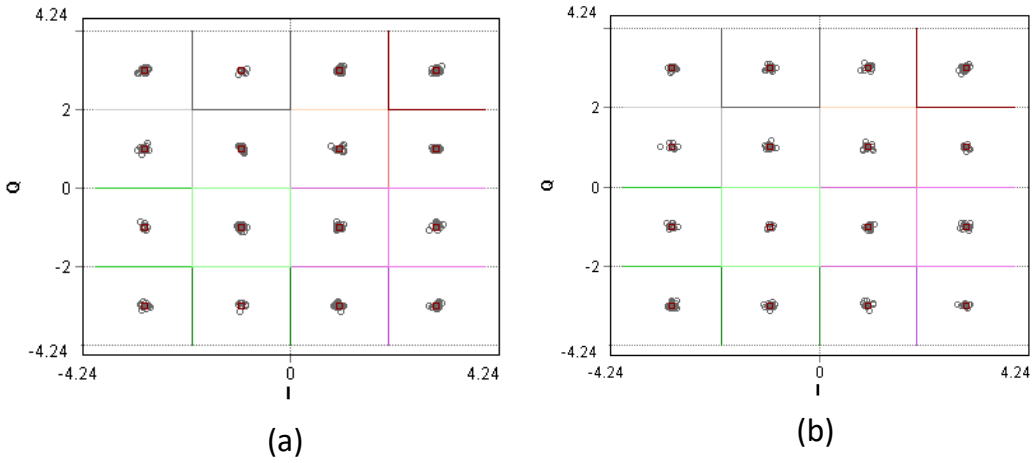

Figure 5.6 Simulation result: received 64QAM constellation diagram using QSB, (a)channel 1 EVM = 2.45% (b)channel 2 EVM = 2.50%

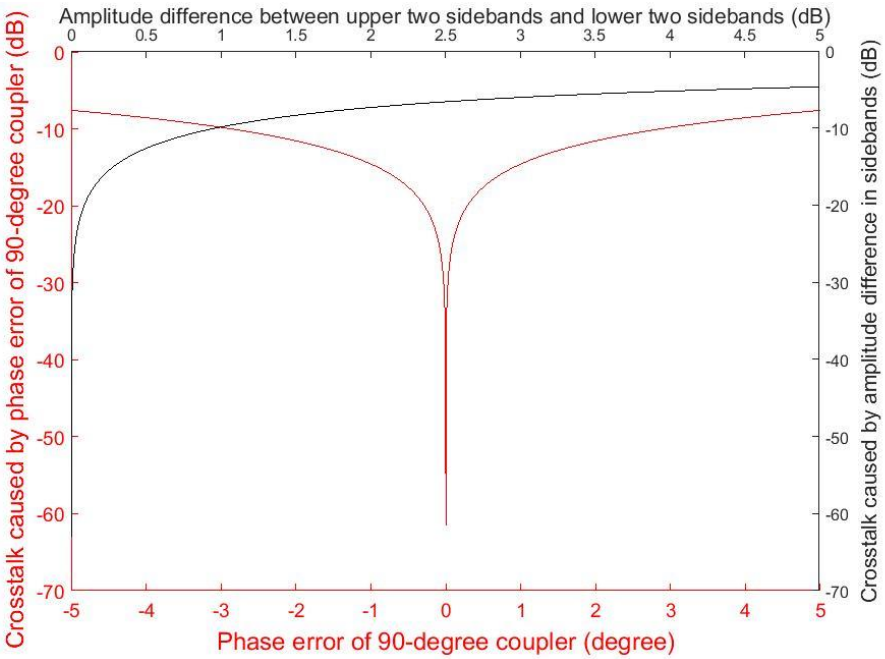

Figure 5.7 System crosstalk vs phase error in 90-degree hybrid couplers for a QSB system.

The crosstalk between two MIMO channels depends on the phase error in the 90-degree hybrid couplers and the amplitude variance among four sidebands as shown in Figure 5.7. If the phase error of the 90-degree hybrid coupler <3°, the crosstalk due to the coupler <-10dB. If the amplitude difference among four sidebands after frequency translation need to be within 1dB, the crosstalk due to the amplitude imbalance <-10dB.

5.6 Summary and conclusion

In a quadrature-multiplexed frequency translation system, two MIMO channels are translated into several frequency bands and multiplexed with each other in quadrature. When the signals from these frequency bands are converted back to the original MIMO signal, the signal power adds up coherently, but the noise power adds in-coherently, giving system higher SNR. Thus the SFDR can be improved. This shows that the optical link bandwidth can be traded for the system SFDR.

In this chapter, the theory for the SFDR improvement in a quadrature-multiplex frequency translation system has been mathematically illustrated. By increasing the number of sidebands in the optical link, the system SFDR can be improved. The major limitations of the

improvement include: i) higher pre-amplifier gain is required to compensate the mixers' conversion loss when the original RF signal is translated into more sidebands; ii) the pre-amplifier noise figure limits system's the highest SFDR; iii) frequency mixers introduce additional nonlinearity products and conversion loss.

Simulations and experiments have been performed, showing that by using DSB and QSB frequency translation, the system can be improved beyond the intrinsic link. The DSB system can improve the system 3rd order SFDR from 102.8dB/Hz$^{2/3}$ to 104.5 dB/Hz$^{2/3}$, while the QSB system has 105.5dB/Hz$^{2/3}$ SFDR3. If the pre-amplifier noise figure>10dB, it is not worth to translate the original RF signal into more than eight sidebands.

Chapter 6 Hybrid DAS using Digital and Analogue RoF

6.1 Introduction

In an analogue RoF system, the loss of SNR and linearity occurs in most of the system stages. In a digital RoF system, however, because the RF signal is digitised, as long as the receiver can recognise the digital signal, the signal quality is not critically affected by the analogue degradation in the optical link. Thus, the digital radio over fibre system has higher dynamic range than the analogue RoF system, but because of the analogue-to-digital (ADC) and digital-to-analogue (DAC) conversion, the digital RoF has higher component cost [100]. However, the comparison between the prices of these two systems is not straightforward. Although the digital DAS has a higher price in ADC and DAC, its greater dynamic range means that each of the RAUs can cover larger areas than the analogue DAS [101]. Moreover, in the digital DAS, standard SFP transceivers can be used [102], making the system's transceivers lower cost than the analogue DAS. On the other hand, in the digital DAS, the high data rate after sampling occupies a high bandwidth [103]. It makes the system hard to cope with the MIMO signals.

In a service-agnostic DAS, multiple wireless services need to be transmitted to the RAUs. In the digital DAS, every service needs to be down-converted and digitised (as illustrated in Section 1.1.3 Figure 1.9), meaning that the system cost increases with the number of services. The digital RoF system has a dynamic range advantage over the analogue RoF, especially for the wide bandwidth services, such as 4G LTE. However, because the 2G/3G services have the relatively narrower bandwidth, the improvement of using digital RoF over analogue RoF is less critical. It is meaningful to have a hybrid digital and analogue DAS to remove narrow bandwidth services from the digital link to the analogue link to lower system's overall cost.

In this chapter, an analogue and digital hybrid DAS is proposed, in which the 3G services are transmitted over the analogue RoF link, and the 4G SISO LTE service is transmitted over the digital RoF link. The proposed hybrid DAS has a lower cost than both the digital DAS and the analogue DAS.

6.2 Proposed hybrid DAS system

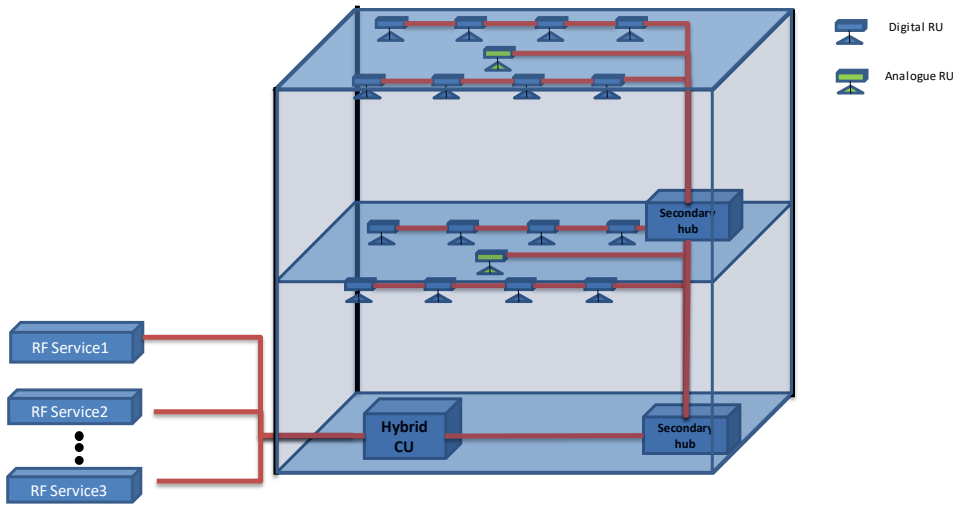

Figure 6.1 Architecture of a hybrid DAS using digital and analogue RoF

The idea of hybrid DAS is to use both the analogue RoF and the digital RoF in the same DAS infrastructure, as shown in Figure 6.1. Different wireless services are connected to the points of interface (POI) or the analogue input port in the central unit (CU) of the hybrid system, as shown in Figure 6.2. The 2G and 3G services are routed through the analogue RoF link, while the 4G LTE service is sent through the digital RoF link. Inside the hybrid central unit, each of the services is delivered by separate service cards. Each of the service cards consists of the signal processing units and optical transceivers. The analogue signal and the digital data are then combined in the CU and sent to the secondary hubs over the same optical fibre. At the secondary hub, the digital and the analogue services are separated and respectively delivered to the analogue/digital remote units (RUs).

At the digital remote units, FPGAs and DACs are required to convert digitised service signal back to the original form, while at the analogue remote units, no digital signal processing is needed. As shown in Figure 6.1, the analogue RUs are more sparsely installed than the digital RUs, in which 4G services are transmitted. This is because the coverage area for the 2G/3G services is much wider than the 4G service at the same power level.

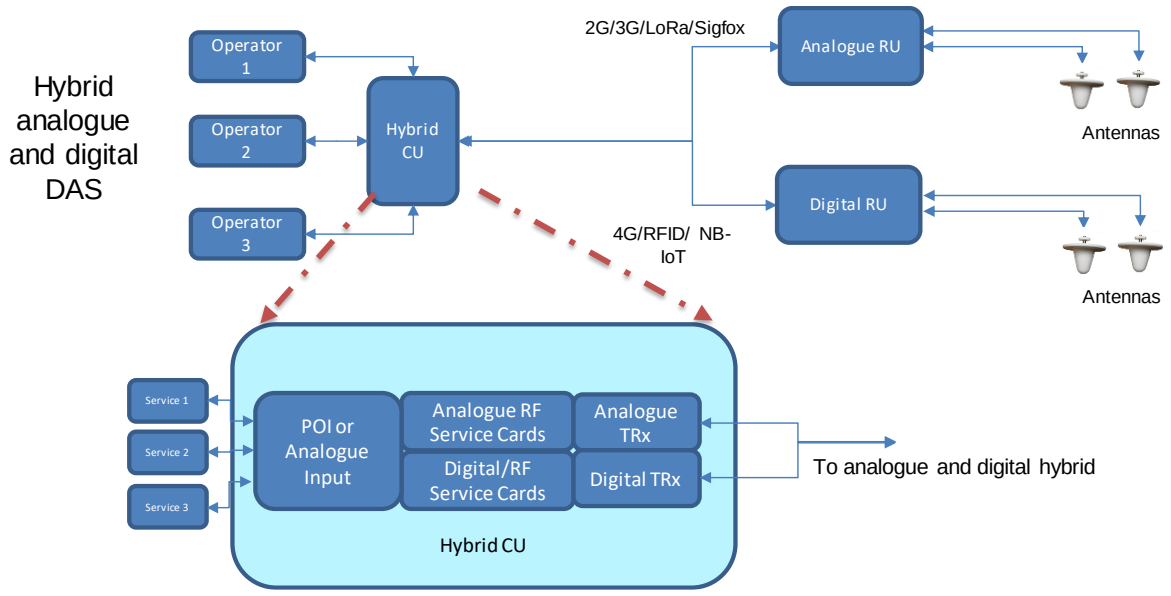

Figure 6.2 Concept for the analogue and digital hybrid RoF [104]

Compared with the traditional analogue or digital RoF system, the cost advantage of the hybrid system is driven by three aspects, which are:

a) The reduction in the number of service cards inside the D-RUs by removing the 2G/3G services from the digital link.
b) Compared with traditional analogue DAS, the fewer number of A-RUs is required.
c) Lower number of 4G signal sources (or base stations) is needed, compared with analogue DAS.

6.3 Signal processing in the digital link

The 3GPP LTE standard defines the LTE with large bandwidth (up to 20MHz) [105] for a single user, meaning that the LTE service suffers from greater performance degradation than the UMTS service when transmitted over an analogue radio over fibre system. Practically, the DAS needs to send service signals from various mobile operators. Take China as an example, as shown in Table 4.3, the total LTE bandwidth from three major mobile operators in China is >400MHz. In a digital radio over fibre system, by using the common public radio interface (CPRI), the data rate generated after digitising is ~20 to 30Gbps [106]. In the proposed digital RoF system, 3-time data compression ratio can be achieved, meaning that the data rate generated by the DRoF system is <10Gbps for all LTE SISO services in China.

In the proposed digital link, the RF service signals are first down-converted to an intermediate frequency (IF) band, which is 31.25MHz here [107]. This IF band is chosen because an ADC samples it with 125 MSPS sampling rate and the IF band is at the centre of the Nyquist zone. The ADC used here has 14-bit resolution.

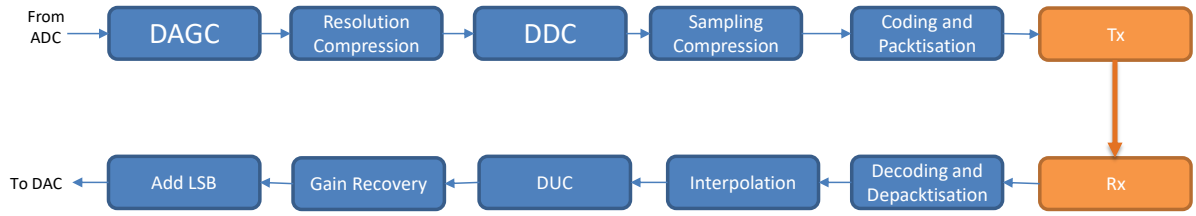

Figure 6.3 Digital signal processing in the DRoF link [104]

After the ADC, digital signal processing is done in an FPGA, in which data rate is compressed using the sampling and quantisation compression [107] as shown in Figure 6.3. A resolution compression is done to compress 14-bit digitised IF signal to the 8-bit data stream while maintaining the signal quality. A digital down conversion (DDC) is then applied to convert compressed IF signal to baseband. Following the DDC, the baseband signal is re-sampled at lower clock rate – 25MHz here. The whole data compression process compresses the data rate from 125MSPS*14bit = 1.75Gbps (at the ADC output) to 25M*8*2 Mbps =400 Mbps for a

20MHz bandwidth LTE channel. The compressed data is coded and then transmitted in serial by an SFP optical transceiver.

At the receiver side, another SFP optical transceiver is used to convert the optical baseband signal back to the electrical domain. After interpolation, the baseband digital signal is digital up-converted to the IF band (in the digital domain). Then the 14-bit data is reconstructed according to the compression bit width by adding the least significant bits (LSB) [107].

The recovered digital data is converted back to the analogue IF band by an analogue to digital converter (ADC) and then upconverted to the original service signal an analogue signal upconverter.

6.4 Simulation of the analogue link

In the analogue and digital hybrid RoF system, because two systems are combined using optical couplers, the loss from the optical coupler can lower the RF performance in the analogue link. A simulation is done in the VPItransmittionMaker®, comparing the analogue RoF link performance in the traditional analogue RoF system (Figure 6.4 (a)) and the hybrid RoF system (Figure 6.4 (b)). A CW DFB laser emitting at a 1530nm wavelength and 10dBm optical power has been used to create the interference from the digital link. The analogue input signal has been pre-amplified before it is directly modulated onto a DFB laser, emitting at a 1550nm wavelength and 6dBm optical power. The DFB laser performance used in the analogue link simulation is identical to the laser used in the experiment. Two optical couplers in the optical link have a 3.5dB loss for each.

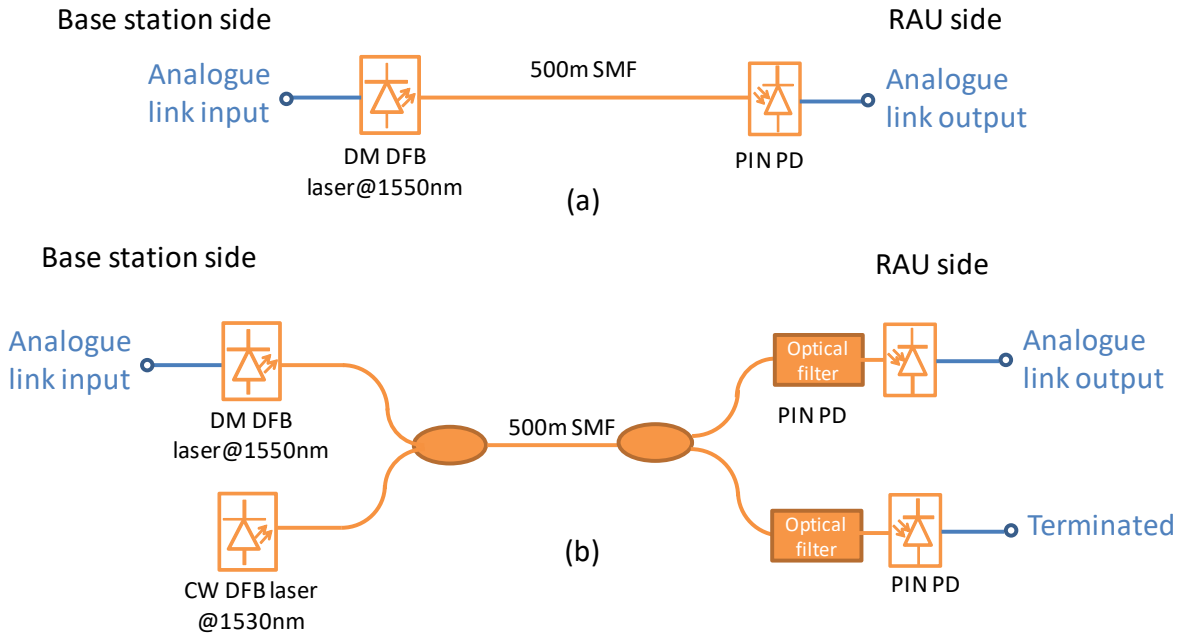

Figure 6.4 Simulation layout for the analogue RoF link: (a) in the traditional analogue RoF system; (b) in the hybrid RoF system

A two-tone test is performed in the simulation at 1800MHz UMTS frequency band. Giving the 0dBm input signal power, the spectrum at analogue link output is as shown in Figure 6.5. The OIP3 for the traditional analogue SISO RoF link can be calculated to be -3.23dBm. If the hybrid system is used, the OIP3 of the analogue link drops to -17.25dBm in the simulation. This is caused by the 7dB optical power loss in the optical link.

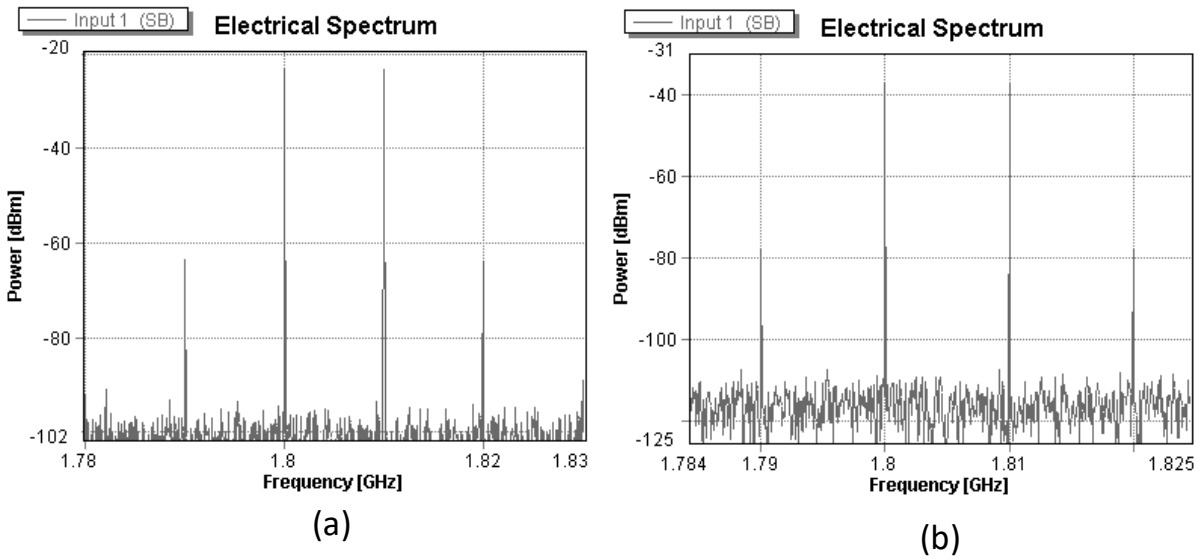

Figure 6.5 Two-tone test simulation result: (a) traditional analogue RoF link; (b) analogue RoF link in the hybrid system (7dB loss for two couplers included)

The output noise floor at the analogue link output is -147.1dBm/Hz for the traditional SISO system and -160.9dBm/Hz for the hybrid system. The 3rd order SFDR of both systems can be derived respectively to be 95.91 dB*Hz$^{-2/3}$ and 95.76 dB*Hz$^{-2/3}$.

Similarly, the second order output interception point (OIP2) for the analogue link in the traditional system and the hybrid system are respectively -9.6 dBm and -23.4 dBm. The SFDR2 for both systems are 68.75 dB*Hz$^{-1/2}$ and 68.74 dB*Hz$^{-1/2}$.

Both systems have similar the 3rd order SFDR and the 2nd order SFDR. This is because the noise of the directly modulated laser is the dominant noise source in the optical link. When the optical power loss from the optical couplers is small, it lowers the RF power and the system RF noise floor simultaneously. Thus it does not decrease the system SFDR, and the optical amplifier is not required in the system.

As shown in Figure 6.6, the optical loss does not significantly influence the value for OIP2 – output noise floor when it is <10dB. If the optical loss >14dB, an EDFA can be used to improve the system's linearity.

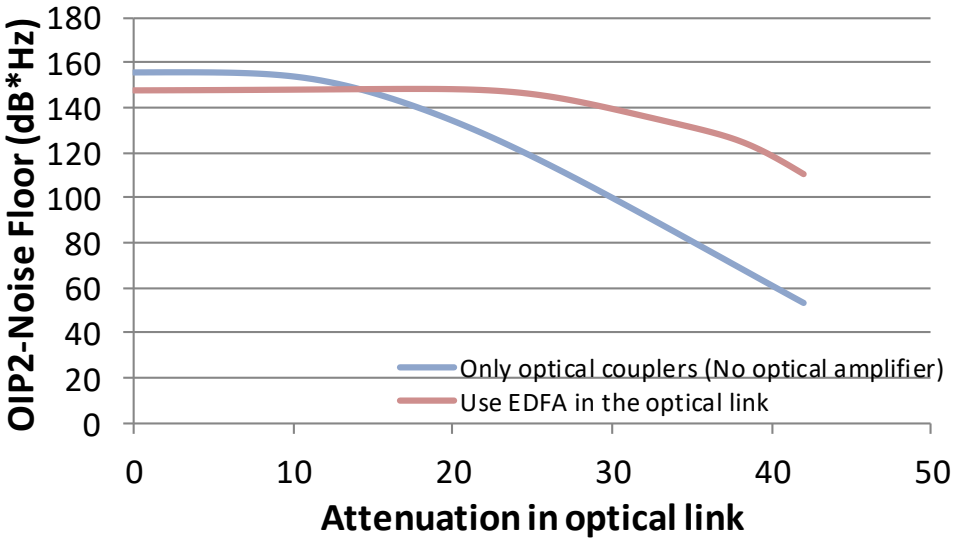

Figure 6.6 OIP2-Noise floor vs optical link loss

6.5 Experimental layout and test results

The analogue and digital hybrid RoF has been demonstrated experimentally, as shown in Figure 6.7. Vector signal generators have been used to produce the 3G and 4G service signals at the input end of the system. The 3G signal used here is WCDMA QPSK with 1800MHz carrier frequency and 3.84MSymbol/s symbol rate. The 4G signal used here is LTE test model 3.1, with 20MHz channel bandwidth.

In the analogue link, a pre-amplifier with 35dB power gain is used to provide the system with optimum performance. The amplified 3G signal is then directly modulated onto a 1550nm wavelength DM DFB laser emitting at ~6dBm optical power.

In the digital link, at the transmitting side, the 4G LTE signal is sampled by an analogue to digital converter (ADC) and to the FPGA, in which a data compression algorithm as illustrated in section 6.5 has been performed, including resolution compression and sampling compression as shown in Figure 6.7. The compressed digital data is then transmitted via the optical link by

a DFB laser emitting at 1530nm wavelength. Both the analogue link and the digital link are combined in optical domain by an optical coupler, then sent to the remote end via a 500km SMF.

At the remote end, the optical signals of the analogue and digital link are split and filtered out into two ways and separately received by photodetectors. They are then converted back to the original 3G and 4G signals at the remote end. A vector signal analyser is used to test the recovered signals. A picture showing the experimental setup has been presented in Figure 6.8.

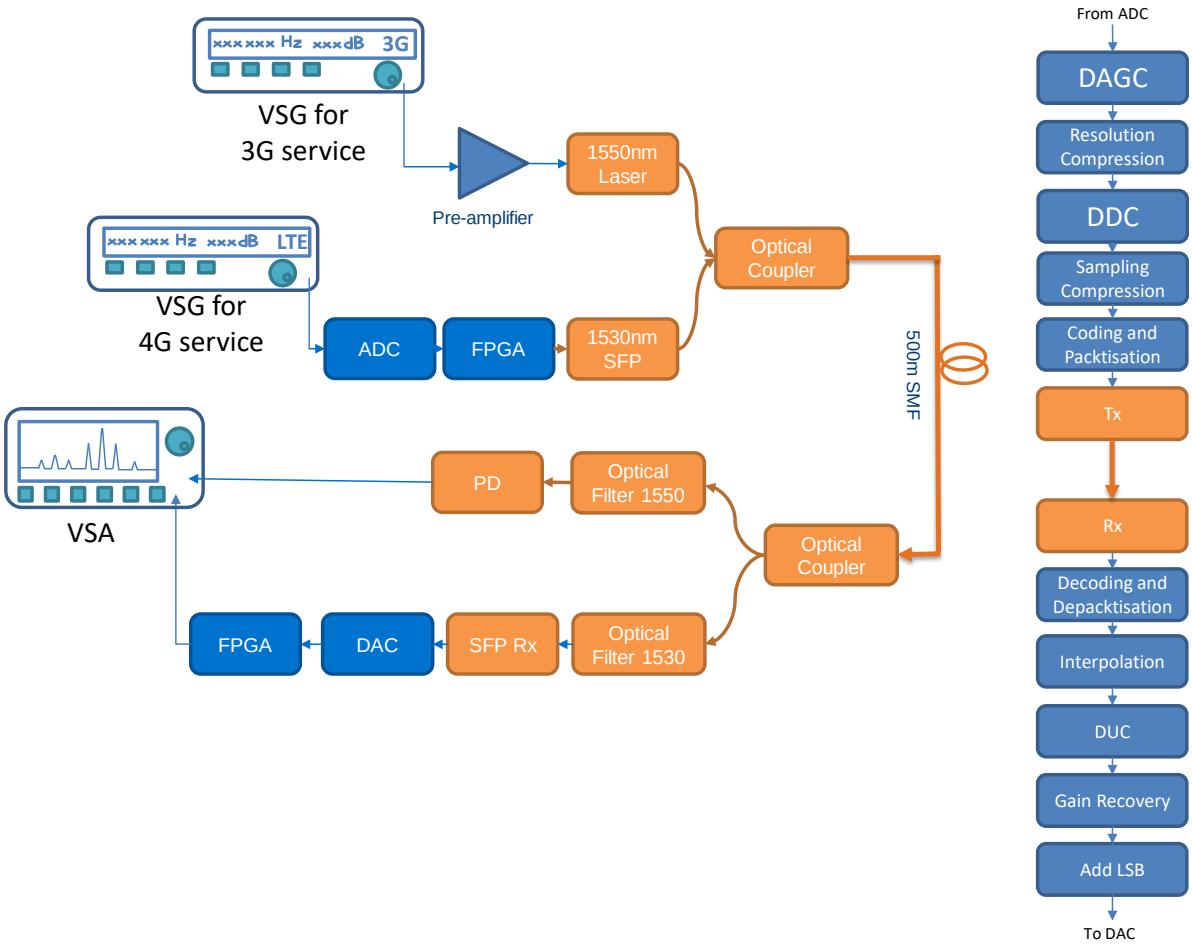

Figure 6.7 Experimental layout for analogue and digital hybrid RoF system.

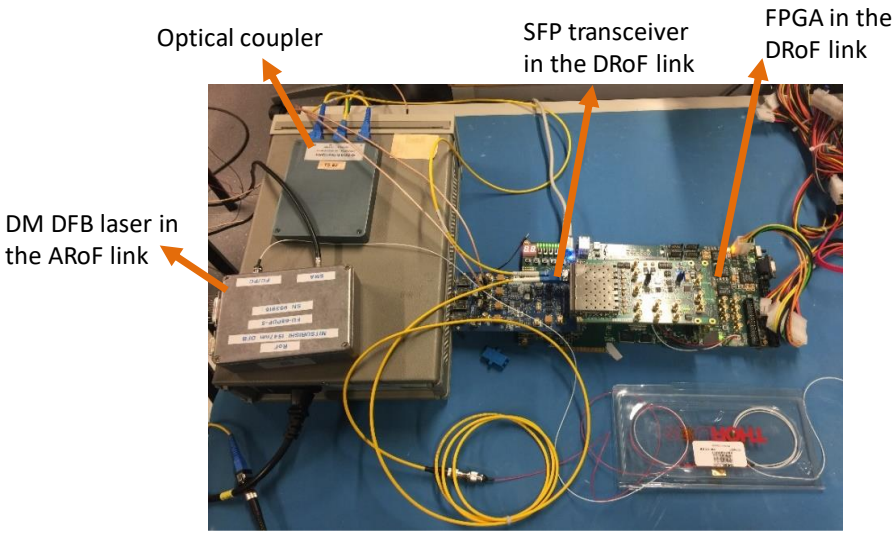

Figure 6.8 Experiment setup for hybrid RoF link

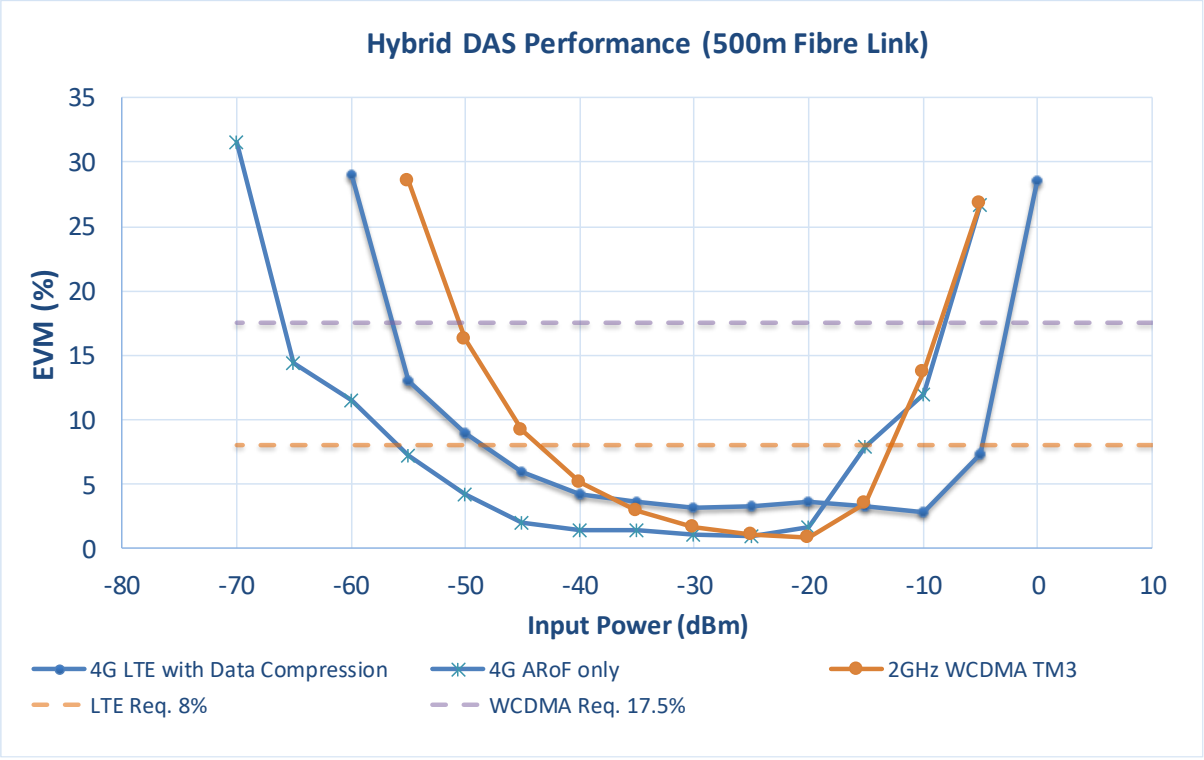

Figure 6.9 EVM dynamic range of the analogue and digital RoF system

Experimentally, the EVM dynamic range for both the analogue RoF link and the digital RoF link have been tested as shown in Figure 6.9. The 3G WCDMA service has ~42dB EVM

dynamic range without using AGC, and the 4G LTE service has ~43dB EVM dynamic range without using AGC. By using digital RoF, the link dynamic range of the 4G LTE service has been improved to be a comparable value as the 3G service. Meaning that, if the hybrid system is compared with the analogue system, the users can get better service for the 4G system. If it is compared with traditional digital RoF system, the hybrid system only does the DSP for the 4G service, but leave the other services in analogue, meaning that the cost for the ADC/DAC and FPGA can be lowered.

6.6 Summary and Conclusion

In a DAS, if the 4G signals and the 3G signals are treated equally, the 4G services will have poorer coverage. By using the analogue and digital hybrid RoF system, the system can have improved QoS without critically increase the cost.

In this chapter, we have proposed a layout for the analogue and digital RoF hybrid DAS. In the digital link, resolution and sampling rate compression have been used, giving the system 3-time compression ratio compared with CPRI. The digital and analogue RoF links are combined using optical couplers.

Simulations show that the optical couplers give the system 7dB optical power loss. However, system's 2^{nd} order and 3^{rd} order SFDR is not significantly lowered (<0.5 dB). This is because the laser diode's RIN is dominant noise source in the system and the optical loss decreases the signal power and noise power simultaneously. Experiments have been carried out transmitting the 4G signal over the DRoF link and the 3G signal over the ARoF link. The experiment result shows that the 4G LTE and 3G WCDMA services have comparable EVM dynamic range in the proposed hybrid RoF system, respectively 43dB and 42dB.

The hybrid DAS potentially has a lower cost than traditional digital or analogue DAS because of three reasons: i) it reduces the number of service cards in the DDAS; ii) reduces the number of RAUs in the ADAS; iii) it reduces the number of signal sources required in the ADAS.

6.7 Acknowledgement

The work in Chapter 6 is the outcome of the calibration with Dr Tongyun Li. The idea of hybrid DAS is generated by Dr Tongyun Li and he designed the hardware and the software part of the digital link in the hybrid system. The author designed and simulated the analogue part of the hybrid system. Both Dr Tongyun Li and the author got involved in the experiments.

Chapter 7 Conclusion and Future Work

7.1 Thesis Summary

A. Motivations

Nowadays the 3G and 4G services are widely deployed, and in the future 5G era, the high capacity wireless communication techniques, such as MIMO will be broadly implemented. Indoor areas, where 80% of the wireless data traffic originates, are difficult to be covered using wireless signal [108]. It is, therefore, necessary to find a cost-effective solution to cover the indoor area by multiple wireless services.

This thesis aims to develop a low-cost solution for next-generation indoor wireless coverage. Among currently available solutions, such as signal repeaters, small cells and distributed antenna systems, the DAS has many benefits: i. Each of the RAUs works together so no inter-cell interference; ii. It delivers the RF signals and does not require the baseband information from the mobile service operators so that it can be operated by neutral hosts, such as the owners of public infrastructure, commercial real estate and enterprises; iii. the DAS is also service-agnostic and broadband, making it suitable for extensive public areas with high user density.

Nowadays, a straightforward solution to transmit MIMO signals over the DAS is to deliver each of the MIMO channels using different strands of fibres (space division multiplexing). This solution gives the system high installation cost, makes it difficult to upgrade current SISO DAS into the MIMO DAS.

B. Principles of DSB frequency translation 2x2 RoF system

For all these reasons, the author developed a low-cost DSB frequency translation system, which can upgrade the current SISO DAS infrastructure into MIMO DAS without installing parallel optical fibres. In the DSB frequency translation system, two MIMO channels were multiplexed

with each other in quadrature, so that the powers in both sidebands after frequency mixing can be kept. The author investigated the performance of the system. The following problems can cause the crosstalk in the MIMO RoF system using DSB frequency translation:

i. The phase error of the 90-degree hybrid coupler;
ii. The amplitude imbalance between the upper sideband and the lower sideband of the frequency mixing products, which is caused by the S21 vibration in the pre-amplifier and the optical link;
iii. The signal's group delay when transmitting from the BS station to the RAUs.

The first problem is caused by the component quality. Usually, the phase error for a commercial 90-degree hybrid coupler can be <2°. The second problem is caused by the modulation bandwidth of the DM DFB laser and the dispersion if it is in an MMF link. A power equaliser has been designed to compensate some of the amplitude imbalance in two sidebands so that the system can operate in LTE bandwidth. The third problem can be overcome by adding a phase shifter to adjust the LO phase at the RAUs.

Experimentally, the DSB frequency translation system was demonstrated to work for LTE signals, and compared with the traditional SSB frequency translation system, the DSB system has higher 1.7dB 3rd order SFDR and effective EVM dynamic range. The system is well conditioned in the power equaliser bandwidth, which is 610MHz to 750MHz in the experiment, meaning the crosstalk between two MIMO channels can be well compensated in this range.

C. Broadband implementation of DSB frequency translation MIMO RoF system

To make the DSB frequency translation system service-agnostic, the author investigated the frequency spectrums in the major countries in world, finding that there are some frequency spectral regions that are reserved for particular uses, such as aeronautical communication and satellite communication. Signals from these frequency bands are not usually required to be

delivered over the DAS. By translating the original MIMO signals into these frequency bands can avoid the overlap between the signals after the frequency translation and other services in the DAS, so that the system can be broadband and service-agnostic. In the UK, US and China, a 2.2 GHz LO can be used to make sure all the LTE frequency bands to be translated into unoccupied bands over DAS. In the other countries, similar but different LO frequencies can be found.

To show the feasibility of the system, a demonstration was made using a 2x2 Wi-Fi MIMO. The MIMO signals and the LO signal was successfully delivered from the central unit to the RAU via a 500m SMF link using the DSB frequency translation. The client can receive the MIMO signals from the RAU with high throughput.

D. SFDR improvement using multiple sidebands quadrature-multiplexed frequency translation technique

By extending the idea of the DSB frequency translation, the MIMO signal can be converted into more than two sidebands so that the SFDR of the RoF system can be further improved. It has been theoretically shown that the DSB and QSB system can improve the system 3rd order SFDR beyond the intrinsic optical link. If an ideal pre-amplifier and mixer are used, the DSB and QSB system can give the system respectively 2dB and 3dB 3rd order SFDR improvement. If the original signals are translated into more sidebands, higher pre-amplifier gain is required to compensate the conversion loss of the frequency mixers. Limited by the noise figure of the high gain amplifier, if the amplifier NF>10dB, the 3rd order SFDR improvement does not increase when the original signals are translated into more than eight sidebands.

Experimentally, the DSB system gives ~1.7dB improvement, while the QSB system can give ~2.7dB increase. The degradation comes from the pre-amplifier noise figure and the nonlinearity of the mixers and the pre-amplifier. The simulation shows the system can support MIMO radio over fibre.

This shows that the optical bandwidth can be traded for the RF SFDR and at the same time, MIMO operation can be supported.

E. Hybrid DAS using analogue and digital RoF

The 3GPP standards have defined wider bandwidth in 4G services than the 3G. Thus if they are treated equally, the wideband 4G services can cover less area than the 3G. Traditional digital radio over fibre system has higher dynamic range than the analogue system but generates a large amount of data when digitising the RF signals. Because the 3G services have relatively narrow bandwidth, the dynamic range improvement by using DDAS is not critical. However, if all the 3G services are to be transmitted using the DDAS, many service cards will be required, giving the system high-cost. Therefore, it is meaningful to transmit 2G and 3G services in the analogue DAS to lower the system cost.

The hybrid analogue and digital radio over fibre system transmit the 4G LTE services in digital while keeping the 3G services in analogue. Compared with the traditional digital DAS and analogue DAS, the hybrid DAS reduces the cost in three means: i) reduces the number of service cards in the DDAS; ii) lowers the number of RAUs in the ADAS; iii) reduces the number of the signal sources required in the ADAS.

The hybrid DAS combines and separates the DRoF and the ARoF links in optical domain by using optical couplers. Simulation shows that the optical power loss introduced by the optical couplers does not significantly decrease the signal SFDR (<0.5dB). Experimentally, by using the hybrid system, the EVM dynamic ranges of the 20MHz bandwidth LTE service in the digital link and 3G WCDMA service in the analogue link are respectively 43 and 42 dB.

7.2 Potential future work

While this thesis has introduced low-cost solutions for next-generation indoor wireless coverage, more research can be carried out to achieve an ultimate deployment of the future DAS.

A. Higher MIMO dimensions on RoF

The 5G era is coming in 2020 and now is the critical transition time from 4G to 5G technology. One of the important solutions to get high capacity in the 5G era is to use a large number of MIMO channels. In the mobile world congress in 2017 (MWC 2017), mobile device vendors have demonstrated their attempts to achieve high dimension MIMO communication. For example, ZTE® has demonstrated their massive MIMO macro basestation solutions with 128 antennas [109]. However, limited by the size of the mobile devices and the wavelength of the mobile signal carrier frequency, it is hard to install high dimension MIMO receivers inside the mobile devices. The current ZTE® Gigabit Phone use 4x4 MIMO and carrier aggregation to achieve Gbps wireless communication [110].

In this thesis, a low-cost 2x2 MIMO RoF system using DSB frequency translation has been demonstrated. There is a strong driver to extend the 2x2 MIMO RoF system into higher dimensions. There are several challenges:

i. In [64], the authors have proposed a 3x3 MIMO RoF system by using DSB frequency translation for two of the MIMO channels, while keeping the third MIMO channel at its original frequency, as shown in Figure 7.1. Practically, because of the RF signal leakage in the frequency mixers, the signal leakage from the first and the second MIMO channels remains in the same frequency band with the 3rd MIMO channels. Therefore, filters must be used to prevent the 3rd MIMO channel from the crosstalk.

   However, because the LTE frequency bands cover from 700MHz to 3.5GHz, different filters need to be installed for different LTE frequency bands. These filters will prevent the system from being agnostic. A method needs to be found out to address this problem.

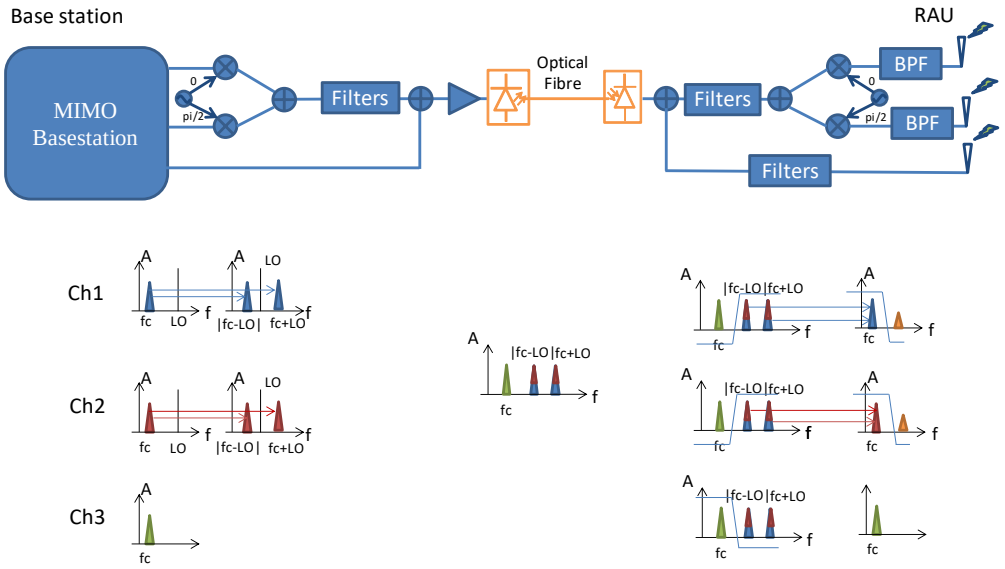

Figure 7.1 3x3 MIMO RoF system using DSB frequency translation [64]

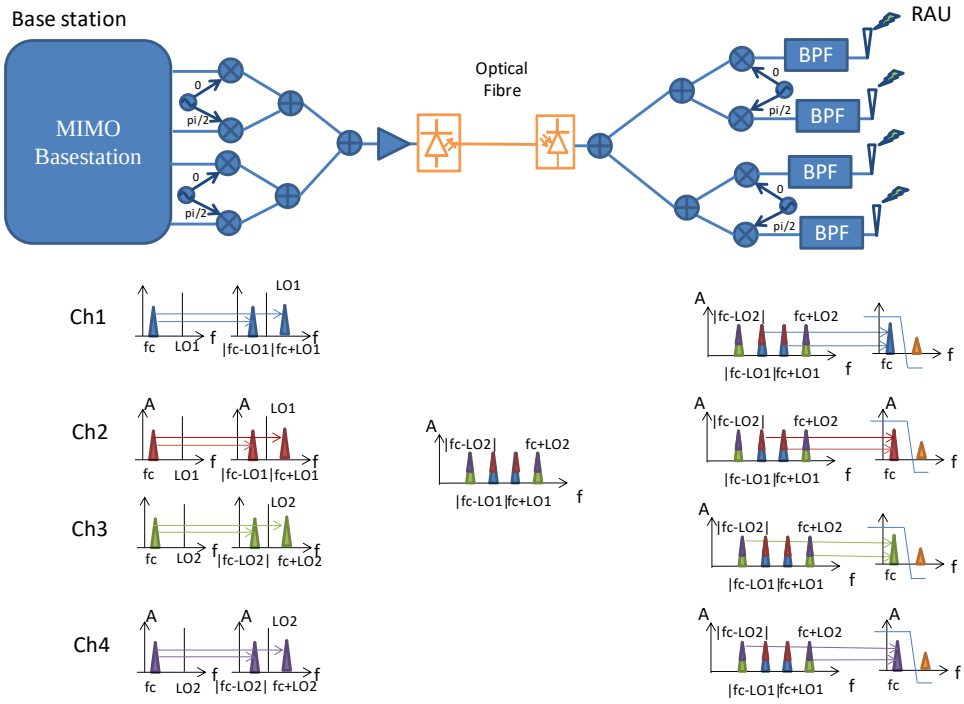

Figure 7.2 4x4 MIMO RoF system using DSB frequency translation

ii. For the case of 4x4 MIMO radio over fibre system, two pairs of LOs need to be used, as shown in Figure 7.2. Each of the local oscillators translates and quadrature-multiplex two MIMO channels. The four MIMO signals after the frequency translation respectively occupy the frequency bands at $fc+f_{LO1}$, $|fc-f_{LO1}|$, $fc+f_{LO2}$ and $|fc-f_{LO2}|$.

Compared with the 2x2 system, the LOs and MIMO signal channels are more likely to create nonlinear products in the 4x4 system. Therefore, the system needs to be more carefully designed.

iii. As mentioned in Chapter 4, many frequency bands are not transmitted over the DAS. 2x2 MIMO signals can be translated into these frequency bands to avoid the overlap with other services over the DAS. However, when there is a higher number of MIMO channels, it is harder to translate all MIMO signal channels into the limited unoccupied frequency bands. Thus, a new frequency map needs to be designed. For the case of massive MIMO, the techniques such as WDM and SCM hybrid system can be used to extend the system bandwidth in the optical domain [111].

B. The convergence of multiple networks including MIMO and IoT networks.

The next generation mobile network (5G) not only have higher capacity than the 4G network but also provides better device-to-device (D2D) connectivity [112]. It has been predicted that entire internet of things (IoT) market will be over $1.7trillion by 2019 [113]. The IoT infrastructure revenue generated in 2015 was approximately $330 billion and is projected to reach $453 billion by 2020 with a CAGR of 6.2% [114]. For the future indoor wireless signal coverage, the traditional cellular network can no longer satisfy users' requirements. The DAS should be a transparent and seamless platform for various of wireless standards, including the IoT services.

The integration of the IoT services over the DAS is necessary. This will include:

i. The integration of multiple-operator cellular networks.

ii. Analogue and digital hybrid DAS, including MIMO: In chapter 6, a hybrid analogue and digital DAS for SISO signals have been proposed. However, as the DRoF generates high data rate when digitising, it is a very high cost to transmit MIMO signals using DRoF. Integrating MIMO analogue RoF system with the DRoF can be a cost-effective way for next-generation indoor wireless coverage.

iii. The integration of the IP interfaces from the IoT services to the DAS: The analogue DAS has many advantages in some certain scenarios. However, many IoT services are transmitted through the IP networks [115]. Thus, it is necessary future indoor wireless coverage infrastructure to support both the mobile cellular networks and IP networks on the same infrastructure.

References

[1] T. S. Rappaport, Wireless Communications: Principles and Practice,, Upper Saddle River, N.J.: Prentice Hall, 2002.

[2] mobiForge "Global mobile statistics 2014 Part A: Mobile subscribers; handset market share; mobile operators, " may 2014. Internet: http://mobiforge.com/research-analysis/.

[3] “GSM World Coverage Map and GSM Country List,” WorldTimeZone, 6 July 2017. [Online]. Available: http://www.worldtimezone.com/gsm.html. [Accessed 10 September 2017].

[4] Evolutionary Study and Performance Analysis of Generations in Wireless Technology, International Journal of Scientific & Engineering Research, Volume 4, Issue 6, June-2013 883.

[5] Cisco, Cisco Visual Networking Index: Global Mobile Data Traffic Forecast Update, 2016–2021, [Online] Available: http://www.cisco.com/c/en/us/solutions/collateral/service-provider/.

[6] CISCO. "Cisco Visual Networking Index: Global Mobile Data Traffic Forecast Update, 2013–2018". Internet: http://www.cisco.com/c/en/us/solutions/collateral/service-provider/visual-networking-index-vni/white_paper_c11-520862.html, Feb. 5, 2015[April. 5].

[7] "Building Repeater Systems," AlternativeWireless, 2017. [Online]. Available: http://www.alternativewireless.com/resources/cell-signal-improvement/building-signal-boosters-help/building-repeater-systems.html. [Accessed 10 September 2017].

[8] "Cisco Visual Networking Index: Forecast and Methodology, 2016–2021," CISCO, 6 June 2017. [Online]. Available: https://www.cisco.com/c/en/us/solutions/collateral/service-provider/visual-networking-index-vni/complete-white-paper-c11-481360.pdf. [Accessed 10 September 2017].

[9] "Home Signal Support," 3 mobile, 2002. [Online]. Available: http://www.three.co.uk/Support/Devices/Phones/Home/Signal_Black. [Accessed 22 September 2017].

[10] "Ericsson Radio Dot System," Ericsson, 2017. [Online]. Available: https://www.ericsson.com/ourportfolio/networks-products/radio-dot-system?nav=fgb_101_0561%7Cfgb_101_0516%7Cfgb_101_0526. [Accessed 10 September 2017].

[11] "LampSite," Huawei, 2017. [Online]. Available: http://carrier.huawei.com/en/products/wireless-network/small-cell/lampsite. [Accessed 10 September 2017].

[12] "Qcell Future-Oriented Indoor MBB Solution," ZTE, 2015. [Online]. Available: http://www.zte.com.cn/global/solutions/access/flexible/Qcell. [Accessed 10 September 2017].

[13] M. Fabbri and P. Faccin, “Radio over Fiber Technologies and Systems: New Opportunities , 2007, vol.3, pp.230-233, 1-5 July 2007,” in *ICTON '07. 9th International Conference on Transparent Optical Network*, Rome, 2007.

[14] “Distributed Antenna Systems (DAS) Market worth 10.78 Billion USD by 2022,” Markets and Markets, 2017. [Online]. Available: Distributed Antenna Systems (DAS) Market worth 10.78 Billion USD by 2022. [Accessed 10 September 2017].

[15] “Zinwave UNITIVITY SYSTEM,” Zinwave, [Online]. Available: https://cdn2.hubspot.net/hubfs/2702507/Data%20Sheets/UNITIVITY%20DATA%20 11.14.2017.pdf?t=1513019148075. [Accessed 12 Dec 2017].

[16] I. Charles H. Cox, Analog Optical Links: Theory and Practice, Cambridge: Cambridge University Press, 2006.

[17] T. Li., M. J. Crisp, R. V. Penty and I. H. White,, “Low Bit Rate Digital Radio Over Fibre System,” in *International Topical Meeting on Microwave Photonics 2009, MWP ’09*, Valencia, 2009.

[18] A. Nirmalathas, P. A. Gamage, C. Lim, D. Novak, R. Waterhouse and Y. Yang, “Digitized RF transmission over fiber,” *IEEE Microwave Magazine,* vol. 10, no. 4, pp. 75-81, 2009.

[19] C. Cox, E. Ackerman, R. Helkey and G. E. Betts, “Direct-detection analog optical links,” *IEEE Transactions on Microwave Theory and Techniques,* vol. 45, no. 8, pp. 1375-1383, Aug 1997.

[20] A. J. Cooper, “'Fibre/radio' for the provision of cordless/mobile telephony services in the access network,” *Electronics Letters,* vol. 26, no. 24, pp. 2054-2056, 1990.

[21] “Cable Basics: Fiber Optic Cable,” BELDEN, 2016. [Online]. Available: http://www.beldencables-emea.com/en/products/cable_basics/fiber-optic-cable/index.phtml. [Accessed 10 September 2017].

[22] International Journal of Applied Engineering Research, ISSN 0973-4562 Vol.7 No.11 (2012).

[23] G.P.Agrawal, Fiber-optic Communication Systesm, New York: John Wiley & Sons INC., 2002..

[24] “Data Sheet RG coaxial cable-RG214U,” Kabelwerk EUPEN, 20 March 2007. [Online]. Available: http://www.romkatel.ro/cataloage/pdf/eupen/RG214.pdf . [Accessed 10 Septermber 2017].

[25] “Photodiode Tutorial,” Thorlab, 2017. [Online]. Available: https://www.thorlabs.com/tutorials.cfm?tabID=787382ff-26eb-4a7e-b021-bf65c5bf164b. [Accessed 10 September 2017].

[26] G. Ducournau et al., "Ultrawide-Bandwidth Single-Channel 0.4-THz Wireless Link Combining Broadband Quasi-Optic Photomixer and Coherent Detection," in IEEE Transactions on Terahertz Science and Technology, vol. 4, no. 3, pp. 328-337, May 2014.

[27] G. Abbas, V. Chan and Ting Yee, "A dual-detector optical heterodyne receiver for local oscillator noise suppression," in Journal of Lightwave Technology, vol. 3, no. 5, pp. 1110-1122, October 1985.

[28] Fuada, Syifaul & Adiono, Trio. (2017). Analysis of Received Power Characteristics of Commercial Photodiodes in Indoor Los Channel Visible Light Communication.

International Journal of Advanced Computer Science and Applications. 8. 2017. 10.14569/IJACSA.20.

[29] G.Keiser, Optical Fiber Communications, 3rd Ed. London: McGraw-Hill, 2004..

[30] G. P. Agrawalm , “Fiber-Optic Communciation Systems,” in *ch. 4: Optical receivers*, 2002.

[31] J. C. Campbell, "Recent Advances in Telecommunications Avalanche Photodiodes," in Journal of Lightwave Technology, vol. 25, no. 1, pp. 109-121, Jan. 2007..

[32] W. Wang, “Optical Detectors,” National Tsinghua University, [Online]. Available: https://depts.washington.edu/mictech/optics/me557/detector.pdf. [Accessed 10 September 2017].

[33] C. Cox III, E. Ackerman, R. Helkey and G. E. Betts, “Techniques and Performance of Intensity-Modulation Direct-Detection Analog Optical Links,” *IEEE TRANSACTIONS ON MICROWAVE THEORY AND TECHNIQUES,* vol. 1383, no. 45, p. 1375, 1997.

[34] A. Goutzoulis, J. Zomp and A. Johnson, “An eight-element, optically powered, directly modulated receive UHF fiber-optic manifold,” *Lightwave Technology, Journal of,* vol. 39, pp. 74-86, Feb. 1996.

[35] E. Ackerman, C. Cox, G. Betts, H. Roussell, K. Ray, and F.O’Donnell, “Input impedance conditions for minimizing the noise figure of an analog optical link,” IEEE Trans. Microwave Theory Tech., vol. 46, pp. 2025-2031, Dec. 1998.

[36] S. Pappert, C. Sun, R. Orazi and T. Weiner, "Microwave fiber optic links for shipboard antenna applications," in *IEEE Int. Conf. Phased Array Systems and Technology*, Dana Point, CA, 2000.

[37] G. Betts, "Linearized modulator for suboctave-bandpass optical analog links," *IEEE Trans. Microwave Theory Tech. ,* vol. 42, pp. 2642-2649, 1994.

[38] D. Tauber, G. Wang, R. Geels, J. Bowers and L. Coldren, "Large and small signal dynamics of vertical cavity surface emitting lasers," *Applied Physics Letters,* vol. 62, pp. 325-327, Jan. 1993.

[39] S. Weisser, E. Larkins, W. Benz, J. Daleiden, I. Espivias, J. Fleissner, J. Ralston, B. Romero, R. Sah, A. Schonfelder and J. Rosenzweig, "Damping-limited modulation bandwidths up to 40 GHz in undoped short-cavity In/sub 0.35/Ga/sub 0.65/As-GaAs multiple-quantum-well lasers," *IEEE Photonics Technology Letters,* vol. 8, no. 5, pp. 608-610, 1996.

[40] T. Chen, J. Ungar, X. Yeh and N. Bar-Chaim, "Very large bandwidth strained MQW DFB laser at 1.3 mm," *IEEE Photon. Technol. Lett.,* vol. 7, pp. 458-460, 1995.

[41] K. Noguchi, O. Mitomi, and H. Miyazawa, "Millimeter-wave Ti:LiNbO3 optical modulators," J. Lightwave Technol., vol. 16, pp.615-617, Apr. 1998..

[42] W. Bridges and F. Sheehy, "Velocity-matched electro-optic modulator," *SPIE, ,* vol. 1371, pp. 68-77, 1990.

[43] Finisar, "FP-1310-4I-LCB," Arrow Electronics, 2017. [Online]. Available: https://www.arrow.com/en/products/fp-1310-4i-lcb/finisar. [Accessed 10 September 2017].

[44] E. Ackerman and C. Cox, “RF fiber-optic link performance,” IEEE Micrw. Mag., vol. 2, no. 4, pp. 50-58, 2001.

[45] E. Ackerman and C. Cox, “RF fiber-optic link performance,” IEEE Micrw. Mag., vol. 2, no. 4, pp. 50-58, 2001.

[46] E. Meland, R. Holmstrom, J. Schlafer, R. Lauer and W. Powazinik, “Extremely high-frequency (24 GHz) InGaAsP diode lasers with excellent modulation efficiency,” *Electron. Lett.,* vol. 26, pp. 1827-1829, 1990.

[47] D. Young, J. Scott, M. Peters, M. Majewski, B. Thiebeault, S. Corzine and L. Coldren, “Enhanced performance of offset-gain high-barrier vertical-cavity surface-emitting lasers,” IEEE J. Quantum Electron., vol. 29, pp. 2013-2022, 1993..

[48] S. Weisser, E. C. Larkins, K. Czotscher and W. Benz, “Damping-limited modulation bandwidths up to 40GHz in undoped short-cavity In0.35Ga0.65As–GaAs multiple-quantum-well lasers,” *Photonics Technology Letters IEEE,* vol. 8, no. 5, pp. 608-610, 1996.

[49] J. Ingham, M. Websterm, A. Wonfer, R. Penty, I. White and K. White, “Wide-frequency-range operation of a high-linearity uncooled FDB laser for next generation radio-over fiber,” *Optical Fiber Communications OFC,* vol. 2, pp. 754-756, 2003.

[50] A. Larsson, C. Carlsson, J. Gustavsson and A. Haglund, “Broadband direct modulation of VCSELs and applications in fiber optic RF links,” in *IEEE International Topical Meeting on Microwave Photonics (MWP 2004)*, Ogunquit, 2004.

[51] "Single Mode vs. Multi-Mode Fiber Optic Cable," Multicom, 2017. [Online]. Available: https://www.multicominc.com/training/technical-resources/single-mode-vs-multi-mode-fiber-optic-cable/. [Accessed 10 September 2017].

[52] L. Pavesi and D. J. Lockwood, Silicon Photonics III: Systems and Applications, Springer, 2016.

[53] M. Rumny, LTE and the Evolution to 4G Wireless - Design and Measurement Challenges, John Wiley & Sons Ltd, 2nd edn, 2013..

[54] "3GPP TS 36.104 V11.2.0 (2012-09) Base Station Radio Transmission and Reception," 3rd Generation Partnership Project (3GPP), 2012.

[55] "Practical Manufacturing Testing of 802.11 OFDM Wireless Devices," Litepoint, 2012. [Online]. Available: http://www.litepoint.com/wp-content/uploads/2014/02/Testing-802.11-OFDM-Wireless-Devices_WhitePaper-1.pdf. [Accessed 10 September 2017].

[56] "ETSI TS 136.101 V13.3.0 (2016-05) - LTE; Evolved Universal Terrestrial Radio Access (E-UTRA); User Equipment (UE) radio transmission and reception (3GPP TS 36.101 version 13.3.0 Release 13," 2016.

[57] X. Ge, H. Cheng, M. Guizani and T. Han, "5G wireless backhaul networks: challenges and research advances," *IEEE Network,* vol. 28, no. 6, pp. 6-11, 2014.

[58] "Distributed Antenna Systems Portfolio," i3 integrated installation inc., 2015. [Online]. Available: http://www.i3install.com/portfolio/das/. [Accessed 10 September 2017].

[59] C. H. Cox, E. I. Ackerman, G. E. Betts and J. L. Prince, "Limits on the performance of RF-over-fiber links and their impact on device design," *IEEE Transactions on Microwave Theory and Techniques,* vol. 54, no. 2, pp. 906-920, 2006.

[60] E. Ackerman, S. Wanuga, D. Kasemset, A. S. Daryoush and N. R. Samant, "Maximum dynamic range operation of a microwave external modulation fiber-optic link," *IEEE Transactions on Microwave Theory and Techniques,* vol. 41, no. 8, pp. 1299-1306, 1993.

[61] Commscope, "Interleaved MIMO: Near-full MIMO performance, nearly half the costs," Feb. 2017. [Online]. Available: https://www.google.co.uk/url?sa=t&rct=j&q=&esrc=s&source=web&cd=1&ved=0ahUKEwiYprny0cfWAhWLJVAKHdAfCy4QFggoMAA&url=http%3A%2F%2Fwww.commscope.com%2FDocs%2FInterleaved_MIMO_white_paper_WP-109965.pdf&usg=AFQjCNH_frMZiZqbpJdSkcsIiqKXdtL-9Q. [Accessed 10 September 2017].

[62] G. Gordon, M. J. Crisp, R. V. Penty and I. H. White, "Experimental Comparison of Antenna Clustering Strategies in MIMO Distributed Antenna Systems," *2014 IEEE 80th Vehicular Technology Conference (VTC2014-Fall),* pp. 1-5, 2014.

[63] E. M. Vitucci, L. Tarlazzi, P. Faccin and V. Degli-Esposti, "Analysis of the performance of LTE systems in an Interleaved F-DAS MIMO indoor environment," in *The 5th European Conference on Antennas and Propagation (EUCAP)*, Rome, 2011.

[64] Z. Zhang, X. Wang, K. Long, A. Vasilakos and L. Hanzo, "Large-scale MIMO-based wireless backhaul in 5G networks," *IEEE Wireless Communications,* vol. 22, no. 5, pp. 58 - 66, 2015.

[65] J. Capmany, B. Ortega, A. Martinez, D. Pastor, M. Popv and P. Fonjall, "Multiwavelength single sideband modulation for WDM radio-over-fiber systems using a fiber grating array tandem device," *Photonics Technology Letters, IEEE,* vol. 17, no. 2, pp. 471-473, 2005.

[66] I. Seto and e. al., , "Optical subcarrier multiplexing transmission for base station with adaptive array antenna," *IEEE Trans. Microw. Theory Tech.,* vol. 49, no. 10, pp. 2036-2041, 2001.

[67] G. Gordon, J. Carpenter, M. Crisp, T. Wilkinson, R. Penty and I. White, "Demonstration of radio-over-fibre transmission of broadband MIMO over multimode fibre using mode division multiplexing," in *European Conference and Exhibition on Optical Communication., Optical Society of America*, Amsterdam, 2012.

[68] G. S. Gordon and e. al, "Demonstration of radio-over-fibre transmission of broadband MIMO over multimode fibre using mode division multiplexing.," in European Conference and Exhibition on Optical Communication., Optical Society of America, 2012..

[69] J. Capmany, B. Ortega, A. Martinez, D. Pastor, M. Popov and P. Fonjallza, "Multiwavelength single sideband modulation for WDM radio-over-fiber systems using a fiber grating array tandem device," *IEEE Photonics Technology Letters,* vol. 17, no. 2, pp. 471-474, 2005.

[70] T. Li, M. Crisp, R. V. Penty and I. H. White, "Low bit rate digital radio over fibre system," in *2009 International Topical Meeting on Microwave Photonics*, Valencia, 2009.

[71] Chin-Pang Liu; A. Seeds, "Transmission of MIMO radio signals over fibre using a novel phase quadrature double sideband frequency translation technique," Microwave photonics, 2008. jointly held with the 2008 asia-pacific microwave photonics conference.

[72] Chin-Pang Liu; Seeds, A.J. "Transmission of Wireless MIMO-Type Signals Over a Single Optical Fiber Without WDM", Microwave Theory and Techniques, IEEE Transactions on, On page(s): 3094 - 3102 Volume: 58, Issue: 11, Nov. 2010.

[73] A. Chowdhury, H. Chien, S. Fan, J. Yu and G. Chang,, "Multi-Band Transport Technologies for In-Building Host-Neutral Wireless Over Fiber Access Systems," *Lightwave Technology, Journal of,* vol. 28, no. 16, pp. 2406-2415, Aug.15, 2010.

[74] J. Zou; H. Chen; F. Huijskens, Z. Cao; E. Tangdiongga, and T. Koonen, "Demonstration of fully functional MIMO wireless LAN transmission over GI-MMF for in-building networks," Optical Fiber Communication Conference and Exposition and the National Fibe.

[75] M. Othman, L. Deng, X. Pang, J. Caminos, W. Kozuch, K. Prince, J. Jensen and I. T. Monroy, "Directly-modulated VCSELs for 2×2 MIMO-OFDM radio over fiber in WDM-PON," in *2011 37th European Conference and Exhibition on Optical Communication (ECOC)*, Geneva, 2011.

[76] L. Maksymiuk; J. Siuzdak, "Successful IEEE 802.11n 2-channel MIMO transmission over standard graded index multimode fiber in passband," Communications (QBSC), 2012 26th Biennial Symposium on, pp.15-18, 28-29 May 2012.

[77] M. Morant, J. Prat and R. Llorente,, "Radio-Over-Fiber Optical Polarization-Multiplexed Networks for 3GPP Wireless Carrier-Aggregated MIMO Provision," *Lightwave Technology, Journal of,* vol. 32, no. 20, pp. 3721-3727, 2014.

[78] G. Gordon, M. Crisp, R. Penty, T. Wilkinson and I. and I. White, "Feasibility Demonstration of a Mode-Division Multiplexed MIMO-Enabled Radio-Over-Fiber Distributed Antenna System," *Journal of Lightwave Technology,* vol. 32, no. 20, pp. 3521-3528, 2014.

[79] Y. Yang, M. J. Crisp, R. V. Penty and I. H. White, "Low-Cost MIMO Radio Over Fiber System for Multiservice DAS Using Double Sideband Frequency Translation," *Journal of Lightwave Technology,* vol. 34, no. 16, pp. 3818-3824, Aug. 15 2016.

[80] Marpaung, David & Roeloffzen, Chris & Heideman, R.G. & Leinse, Arne & Sales, Salvador & Capmany, J. (2013). Integrated Microwave Photonics. Laser & Photonics Review. 7. . 10.1002/lpor.201200032..

[81] "Amplifier ZHL-42W+," Minicircuits, 2017. [Online]. Available: https://www.minicircuits.com/pdfs/ZHL-42W+.pdf. [Accessed 10 September 2017].

[82] "Low Noise Bypass Amplifier ZX60-53LNB+," Minicircuits, 2017. [Online]. Available: https://www.minicircuits.com/pdfs/ZX60-53LNB+.pdf. [Accessed 10 September 2017].

[83] "Power Combiner ZX10Q-2-25.pdf," Minicircuits, 2017. [Online]. Available: https://ww2.minicircuits.com/pdfs/ZX10Q-2-25.pdf. [Accessed 10 September 2017].

[84] A. Flatman, "In-Premises Optical Fibre In-Premises Optical Fibre Installed Base Analysis to Installed Base Analysis to 2007," LAN Technologies UK, 2007. [Online]. Available:

http://ieee802.org/3/10GMMFSG/public/mar04/flatman_1_0304.pdf. [Accessed 10 September 2017].

[85] "MIMO Performance and Condition Number in LTE," keysight, 31 July 2014. [Online]. Available: http://literature.cdn.keysight.com/litweb/pdf/5990-4759EN.pdf. [Accessed 10 September 2017].

[86] M. Jackson, "ISP News," 15 10 2014. [Online]. Available: https://www.ispreview.co.uk/index.php/2014/10/vodafone-uk-deploy-lte-advanced-ultra-fast-4g-mobile-broadband-speed.html. [Accessed 13 09 2017].

[87] "3 (Three) (United Kingdom) uses 1 UMTS band and 2 LTE bands," Frequency Check, 2017. [Online]. Available: https://www.frequencycheck.com/carriers/3-three-united-kingdom. [Accessed 13 09 2018].

[88] "EE (Everything Everywhere) (United Kingdom) uses 1 GSM band, 1 UMTS band, and 3 LTE bands. Find out if your unlocked phone or mobile device will work with EE (Everything Everywhere) (United Kingdom)," Frequency check, 2017. [Online]. Available: https://www.frequencycheck.com/carriers/ee-everything-everywhere-united-kingdom. [Accessed 13 09 2018].

[89] "O2 (United Kingdom) uses 2 GSM bands, 2 UMTS bands, and 2 LTE bands.," Frequency check, 2017. [Online]. Available: https://www.frequencycheck.com/carriers/o2-united-kingdom. [Accessed 13 09 2018].

[90] "Vodafone (United Kingdom) uses 2 GSM bands, 2 UMTS bands, and 2 LTE bands.," Frequency check, 2017. [Online]. Available:

https://www.frequencycheck.com/carriers/vodafone-united-kingdom. [Accessed 13 09 2018].

[91] "UK frequency allocation table," Ofcom, 12 01 2017. [Online]. Available: https://www.ofcom.org.uk/__data/assets/pdf_file/0016/103309/uk-fat-2017.pdf. [Accessed 13 09 2018].

[92] "LTE;Evolved Universal Terrestrial Radio Access (E-UTRA); User Equipment (UE) radio transmission and reception (3GPP TS 36.101 version 14.3.0 Release 14)," ETSI, 04 2017. [Online]. Available: http://www.etsi.org/deliver/etsi_ts/136100_136199/136101/14.03.00_60/ts_136101v140300p.pdf. [Accessed 13 09 2018].

[93] "Nex-Tech set to deploy LTE in Kansas using 1900MHz spectrum," TeleGeography, 05 09 2013. [Online]. Available: https://www.telegeography.com/products/commsupdate/articles/2013/09/05/nex-tech-set-to-deploy-lte-in-kansas-using-1900mhz-spectrum/. [Accessed 13 09 2017].

[94] "FCC 700 MHz Band Auction," Federal Communications Commission, 19 03 2008. [Online]. Available: https://apps.fcc.gov/edocs_public/attachmatch/DA-08-595A2.pdf. [Accessed 13 09 2017].

[95] "700 MHz Lower Band (Blocks C, D) License - WPWU903 - T-Mobile License LLC," Federal Communications Commission , 24 01 2003. [Online]. Available: http://wireless2.fcc.gov/UlsApp/UlsSearch/license.jsp?licKey=2479842. [Accessed 13 09 0013].

[96] 2. U. b. a. 3. L. b. China Mobile (China) uses 2 GSM bands, "China Mobile (China) uses 2 GSM bands, 2 UMTS bands, and 3 LTE bands," Frequency check, 2017.

[Online]. Available: https://www.frequencycheck.com/carriers/china-mobile-china. [Accessed 20 09 2018].

[97] "China Unicom (China) uses 2 GSM bands, 1 UMTS band, and 2 LTE bands.," Frequency check, 2017. [Online]. Available: https://www.frequencycheck.com/carriers/china-unicom-china. [Accessed 20 09 2017].

[98] "China Telecom (China) uses 2 LTE bands and 2 CDMA bands," Frequency check, 2017. [Online]. Available: https://www.frequencycheck.com/carriers/china-telecom-china. [Accessed 20 9 2017].

[99] Y. Yang, M. J. Crisp, T. Li, R. V. Penty and I. H. White, "MIMO Capable RoF System with Improved SFDR using Quadruple Sidebands," in *2017 IEEE International Topical Meeting on Microwave Photonics (MWP)*, Beijing, China, 2017.

[100] D. Wake, A. Nkansah and N. J. Gomes, "Radio Over Fiber Link Design for Next Generation Wireless Systems," *Journal of Lightwave Technology,* pp. 2456-2464, 15 August 2010.

[101] S. R. Abdollahi, A. Raweshidy, S. M. Fakhraie and R. Nilavalan, "Digital Radio over Fibre for Future Broadband Wireless Access Network Solution," in *2010 6th International Conference on Wireless and Mobile Communications*, Valencia, 2010.

[102] "Cisco SFP-10G-LRM Compatible 10GBASE-LRM SFP+ 1310nm 220m DOM Transceiver," Fiber Store, 2017. [Online]. Available: http://www.fs.com/products/11556.html. [Accessed 20 09 2017].

[103] M. Hinrichs, L. F. del Rosal, C. Kottke and V. Jungnickel, "Analog vs. next-generation digital fronthaul: How to minimize optical bandwidth utilization," in *2017 International Conference on Optical Network Design and Modeling (ONDM)*, Budapest, 2017.

[104] T. Li, Y. Yang, R. Penty and I. White, "Digital and Analogue Hybrid Radio over Fiber System for Indoor Wireless Coverage," in *IEEE International Conference on Communications (ICC)*, Kansas City, 2018.

[105] 3GPP, "Technical Specifications and Technical Reports for a UTRAN-based 3GPP system, Specification #: 21.101," 2015 .

[106] " CPRI specification 6.1 [available: www.cpri.info]," Ericsson AB et al., Jul. 2014.

[107] T. Li, R. Penty and I. White, "Novel digital radio over fibre for 4G-LTE," in *2015 IEEE International Conference on Communication Workshop (ICCW)*, London, 2015.

[108] T. Norman, "Research forecast report—Wireless network traffic 2010–2015: forecasts and analysis," AnalysysMason, London, 2010.

[109] "ZTE Releases World's First Pre5G FDD Massive MIMO Solution, Verified by Joint Field Tests with China Unicom," ZTE, 30 December 2016. [Online]. Available: http://www.zte.com.cn/global/about/press-center/news/201612ma/1230. [Accessed 20 September 2017].

[110] "ZTE Unveils Forward-looking "5uper Generation" Smartphone with Download Speeds Reaching up to 1Gbps," ZTE, 26 Febrary 2017. [Online]. Available:

http://www.zte.com.cn/global/about/press-center/news/201702Ma/0227ma2. [Accessed 20 September 2017].

[111] A. Kaszubowska, L. P. Barry, . P. Anandarajah and L. Hu, "Characterization of wavelength interleaving in radio-over-fiber systems employing WDM/SCM," *Optics Communications,* vol. 260, no. 1, pp. 144-149, 2006.

[112] O. Said and M. Masud, "Towards Internet of Things: Survey and Future Vision," *International Journal of Computer Networks (IJCN),* 2013.

[113] "The 'Internet of Things' will be the world's most massive device market and save companies billions of dollars," Business Insider, 18 February 2015. [Online]. Available: http://uk.businessinsider.com/the-internet-of-things-market-growth-and-trends-2015-2. [Accessed 20 September 2017].

[114] "Internet of Things (IoT) Infrastructure: Market for IoT Platforms, Hardware, and Software 2015 - 2020," CISION, 19 January 2016. [Online]. Available: http://www.prnewswire.com/news-releases/internet-of-things-iot-infrastructure-market-for-iot-platforms-hardware-and-software-2015---2020-300206623.html. [Accessed 20 Spetember 2017].

[115] A. Zanella, N. Bui, A. Castellani, L. Vangelista and M. Zorzi, "Internet of Things for Smart Cities," *IEEE Internet of Things Journal,* vol. 1, no. 1, pp. 22-32, 2014.